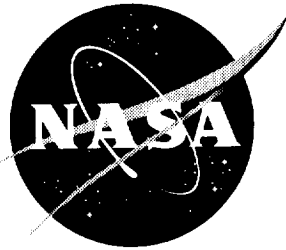


NASA/CR-1999-209326



# High Reynolds Number Hybrid Laminar Flow Control (HLFC) Flight Experiment IV. Suction System Design and Manufacture

*Boeing Commercial Airplane Group, Seattle, Washington*

National Aeronautics and  
Space Administration

Langley Research Center  
Hampton, Virginia 23681-2199

Prepared for Langley Research Center  
under Contract NAS1-18574

---

April 1999

The data in this volume, D6-655648-4, was collected by members of The Boeing Company in a cooperative effort with the National Aeronautics and Space Administration and the United States Air Force under contract NAS1-18574.

---

Available from:

NASA Center for AeroSpace Information (CASI)  
7121 Standard Drive  
Hanover, MD 21076-1320  
(301) 621-0390

National Technical Information Service (NTIS)  
5285 Port Royal Road  
Springfield, VA 22161-2171  
(703) 605-6000

# CONTENTS

|  | <u>Page</u> |
|--|-------------|
| 1.0 SUMMARY .....                          | 1           |
| 2.0 INTRODUCTION .....                     | 3           |
| 2.1 Background .....                       | 3           |
| 2.2 Technical Approach .....               | 3           |
| 2.3 Program Tasks .....                    | 4           |
| 3.0 SUCTION SYSTEM REQUIREMENTS .....      | 5           |
| 3.1 Theoretical Suction Distribution ..... | 5           |
| 3.2 Practical Suction Distribution .....   | 6           |
| 4.0 SYSTEM DESIGN .....                    | 15          |
| 4.1 Flow Path .....                        | 15          |
| 4.2 Design Flows and Pressures .....       | 17          |
| 4.3 Flow and Pressure Analysis .....       | 17          |
| 4.4 Flutes and Suction Panel .....         | 22          |
| 4.4.1 Flute Width Selection .....          | 23          |
| 4.4.2 Skin Porosity .....                  | 30          |
| 5.0 HARDWARE DESIGN .....                  | 39          |
| 5.1 Requirements .....                     | 39          |
| 5.2 System Arrangement .....               | 39          |
| 5.3 Special Features .....                 | 44          |
| 5.3.1 Flapper Valves .....                 | 44          |
| 5.3.2 Check Valves .....                   | 44          |
| 5.3.3 Pressure Regulating Valve .....      | 44          |
| 5.3.4 Shutoff Valve .....                  | 46          |
| 5.3.5 Plenum .....                         | 48          |
| 5.3.6 Muffler .....                        | 49          |
| 5.3.7 Filter .....                         | 49          |
| 5.4 Turbocompressor Modifications .....    | 50          |
| 6.0 SUCTION CONTROL SCHEME .....           | 51          |
| 6.1 Spanwise Control .....                 | 51          |
| 6.2 Chordwise Adjustment .....             | 54          |
| 7.0 ANTI-ICE AND PURGE OPERATION .....     | 57          |
| 7.1 Anti-Ice .....                         | 57          |
| 7.1.1 External Heat Loads .....            | 57          |
| 7.1.2 System Performance .....             | 60          |
| 7.2 Purge .....                            | 67          |
| 8.0 REFERENCES .....                       | 71          |

## CONTENTS (CONTINUED)

|   | <u>Page</u> |
|---|-------------|
| Appendix A Equations Used in Duct Analysis .....                                  | A-1         |
| Appendix B "Corrected" Flow Parameters .....                                      | B-1         |
| Appendix C Example Flute Pressure Drop Calculation .....                          | C-1         |
| Appendix D Hole Flow Pressure Drop Code "ADBTDIF.BAS" .....                       | D-1         |
| Appendix E Tapered Hole Flow Pressure Drop Code "ADBTSTC.BAS" .....               | E-1         |
| Appendix F Icing Tunnel Test of HLFC Transpiration Thermal Anti-Icing (TAI) ..... | F-1         |
| Appendix G Leading-Edge Heating Load at Icing Conditions .....                    | G-1         |
| Appendix H Heat Exchanger Sizing Calculation .....                                | H-1         |

## FIGURES

| <u>Figure</u> | <u>Title</u>  | <u>Page</u> |
|---------------|---|-------------|
| 3.1-1         | Suction Coefficient Requirement .....   | 6           |
| 3.1-2         | Suction Coefficient Variations With Attachment-Line Location .....  | 6           |
| 3.2-1         | Wing Buttock Line and Outboard Slat Station Coordinates .....   | 7           |
| 3.2-2         | Increased Suction Rates Based On Area Ratios .....  | 8           |
| 3.2-3         | Typical $c_{q'}$ Curve in High-Suction Zone .....   | 8           |
| 3.2-4         | Practical $c_{q'}$ for the Design Case ( $C_L = 0.5$ , 0.8M, 39,000 ft)<br>High-Suction Zone .....                          | 10          |
| 3.2-5         | Typical $c_{q'}$ Curve in Transition Zone .....   | 11          |
| 3.2-6         | Local $c_{q'}$ for the Design Case ( $C_L = 0.5$ , 0.8M, 39,000 ft)<br>Transition Zone (Flutes 7 and 8) .....               | 12          |
| 3.2-7         | Typical $c_{q'}$ Curve Aft Zone (TS Instability Control) .....  | 13          |
| 3.2-8         | Practical $c_{q'}$ for the Design Case ( $C_L = 0.5$ , 0.8M, 39,000 ft)<br>Flutes 9 through 20, Aft Zone (TS Control) ..... | 14          |
| 4.1-1         | Airflow Path During Normal Suction System Operation .....   | 15          |
| 4.1-2         | HLFC Pneumatic System Schematic .....   | 16          |
| 4.2-1         | Conditions at Collectors for the Design Case ( $C_L = 0.5$ , 0.8M, 39,000 ft) .....   | 18          |
| 4.2-2         | Duct Pressures Versus Spanwise Location .....   | 19          |
| 4.3-1         | Friction Factor for Anticipated Duct Roughness .....  | 20          |
| 4.3-2         | Turbocompressor Map .....   | 21          |
| 4.4-1         | Flute Layout and Isobar Location .....  | 22          |
| 4.4-2         | Theoretical Flute Pressure and Measured Drops .....   | 23          |
| 4.4-3         | Flow Network for Off-Design Analysis of Flute 15 .....  | 24          |
| 4.4-4         | Flow Versus Span, 0.5 $C_L$ Design Case .....   | 25          |
| 4.4-5         | Effect of $C_L$ on Suction Distribution, Flute 2 (CF Control Zone) .....  | 25          |
| 4.4-6         | Distribution of $c_{q'}$ Across Flute at a Constant Flow for Various Hole<br>Spacings ( $\delta$ ) .....                    | 26          |
| 4.4-7         | Flow at Flute Reverse-Flow Threshold .....  | 27          |
| 4.4-8         | Effect of Hole Diameter on Minimum Flute Spacing .....  | 28          |
| 4.4-9         | Flutes Enlarged To Reduce Spanwise $\Delta P$ .....   | 29          |
| 4.4-10        | Laser-Drilled Holes .....   | 30          |
| 4.4-11        | Flow Models Used for Perforation Analysis .....   | 31          |
| 4.4-12        | Methods of Modeling Flow Through Laser-Drilled Holes .....  | 32          |
| 4.4-13        | Computed and Measured Pressure Drop for Three Hole Diameters .....  | 32          |
| 4.4-14        | Diffuser Recovery Effect of a Laser-Drilled Hole .....  | 33          |
| 4.4-15        | Flow Characteristics for the Two Hole Sizes Used<br>(at Design Conditions) .....  | 35          |
| 4.4-16        | Hole Spacing Required To Obtain $c_{q'}$ in Aft Zone .....  | 36          |
| 4.4-17        | Outer Skin Perforation Pattern .....  | 37          |
| 4.4-18        | Variation of $c_{q'}$ Due To Perforation Pattern Steps .....  | 38          |
| 5.2-1         | Turbocompressor Installation (Viewed From Inboard Side) .....   | 40          |
| 5.2-2         | Turbocompressor Installation (Viewed From Outboard Side) .....  | 41          |
| 5.2-3         | General Arrangement of Wing Suction System .....  | 42          |

## FIGURES (CONTINUED)

| <u>Figure</u> | <u>Title</u>   | <u>Page</u> |
|---------------|--|-------------|
| 5.2-4         | Typical Wing Leading-Edge Bay (Krueger Flap Drive Not Shown) .....   | 43          |
| 5.3-1         | Typical Flapper Valve Arrangement.....   | 44          |
| 5.3-2         | Flapper Valve Drive and Position Indication.....   | 45          |
| 5.3-3         | Anti-Ice Check Valve.....  | 46          |
| 5.3-4         | Check Valve.....   | 46          |
| 5.3-5         | Attachment-Line Flow Control Duct and Shutoff Valve.....   | 47          |
| 5.3-6         | Plenum Assembly.....   | 48          |
| 5.3-7         | Muffler.....   | 49          |
| 5.3-8         | Air Filter.....  | 50          |
| 6.1-1         | Flapper Valve Numbering Convention.....  | 52          |
| 6.1-2         | Overall System Control Method.....   | 53          |
| 6.2-1         | Streamwise Pressure Display.....   | 55          |
| 7.1-1         | Icing Tunnel Test.....   | 58          |
| 7.1-2         | Reduction in Heat Transfer Rate Due To Fluid Injection (Air to Air).....                                   | 59          |
| 7.1-3         | Comparison of Ice Protection Methods.....  | 60          |
| 7.1-4         | Flute Thermal Load at Maximum Icing Conditions.....  | 61          |
| 7.1-5         | Flute Temperature Distribution (Anti-Icing Conditions).....  | 62          |
| 7.1-6.        | Flute Temperature Distribution (Still, on the Ground).....   | 63          |
| 7.1-7         | Flute Temperature Distribution (Normal Takeoff Purge).....   | 64          |
| 7.1-8         | Metering Screen Location Required for Suction Versus Anti-Ice.....   | 65          |
| 7.1-9         | Air Temperature During Anti-Ice (No Ice Load).....   | 66          |
| 7.1-10        | Effect of Icing Rates on Air Temperature During Anti-Icing.....  | 68          |
| 7.1-11        | Theoretical Ice Formation at Various Icing Rates.....  | 69          |
| F-1           | Proof-of-Concept Test Model.....   | F-2         |
| F-2           | Details of Test Model.....   | F-3         |
| F-3           | Skin Temperatures in Dry-Air Tests of HLFC TAI System.....   | F-5         |
| F-4           | Leading Edge After 60 sec in FAA Maximum Continuous Icing With<br>350°F TAI Air, Ambient Air at -20°F..... | F-6         |
| F-5           | Leading Edge After 60 sec in FAA Maximum Continuous Icing With<br>200°F TAI Air, Ambient Air at -20°F..... | F-7         |
| F-6           | Leading-Edge Temperatures With TAI in FAA Maximum Continuous Icing.....                                    | F-8         |

## TABLES

| <u>Table</u> | <u>Title</u>  | <u>Page</u> |
|--------------|---|-------------|
| 3-1          | Suction Coefficients (Local $c_q' \times 10^4$ ), Flutes 1 Through 6 .....  | 9           |
| 3-2          | Suction Coefficients (Local $c_q' \times 10^4$ ), Flutes 7 and 8 .....      | 11          |
| 3-3          | Suction Coefficients (Local $c_q' \times 10^4$ ), Flutes 9 Through 20 ..... | 13          |

## PREFACE

The program was jointly sponsored by NASA; the United States Air Force, Wright Laboratory, Flight Dynamics Directorate; and The Boeing Company. The contract was managed by Mr. R. D. Wagner, Head of Laminar Flow Control Project Office, and Mr. D. V. Maddalon, Technical Monitor. Mr. R. L. Clark was the Wright Laboratory (WL/FIMM, Wright-Patterson Air Force Base, OH) Program Manager. The period of performance was from December 1987 through August 1991.

The program was conducted by the Advanced Development Aerodynamics organization of Boeing Commercial Airplane Group (BCAG), supported by the BCAG Nacelle, Strut, and Propulsion System Engineering, BCAG Structures Engineering, BCAG Mechanical/Electrical Systems Engineering, and BCAG Flight Test organizations.

The principal contributors to the work described herein are Mr. M. Hamamoto, lead engineer for systems, Mr. R. H. Horstman, principal analyst, Mr. H. A. Cruver, design supervisor, Mr. R. Woodcock, lead designer, and Mr. A. Shariatmadar, who conducted the laboratory calibrations of the skins and internal flow components. Mr. F. J. Davenport provided technical and document integration services. Mr. A. L. Nagel was HLFC program manager.

Special thanks are owed to Mr. R. D. Wagner and Mr. D. V. Maddalon of NASA Langley Research Center, who generously contributed time and effort to make their unique backgrounds of laminar flow expertise and flight test experience available to Boeing personnel.

Finally, the authors wish to acknowledge the vital contribution of Dr. Werner Pfenninger. In addition to being a mentor to all participants in modern laminar flow control work, he made several specific contributions to the present system design, such as advising the adoption of low turbulence flow control ("flapper") valves and suggesting many aspects of the suction system arrangement.

## SYMBOLS AND ABBREVIATIONS

**Note:** Symbols and abbreviations appearing in the appendixes are defined where used.

|          |  |
|----------|--|
| $A_p$    | Projected area for droplet impingement   |
| $A_s$    | Heated surface area  |
| $b$      | Hole flow exponent; flow exponent  |
| CAD      | Computer Aided Design  |
| CATIA    | Computer Aided Three-Dimensional Interactive Application (a commercial CAD/CAM system) |
| CF       | Crossflow  |
| $C_L$    | Airplane lift coefficient, $W/q_\infty S$  |
| $C_p$    | Pressure coefficient, $(P-P_\infty)/q_\infty$  |
| $C_p$    | Specific heat of air at constant pressure  |
| $c$      | Local wing chord; specific heat of water   |
| $c_q$    | Chord suction coefficient, $(\text{mass flow per unit span})/\rho_\infty V_\infty c$   |
| $c_q'$   | Local suction coefficient, $(\text{mass flow per unit area})/\rho_\infty V_\infty$     |
| $D$      | Diameter (of duct, hole, or tube, depending on context)                                |
| $f$      | Friction factor (for internal flow)  |
| $g$      | Acceleration of gravity  |
| HLFC     | Hybrid laminar flow control  |
| HX       | Heat exchanger   |
| $h$      | Heat transfer coefficient  |
| $h_{fg}$ | Heat of vaporization of water  |
| $k$      | Hole flow coefficient  |
| $L$      | Distance along flute between collectors  |
| $M$      | Mach number  |
| OSS      | Outboard slat station  |
| $P$      | Pressure (as indicated by context or subscript)  |
| PRSOV    | Pressure Regulating Shutoff Valve  |
| psf      | Pounds per square foot   |

## **SYMBOLS AND ABBREVIATIONS (CONTINUED)**

|            |  |
|------------|--|
| $Q_T$      | Anti-icing heat load   |
| $q_\infty$ | Free stream dynamic pressure $\rho_\infty V_\infty^2 / 2$  |
| R          | Gas constant for air   |
| Re         | Reynolds number, $\rho V l / \mu$ ( $V$ , $l$ depend on context)                                     |
| S          | Airplane reference wing area (1,951 ft <sup>2</sup> for a Boeing 757)                                |
| s          | Streamwise arc length on wing surface  |
| T          | Temperature (as indicated by context or subscript)   |
| TAI        | Thermal anti ice   |
| t/c        | Thickness to chord ratio   |
| TS         | Tollmien-Schlichting   |
| V          | Velocity (as indicated by context or subscript)  |
| W          | Airplane weight  |
| WBL        | Wing buttock line  |
| $\dot{w}$  | Weight flow (hole, suction surface, flute, duct or compressor, as indicated by context or subscript) |
| $w_F$      | Flute width  |

## **GREEK LETTERS**

|            |   |
|------------|---|
| $\beta$    | Droplet impingement efficiency  |
| $\gamma$   | Ratio of specific heats (1.40 for air); supercooled moisture density in atmosphere; surface tension |
| $\delta$   | Hole spacing; ratio of pressure to sea level standard pressure                                      |
| $\epsilon$ | Duct internal roughness; surface emissivity   |
| $\theta$   | Ratio temperature to sea level standard temperature; wetting angle                                  |
| $\mu$      | Viscosity   |
| $\rho$     | Density   |
| $\sigma$   | Stefan-Boltzmann constant   |

## **SUBSCRIPTS**

|          |   |
|----------|---|
| $\infty$ | Referring to atmospheric ambient (free stream) conditions |
|----------|---|

## 1.0 SUMMARY

A pneumatic system to suck boundary layer air through a porous leading-edge panel was designed, built, and installed on a Boeing 757 airplane. The panel and suction system were developed to permit flight demonstration of Hybrid Laminar Flow Control (HLFC) at high Reynolds number on a modern turbofan-powered transport and to conduct flight research on laminar flow control technology.

The system was designed to provide a suction flow of 11.5 lb/min at Mach 0.80 and 39,000 ft altitude, with exterior surface pressures corresponding to an airplane lift coefficient of 0.50. The overall flow was controlled by varying the speed of the turbocompressor that served as its suction source. The distribution of suction flow was controlled by a system of remotely adjustable internal valves, working in conjunction with ground-replaceable pressure reducing screens.

The design requirements prohibited both local outflow and large spanwise discontinuities of suction flow, because of concern that either one would cause boundary layer transition. To achieve this, the six spanwise flow channels ("flutes") under the skin near the nose were made very narrow (0.30 in) and aligned with the theoretical local isobars of the wing pressure distribution. Farther aft, it was possible to make the flutes wider and to let them run across isobars, tailoring the flow quantity by varying the skin porosity. Because of possible boundary layer tripping due to internal acoustic effects, substantial effort was also devoted to developing "flapper" control valves. These valves permitted adjustment of suction distribution without the internal turbulence characteristic of conventional butterfly valves.

Five separate main spanwise ducts were required because of the varying pressure levels of the skin areas they served. Furthermore, the available space was severely constrained by the need to accommodate the retracted Krueger flap and its actuators. Nevertheless, use of the CATIA computer-aided design system made it possible to develop the pneumatic hardware and its arrangement without the added cost of a mockup.

Purging and thermal anti-icing capabilities were provided by valving engine bleed air into the system and blocking the turbocompressor inlet. The bleed flow then pressurized the ducts and flutes, providing transpiration heating of the leading edge.

**THIS PAGE INTENTIONALLY LEFT BLANK**

## 2.0 INTRODUCTION

### 2.1 BACKGROUND

The potential for reducing wing friction drag by increasing the extent of laminar flow was recognized more than half a century ago. However, boundary layer instabilities associated with high Reynolds number and with sweepback prevented achievement of significant laminar runs on the wings of large high-performance airplanes. In the 1960s, the USAF X-21 program showed that those problems could be overcome by using slot suction to stabilize the boundary layer if care was taken to control wing surface roughness and waviness. The program failed as a demonstration of practical laminar flow control because of a flawed joint design that required continual repair or replacement of aerodynamic smoothing material. There was also debate as to whether the complexity of a suction system that covered the entire wing with slots and subsurface plumbing was justified by the performance gain.

The concept of Hybrid Laminar Flow Control (HLFC), patented by L. B. Gratzler of The Boeing Company (U. S. Patent No. 4,575,030), greatly simplifies laminar flow control by confining suction surfaces and plumbing to the leading edge. HLFC maintains laminar flow downstream of the wing front spar solely by tailoring the pressure distribution.

Other concerns, relating to anti-icing and to clogging or roughening of suction surfaces due to insect accretion, were addressed by the NASA Leading Edge Flight Test Program (refs. 1 and 2). A modified Lockheed JetStar airplane equipped with an HLFC "glove" over a portion of the wing span was flown in a variety of hostile environments and demonstrated reliable operation.

The present program was undertaken by The Boeing Company, with partial NASA and USAF sponsorship, to—

- a. Perform high Reynolds number flight research on HLFC.
- b. Obtain data on the effectiveness of HLFC on a large, high-subsonic-speed transport airplane.
- c. Develop and demonstrate practical design concepts for HLFC systems.

### 2.2 TECHNICAL APPROACH

A Boeing-owned 757 airplane (No. NA 001, the first 757 built) was modified to include all the critical systems for a full-scale HLFC application, plus flight-operable suction controls and extensive instrumentation to meet HLFC research requirements. The 757 was ideally suited to the program because its advanced aerodynamic technology wing permitted attainment of the needed HLFC pressure distribution with only a small contour change ahead of the front spar, and the smoothness of the existing between-spar structure allowed the test to be conducted with minimal fairing or coating beyond normal paint. This ensured that the data obtained would have practical application to standard production wings and not be restricted to ideally smooth surfaces.

## 2.3 PROGRAM TASKS

The program effort consisted of—

- a. **Aerodynamic Design.** Definition of the surface pressures and suction quantities required to achieve extended laminar flow, followed by geometric design of the wing contours needed to obtain the surface pressures. This task is treated in volume II.
- b. **Leading-Edge Structural Design and Fabrication.** The design, construction, and installation of a 22-ft section of wing leading edge having provisions for suction through a porous outer skin and for a Krueger-type leading-edge flap serving both as an integral part of the airplane high-lift system and as a shield against insect accretion at low altitude. The leading edge was required to meet stringent aerodynamic smoothness and waviness requirements under load, as well as to provide structural integrity. This task is discussed in volume III.
- c. **Suction System Design and Manufacture.** The design of the system of air passages, ducts, valves, and pump, and the specification of leading-edge outer skin porosities. The system was required not only to provide the suction flows required for laminarization but also to demonstrate anti-icing capability. To achieve this, hot pressurized air was required to flow out through certain portions of the porous skin. The system was also required to provide a wide range of suction flow adjustment to permit optimization of HLF C suction quantities and to permit generation of boundary layer behavior data under a variety of suction conditions, in support of research on boundary layer analysis methods. This task is reported in this volume (vol. IV).
- d. **Flight Test and Data Analysis.** The definition and installation of suitable instrumentation to evaluate boundary layer conditions and suction system performance, followed by the conduction of the tests, acquisition of data, and evaluation of test results. This task is reported in volume I, together with an overview of the program as a whole.

### 3.0 SUCTION SYSTEM REQUIREMENTS

The system must provide a maximum suction quantity distributed as discussed in sections 3.1 and 3.2. To satisfy research requirements, there is also a need for the ability to operate at reduced suction levels and with considerable flexibility of suction distribution, both chordwise and spanwise. Note that the system cannot be "shut off" (i.e., operated at zero flow everywhere). Flows between internally connected skin regions will be driven by external pressure differences, resulting in a patchwork of local suction and efflux.

Abrupt spanwise variations in suction flow must be avoided because they are likely to cause boundary layer transition. This implies that the "flutes" (air passages under the skin) must not be blocked except at their extremities. The pressure drops through the skin must therefore be great enough to accommodate expected spanwise pressure variations. At the same time, the permissible flow per hole is limited by the effective aerodynamic roughness associated with individual holes (versus the ideal of continuously distributed porosity). The holes must therefore be very small to provide the needed flow resistance.

The system must also be able to operate in reverse flow, to distribute hot engine bleed air to the leading edge for anti-icing, and to permit purging the system of ingested water.

#### 3.1 THEORETICAL SUCTION DISTRIBUTION

The initial design suction requirement was based on the boundary layer stability theory in general use in early 1988. (Details are provided in vol. II of this series.) Later in the program, an improved analysis by F. Collier of NASA showed that the overall effect of the curvature terms neglected in the classical theory is stabilizing, and a lower suction level should be sufficient. However, because the new method was as yet unproven, the original suction level was used for design, but the safety margin first contemplated was not applied.

The suction requirement was expressed as a continuous distribution of "local suction coefficient" ( $c_q$ ) as a function of arc length along the airfoil surface. The  $c_q$  is defined as the mass flow of suction air per unit area divided by the product of freestream velocity and freestream density. Figure 3.1-1 shows the theoretical requirement at a section close to the inboard end of the HLFC panel. The arc length was measured from the attachment line (i.e., from the point on the leading edge where the flow divides to pass over or under the wing). Because the attachment line moved up and down depending on the flight condition, the relative position of the  $c_q$  distribution and the flutes also changed (fig. 3.1-2). Therefore, if the shape of the suction curve was to follow the flight conditions, some system adjustment was required.

The suction distribution was characterized by an initial high-suction zone (see fig. 3.1-1) to stabilize the boundary layer against crossflow (CF) instability. This was followed by a change zone that ramped the suction to a uniform low level required in the aft zone to control Tollmien-Schlichting (TS) instability.

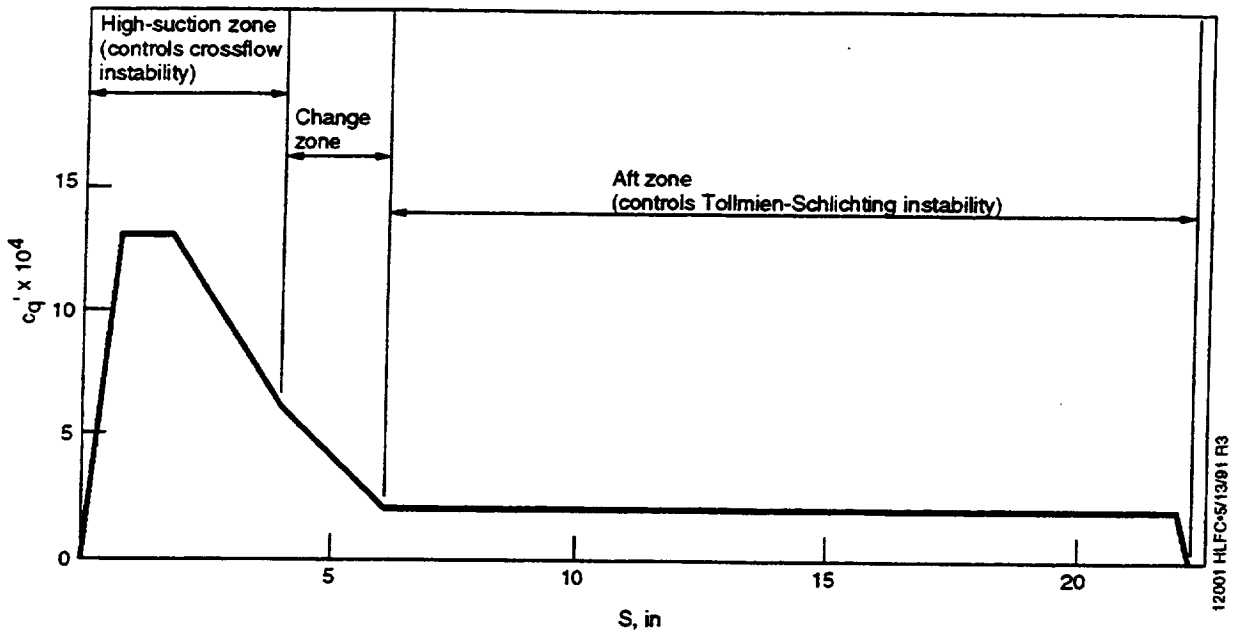


Figure 3.1-1. Suction Coefficient Requirement

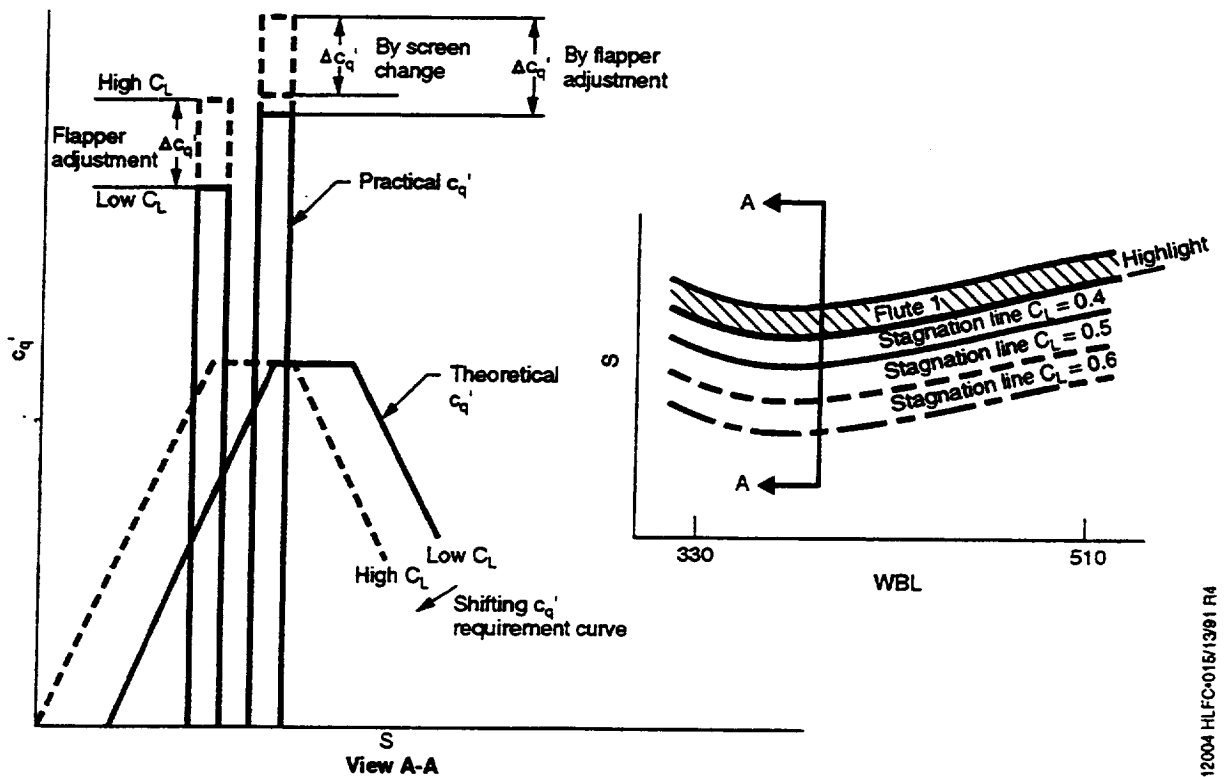


Figure 3.1-2. Suction Coefficient Variations With Attachment-Line Location

### 3.2 PRACTICAL SUCTION DISTRIBUTION

The discussions of practical suction requirements in this section will refer to spanwise locations on the wing using wing buttock line (WBL) axes. These locations are the natural choice for aerodynamic analysis because they are oriented to the wing chord plane and the freestream wind vector. For

purposes of system or structural design, however, it is usually more convenient to use outboard slat station (OSS) axes oriented to the physical leading edge of the wing. Figure 3.2-1 shows the relation of the two coordinate systems, each of which was used where applicable in this report.

Because the porous leading edge was blocked at intervals by the supporting stringers, local suction rates through the open areas (over the flutes) had to increase to compensate. Figure 3.2-2 shows a practical  $c_q'$  distribution in which the local suction at the flutes was increased by the ratio of total to open surface area. Within the accuracy of the stability theory, the interruptions were short enough to provide adequate protection, because the area-averaged suction quantity was the same.

To determine the flow requirement over the test span, the high-suction crossflow (CF control) zone was analyzed at seven wing locations. The six flutes contained within this zone were designed to follow isobars, thereby ensuring an even flow throughout the span. The  $c_q'$  curve defining the suction requirement, in the six flutes, is shown in figure 3.2-3, and consists of—

- a. Line 1—from the stagnation line to isobar  $C_p = 0.7$ , increase the  $c_q'$  from 0 to  $13 \times 10^{-4}$  as a linear ramp.
- b. Line 2—from isobar  $C_p = 0.7$  to  $C_p = 0.2$ , maintain a constant  $c_q' = 13 \times 10^{-4}$ .
- c. Line 3—from isobar  $C_p = 0.2$  to  $C_p = -0.5$ , decrease the  $c_q'$  from  $13 \times 10^{-4}$  to  $6 \times 10^{-4}$  as a linear ramp.

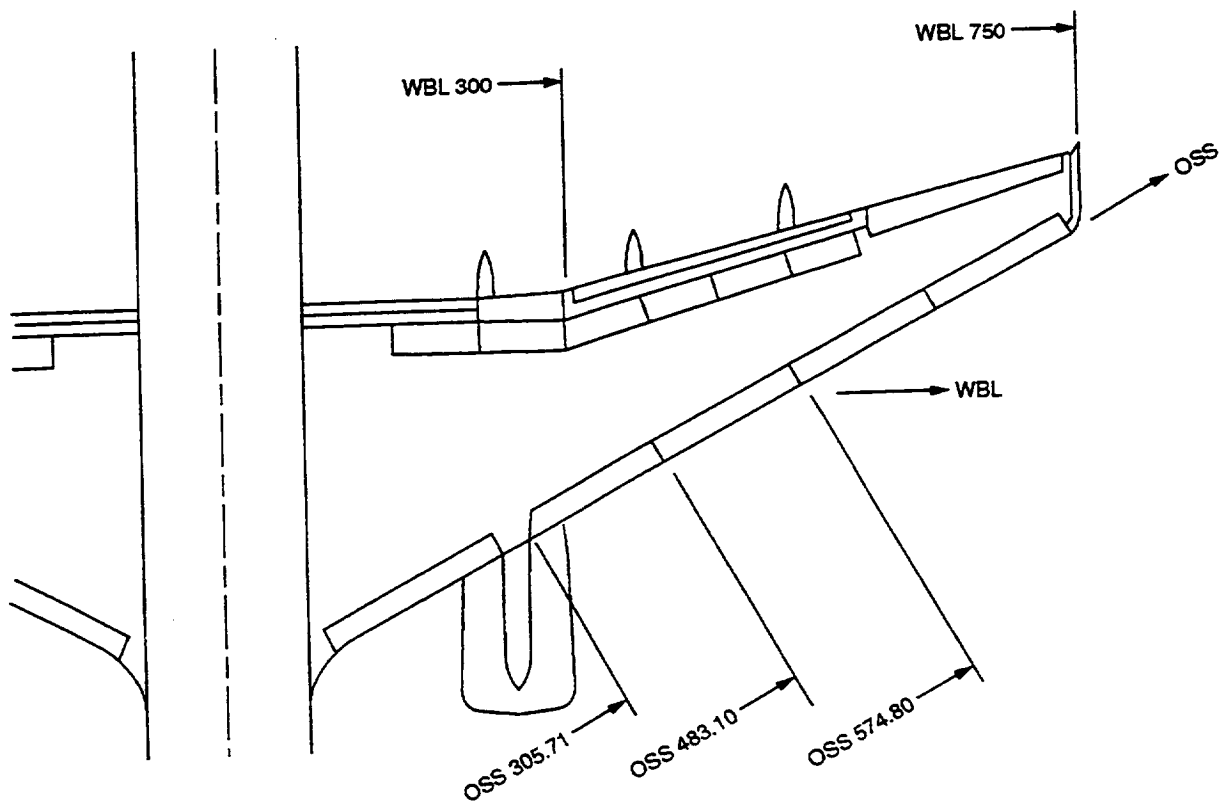


Figure 3.2-1. Wing Buttock Line and Outboard Slat Station Coordinates

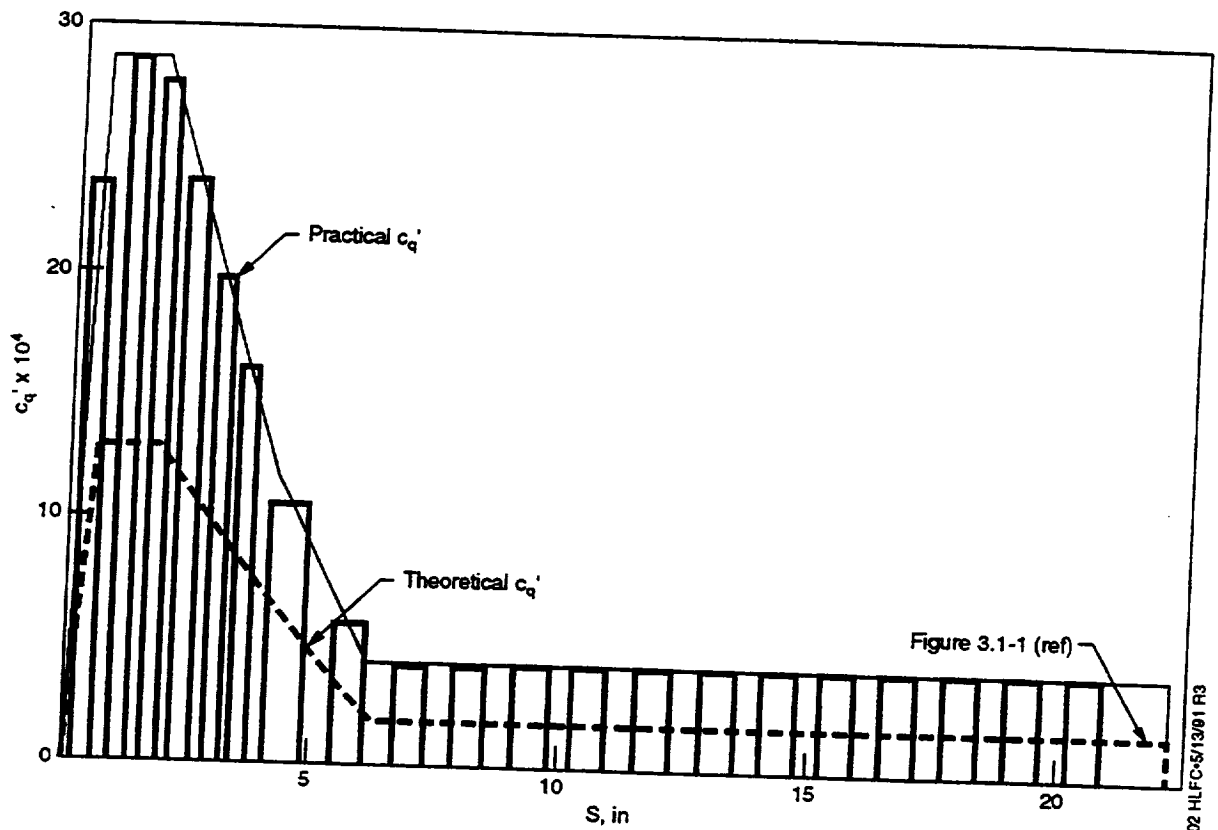


Figure 3.2-2. Increased Suction Rates Based On Area Ratios

12002 HLCF-5/13/01 R3

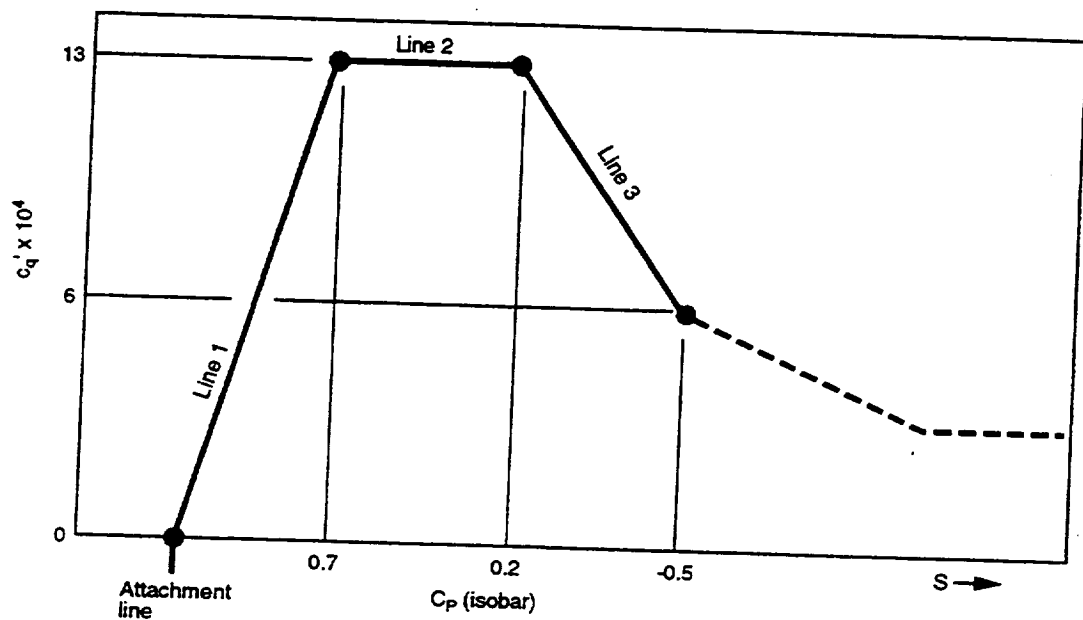


Figure 3.2-3. Typical  $c_q'$  Curve in High-Suction Zone

12005 HLCF-5/13/01 R3

Table 3-1 shows a breakdown of the flute suction requirements for the seven spanwise locations based on the percentage of open area and relative flute position along the  $c_q'$  curve. These data are presented graphically in figure 3.2-4.

The isobars aft of  $C_p = -0.5$  were highly irregular and having the stringers follow them was impractical. The suction area aft of  $C_p = -0.5$  (flute 6) and forward of the front spar was divided into 14 equally spaced flutes. The first two of these equally spaced flutes (flutes 7 and 8) lay in a change zone where the  $c_q'$  requirement was changing from crossflow control ( $c_q' = 6 \times 10^{-4}$ ) to TS instability control ( $c_q' = 2 \times 10^{-4}$ ). The bounds of this transition were isobar  $C_p = -0.5$  upstream and approximately 4% of chord downstream, which corresponded to the aft edge of flute 8. Figure 3.2-5 shows this typical  $c_q'$  curve and table 3-2 shows the practical  $c_q'$  based on the percentage of open area and relative flute position along the  $c_q'$  curve, which is presented graphically in figure 3.2-6.

The remaining 12 flutes in the aft zone were designed to provide a constant  $c_q'$  of approximately  $2 \times 10^{-4}$ . These 12 flutes were bounded by  $s/c = 0.04$  (flute 8) forward and the wing front spar aft. The typical  $c_q'$  curve for this zone is shown in figure 3.2-7. The practical  $c_q'$  based on the percentage of open area is shown in table 3-3 and is presented graphically in figure 3.2-8.

Table 3-1. Suction Coefficients (Local  $c_q' \times 10^4$ ), Flutes 1 Through 6

| Flute Number | Segment     | 1    | 2    | 3    | 4    | 5    | 6    | 7    |
|--------------|-------------|------|------|------|------|------|------|------|
|              | WBL         | 345  | 371  | 398  | 424  | 450  | 477  | 503  |
|              | % Open Area | 45.4 | 44.5 | 45.9 | 46.5 | 45.9 | 45.9 | 46.8 |
| 1            |             | 26.0 | 24.0 | 23.5 | 24.5 | 25.5 | 26.0 | 24.5 |
| 2            |             | 28.5 | 29.0 | 28.5 | 28.0 | 28.5 | 28.5 | 28.0 |
| 3            |             | 27.5 | 28.5 | 27.5 | 27.0 | 27.0 | 27.0 | 26.5 |
| 4            |             | 24.5 | 24.0 | 23.5 | 22.5 | 22.5 | 22.5 | 22.5 |
| 5            |             | 21.0 | 19.5 | 19.5 | 18.5 | 19.0 | 18.5 | 18.0 |
| 6            |             | 17.0 | 15.0 | 16.0 | 14.5 | 15.0 | 14.5 | 14.0 |

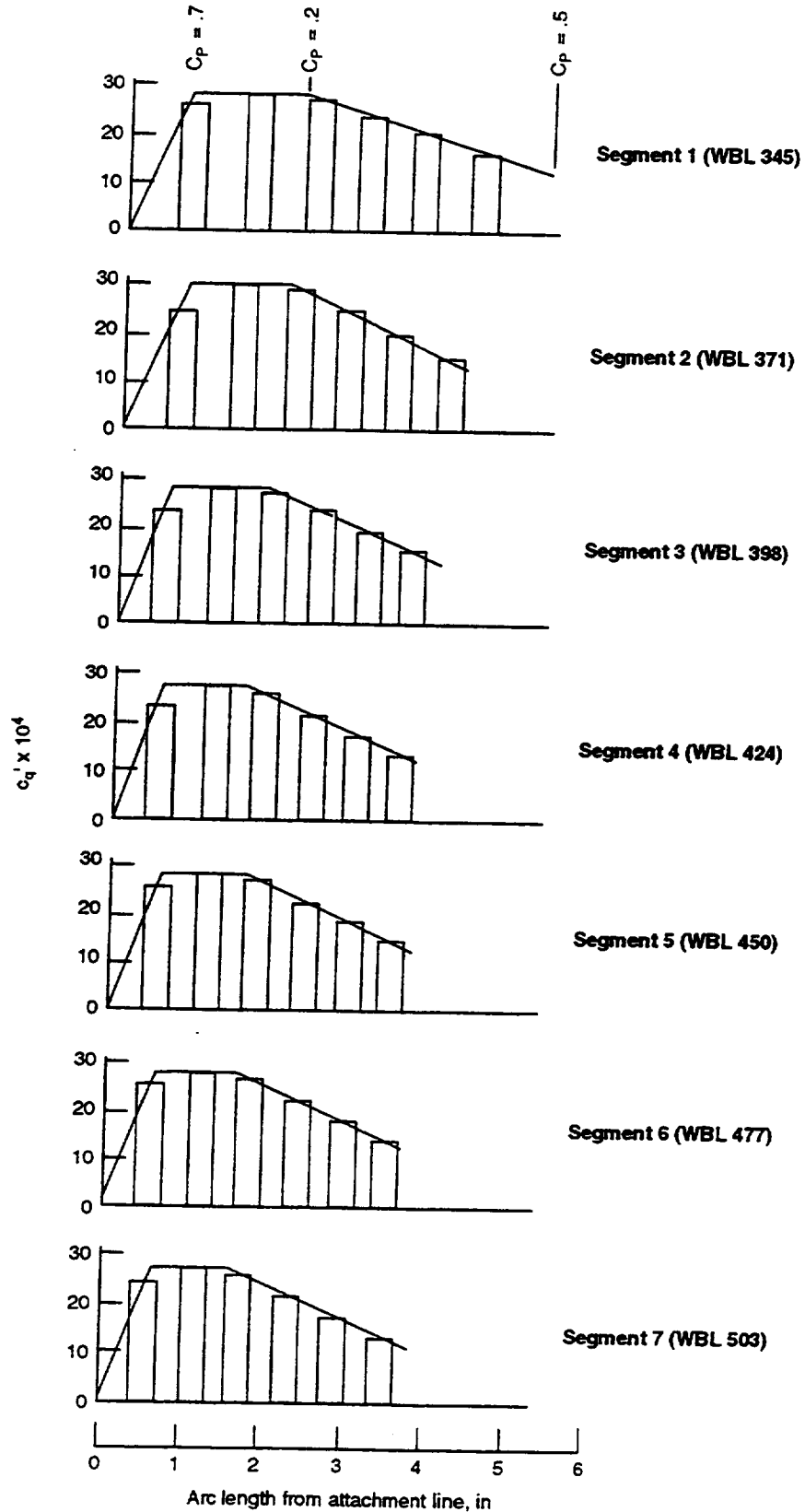


Figure 3.2-4. Practical  $c_q'$  for the Design Case ( $C_L = 0.5, 0.8M, 39,000$  ft) High-Suction Zone

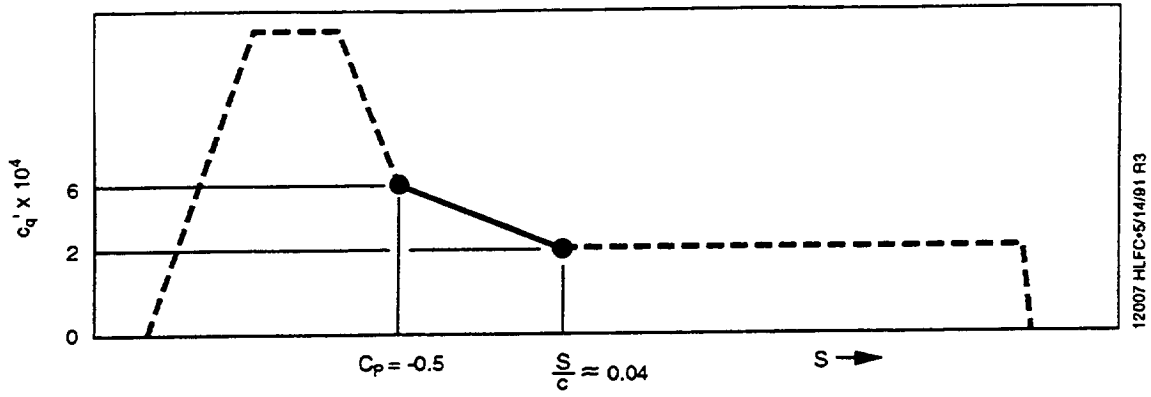


Figure 3.2-5. Typical  $c_q'$  Curve in Transition Zone

Table 3-2. Suction Coefficients (Local  $c_q' \times 10^4$ ), Flutes 7 and 8

| Flute Number | Segment | 1    | 2    | 3    | 4    | 5    | 6    | 7    |
|--------------|---------|------|------|------|------|------|------|------|
|              | WBL     | 345  | 371  | 398  | 424  | 450  | 477  | 503  |
| % Open Area  | 58.1    | 59.4 | 60.1 | 60.1 | 59.0 | 58.3 | 58.3 |      |
| 7            |         | 10   | 11   | 10.5 | 11   | 11   | 11   | 11.5 |
| 8            |         | 5    | 5    | 5    | 5    | 5.5  | 5.5  | 5.5  |

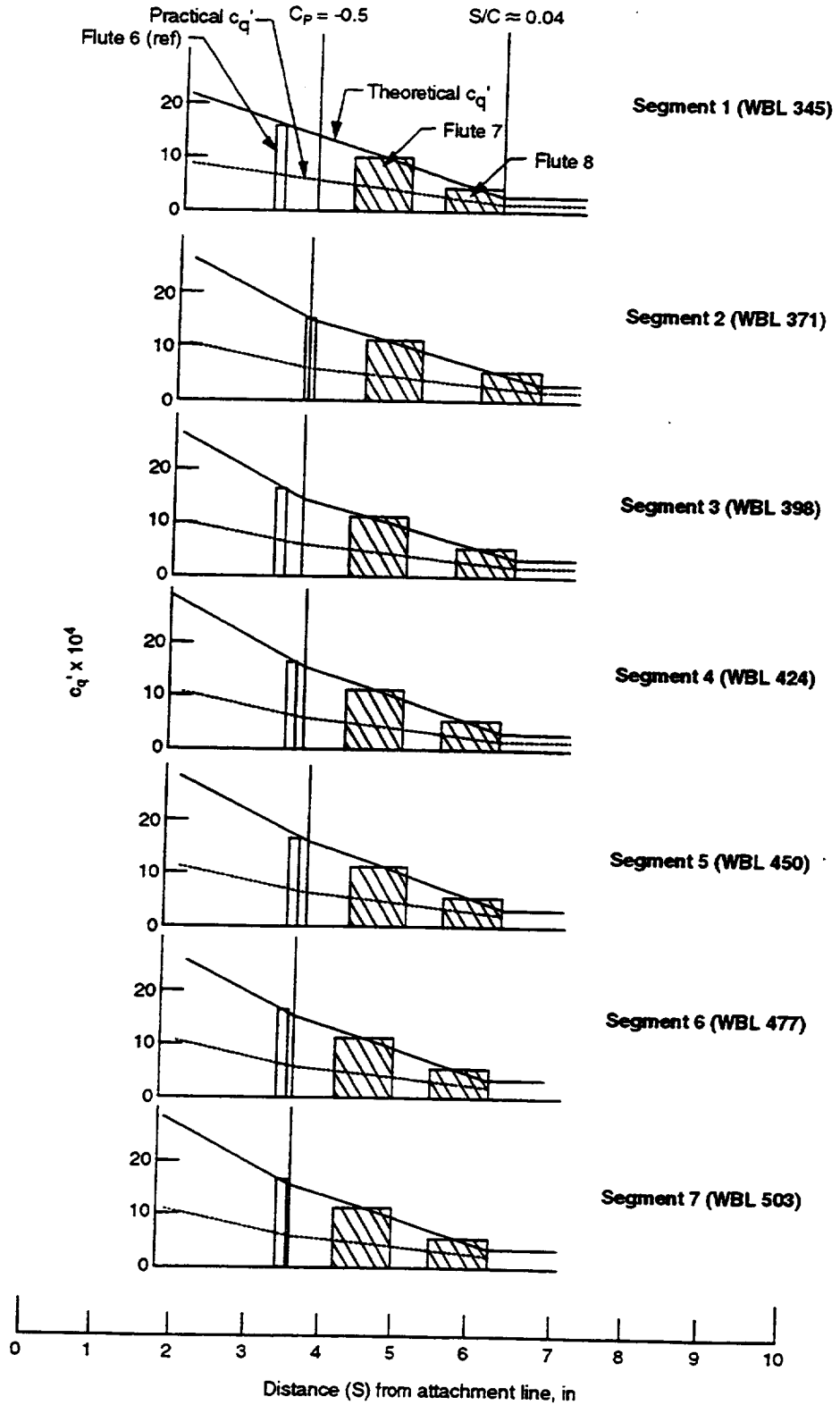


Figure 3.2-6. Practical  $c_q'$  for the Design Case ( $C_L = 0.5, 0.8M, 39,000$  ft) Transition Zone (Flutes 7 and 8)

12008.HLFC-15/14/81 R3

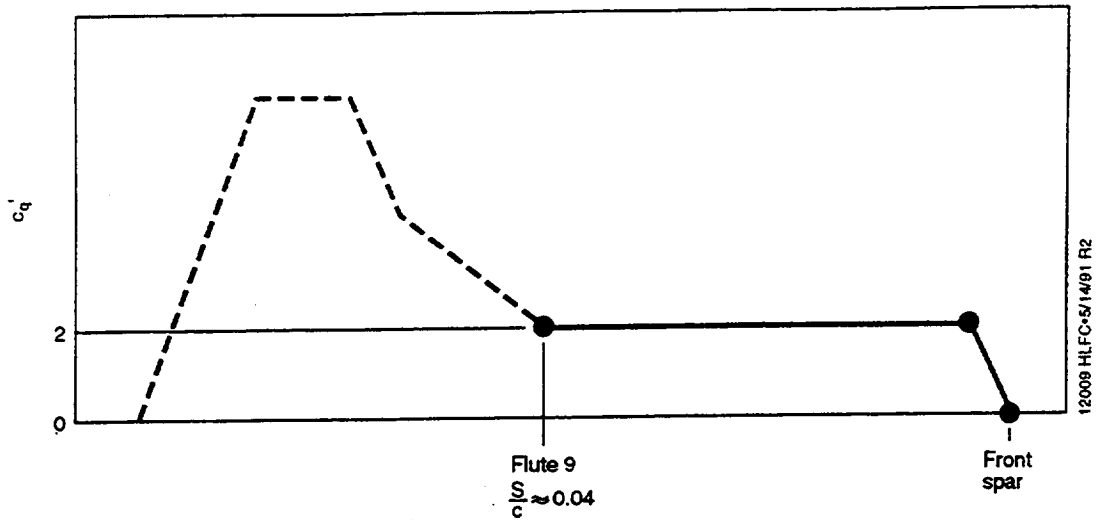
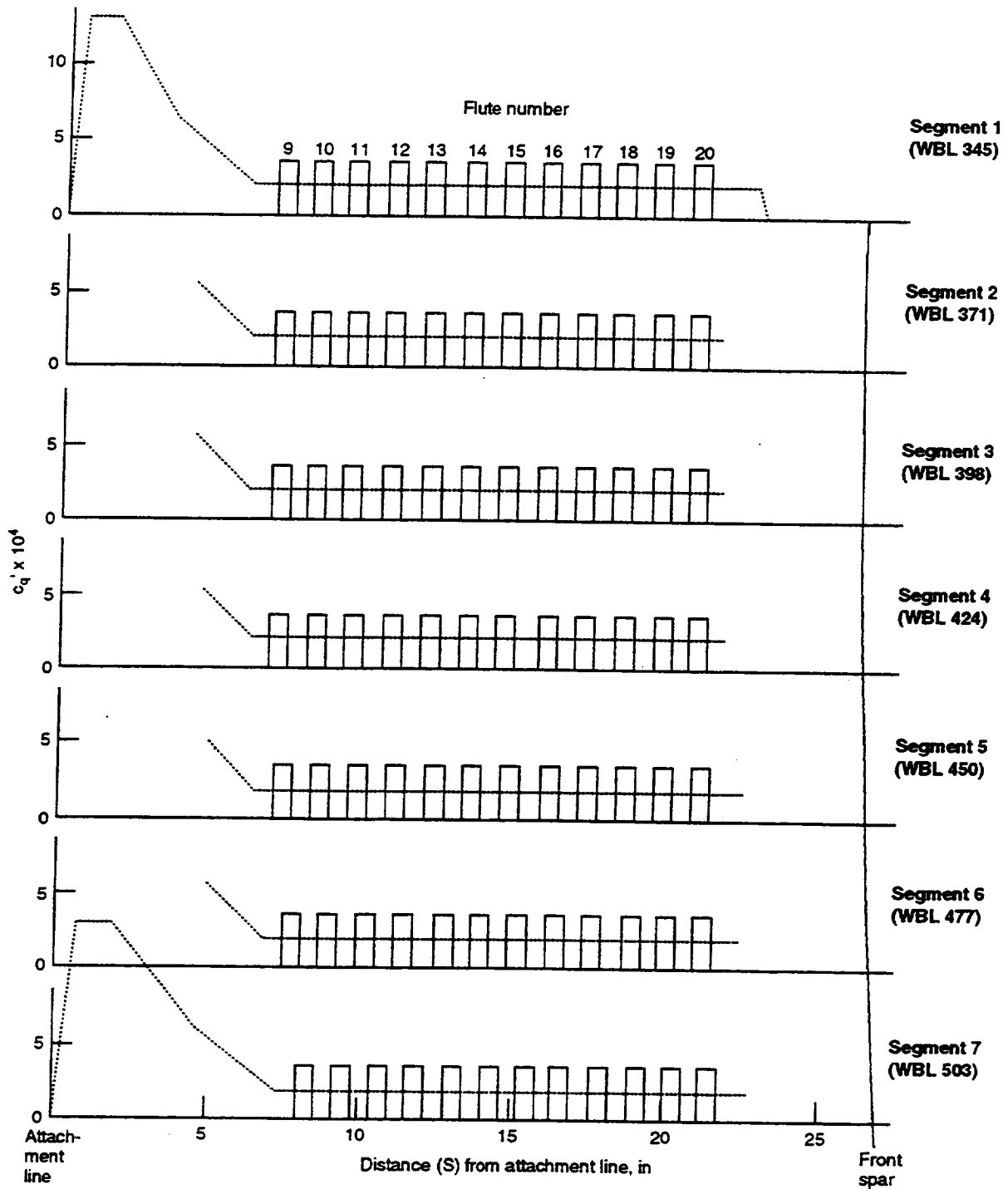


Figure 3.2-7. Typical  $c_q'$  Curve Aft Zone (TS Instability Control)

Table 3-3. Suction Coefficients (Local  $c_q' \times 10^4$ ), Flutes 9 Through 20

| Flute Number | Segment     | 1    | 2    | 3    | 4    | 5    | 6    | 7    |
|--------------|-------------|------|------|------|------|------|------|------|
|              | WBL         | 345  | 371  | 398  | 424  | 450  | 477  | 503  |
|              | % Open Area | 58.1 | 59.4 | 60.1 | 60.1 | 59.0 | 58.3 | 58.3 |
| 9            |             | 3.6  | 3.5  | 3.5  | 3.5  | 3.6  | 3.6  | 3.6  |
| 10           |             | 3.6  | 3.5  | 3.5  | 3.5  | 3.6  | 3.6  | 3.6  |
| 11           |             | 3.6  | 3.5  | 3.5  | 3.5  | 3.6  | 3.6  | 3.6  |
| 12           |             | 3.6  | 3.5  | 3.5  | 3.5  | 3.6  | 3.6  | 3.6  |
| 13           |             | 3.6  | 3.5  | 3.5  | 3.5  | 3.6  | 3.6  | 3.6  |
| 14           |             | 3.6  | 3.5  | 3.5  | 3.5  | 3.6  | 3.6  | 3.6  |
| 15           |             | 3.6  | 3.5  | 3.5  | 3.5  | 3.6  | 3.6  | 3.6  |
| 16           |             | 3.6  | 3.5  | 3.5  | 3.5  | 3.6  | 3.6  | 3.6  |
| 17           |             | 3.6  | 3.5  | 3.5  | 3.5  | 3.6  | 3.6  | 3.6  |
| 18           |             | 3.6  | 3.5  | 3.5  | 3.5  | 3.6  | 3.6  | 3.6  |
| 19           |             | 3.6  | 3.5  | 3.5  | 3.5  | 3.6  | 3.6  | 3.6  |
| 20           |             | 3.6  | 3.5  | 3.5  | 3.5  | 3.6  | 3.6  | 3.6  |



12010 HLF-C-5/14/01 R3

Figure 3.2-8. Local  $c_q'$  for the Design Case ( $C_L = 0.5, 0.8M, 39,000$  ft)  
Flutes 9 Through 20, Aft Zone (TS Control)

## 4.0 SYSTEM DESIGN

### 4.1 FLOW PATH

The airflow path in the suction system during normal operation is as follows (fig. 4.1-1):

- a. Air enters the system through perforations in the wing outer surface (skin).
- b. Passages (flutes) under the surface direct the air spanwise. These passages are created by the support structure (stringers) and the wing skins.
- c. Air exits from the flutes at evenly spaced locations through collectors. The flow rates from the flutes are balanced by screens located in the collectors. From two to nine flutes may feed each collector.
- d. From the collectors, air enters the spanwise ducting system. Tributaries merge through aerodynamic valves (flapper valves) in a sequence that ensures flow controllability for all sections.
- e. Finally, the air exits the system, and the airplane, through a turbocompressor mounted in the strut.

Figure 4.1-2 is a schematic diagram of the entire HLFC pneumatic system, with duct pressures and collector airflows for the design operating condition ( $M = 0.8$ ,  $C_L = 0.5$ , 39,000 ft altitude) noted.

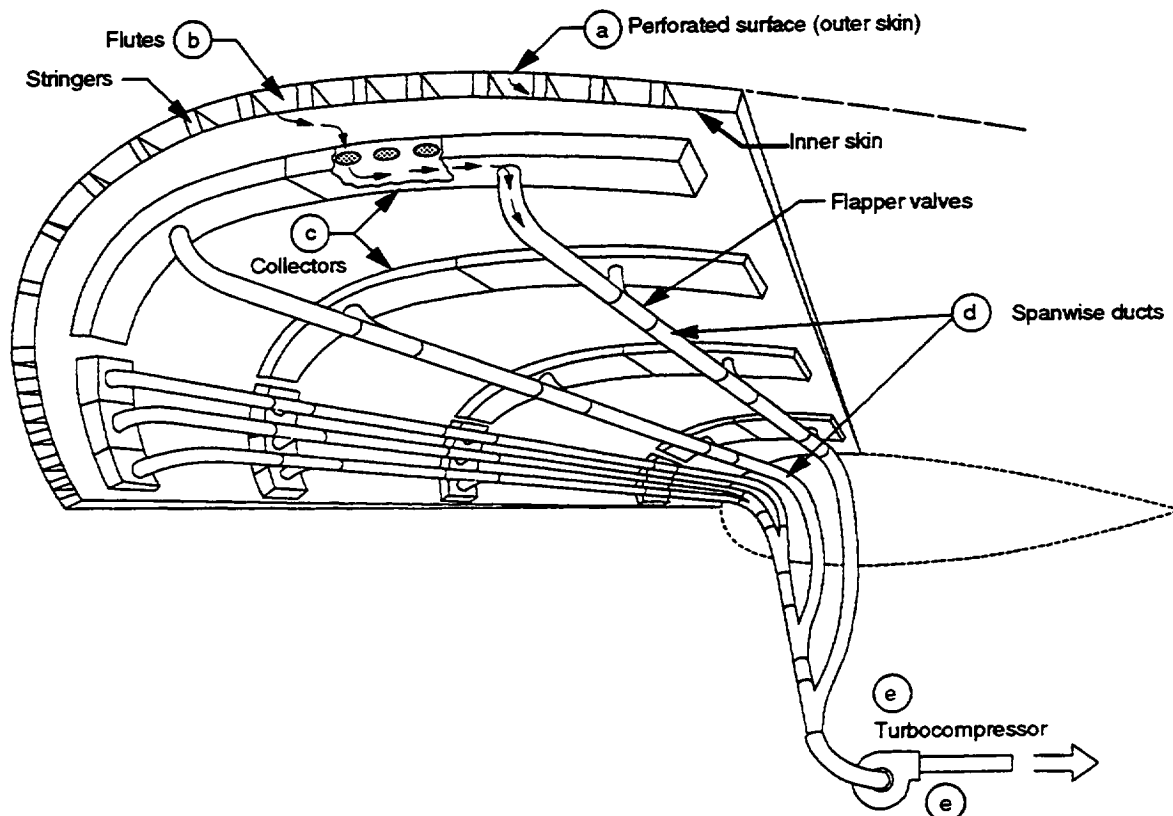


Figure 4.1-1. Airflow Path During Normal Suction System Operation



## 4.2 DESIGN FLOWS AND PRESSURES

Valve settings and screens were selected to balance and distribute suction rates through the wing skin. The resulting system conditions for the design case are shown in figure 4.2-1 for the flutes and collectors and in figure 4.2-2 for the ducts and the turbocompressor. The design philosophy was to install the largest possible duct. Nevertheless, an internal Mach number of about 0.4 occurs along the inboard section of duct 2 and again near the entrance of the turbocompressor.

## 4.3 FLOW AND PRESSURE ANALYSIS

The duct pressure-drop analysis was conducted using a computer code having component subroutines that were easily adapted to different configurations. Each duct was analyzed segment by segment until it merged with another. At that point the lower pressure was selected and the analysis continued for the merged flows. The equations used in the duct analysis are given in appendix A.

The friction factor used in duct pressure drop analyses was expected to range widely because of varying roughness. As a practical approximation, a single roughness value ( $\epsilon$ ) of 0.0001 ft was used throughout (fig. 4.3-1).

A NASA-owned turbocompressor, previously used as a suction pump on other laminar flow control flight test programs, was loaned to Boeing and modified for the present application. Its suction capacity was verified when the flow requirement had been determined. Figure 4.3-2 is a turbocompressor performance map provided by the manufacturer. It shows curves of pressure ratio versus corrected flow rate\* for a series of corrected rotor speeds overlaid on efficiency contour lines. This map, however, was developed for applications where the air being compressed enters at a pressure that is approximately equal to ambient. In the present system, the inlet pressure was as low as one-third of ambient, and the leakage direction (for shaft seals and so forth) was opposite to that for which the turbocompressor was designed. Consequently, greater losses were expected.

Therefore, the turbocompressor was bench-tested as a suction pump to determine its performance in the present application. The line labeled "suction curve" in figure 4.3-2 shows the measured performance at the topping speed, 48,000 rpm. Pumping capacity is substantially reduced in this mode of operation, with the suction curve well below and to the left of the corresponding "pressure curve."

The HLFC system requires a pressure ratio of 2.86 at a flow rate of 11.5 lb/min at altitude. Correcting to sea level standard conditions, 152 lb/min are required at the same pressure ratio. The available pressure ratio, indicated by the symbol on the suction curve, is 3.86. A comfortable margin over the requirement is therefore available. (In fact, because of the low temperature at altitude, the 48,000-rpm topping speed actually corresponds to a corrected speed of around 53,000 rpm, and the indicated margin is conservative.)

---

\* "Corrected" quantities are referred to sea level standard conditions. An example is given in appendix B.

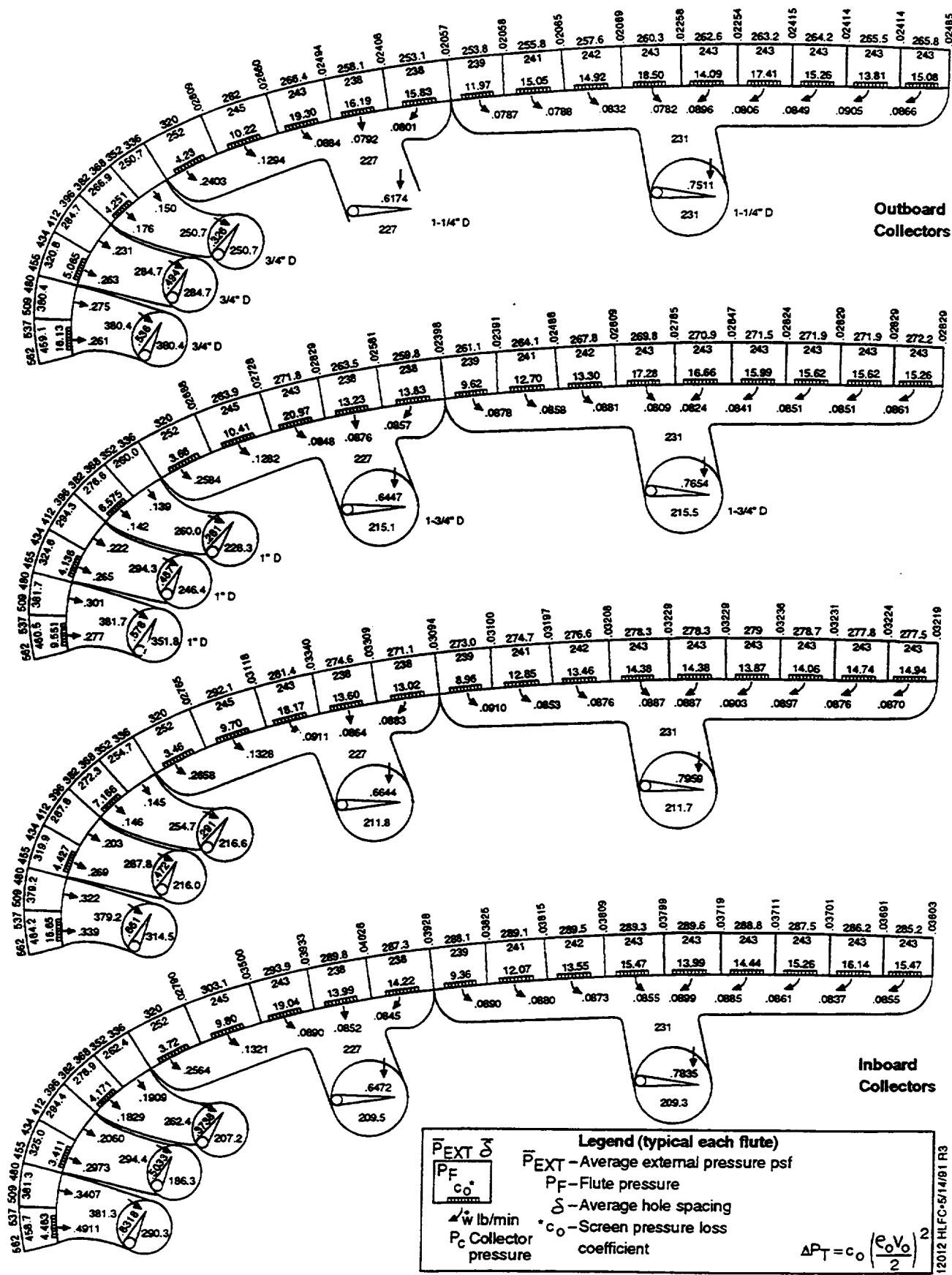


Figure 4 2-1 Conditions at Collectors for the Design Case ( $C_1 = 0.5, 0.8M, 39,000 \text{ ft}$ )

12012 H.L.F.C-5/14/91 R3

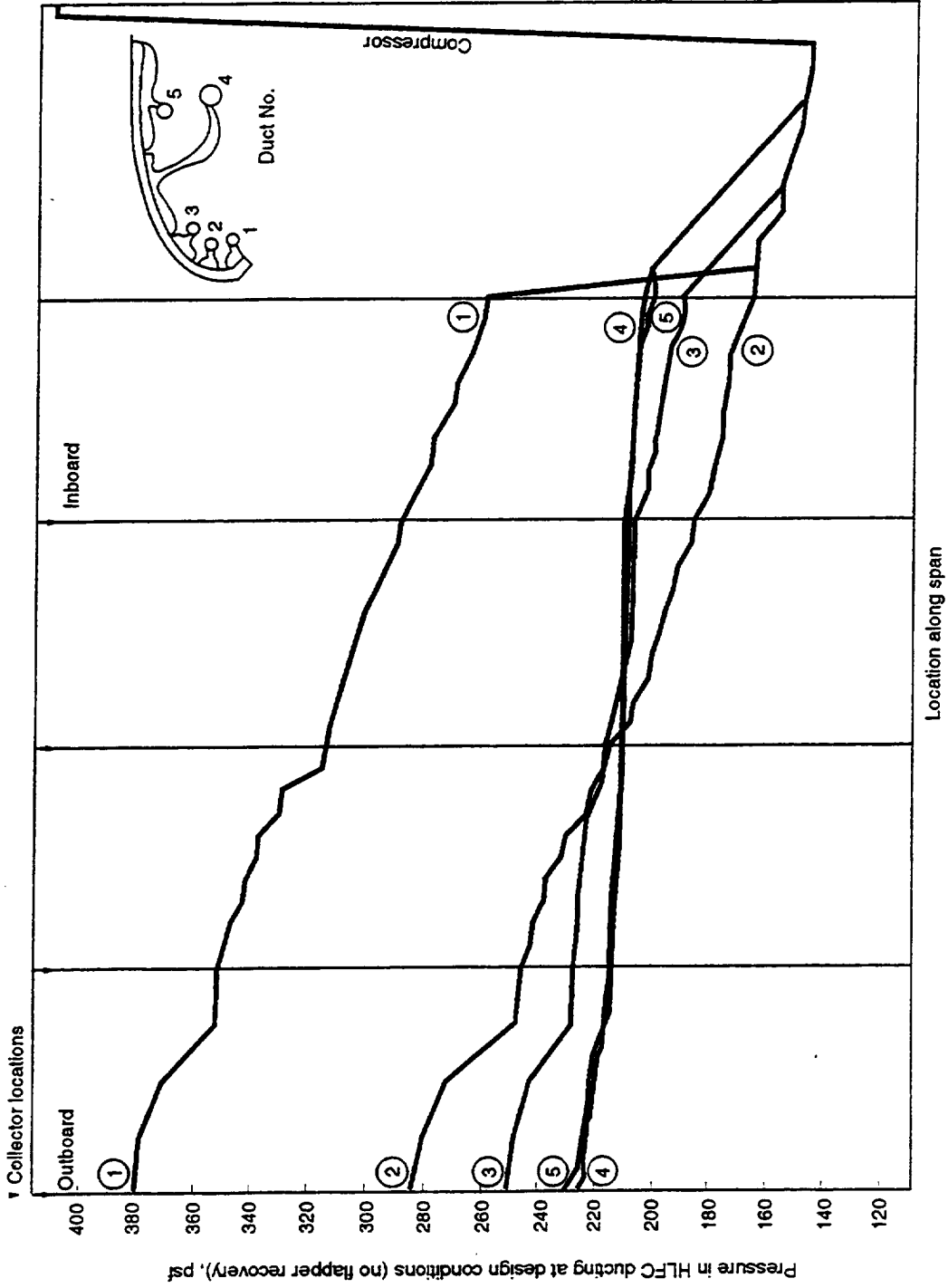


Figure 4.2-2. Duct Pressures Versus Spanwise Location

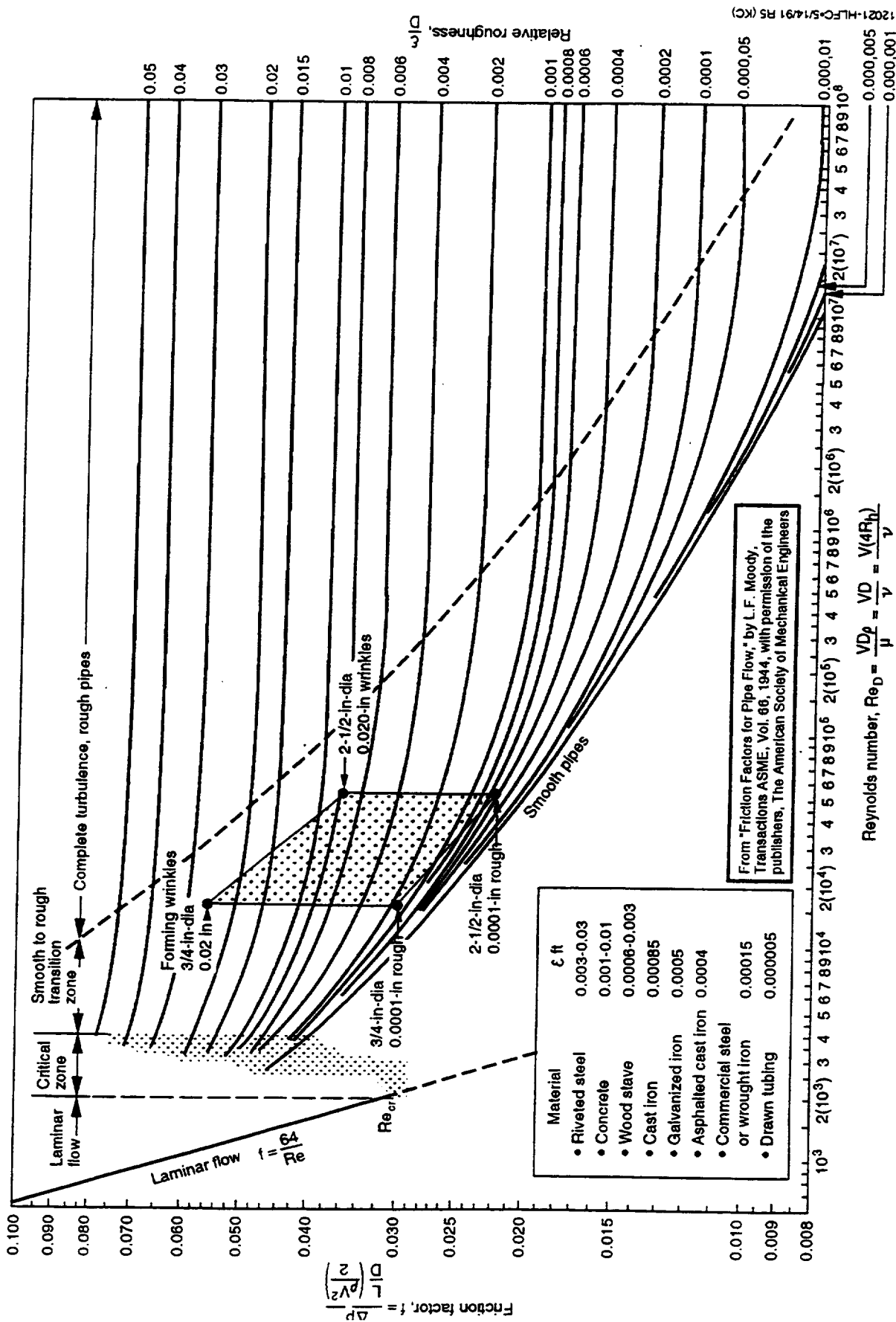


Figure 4.3-1. Friction Factor for Anticipated Duct Roughness

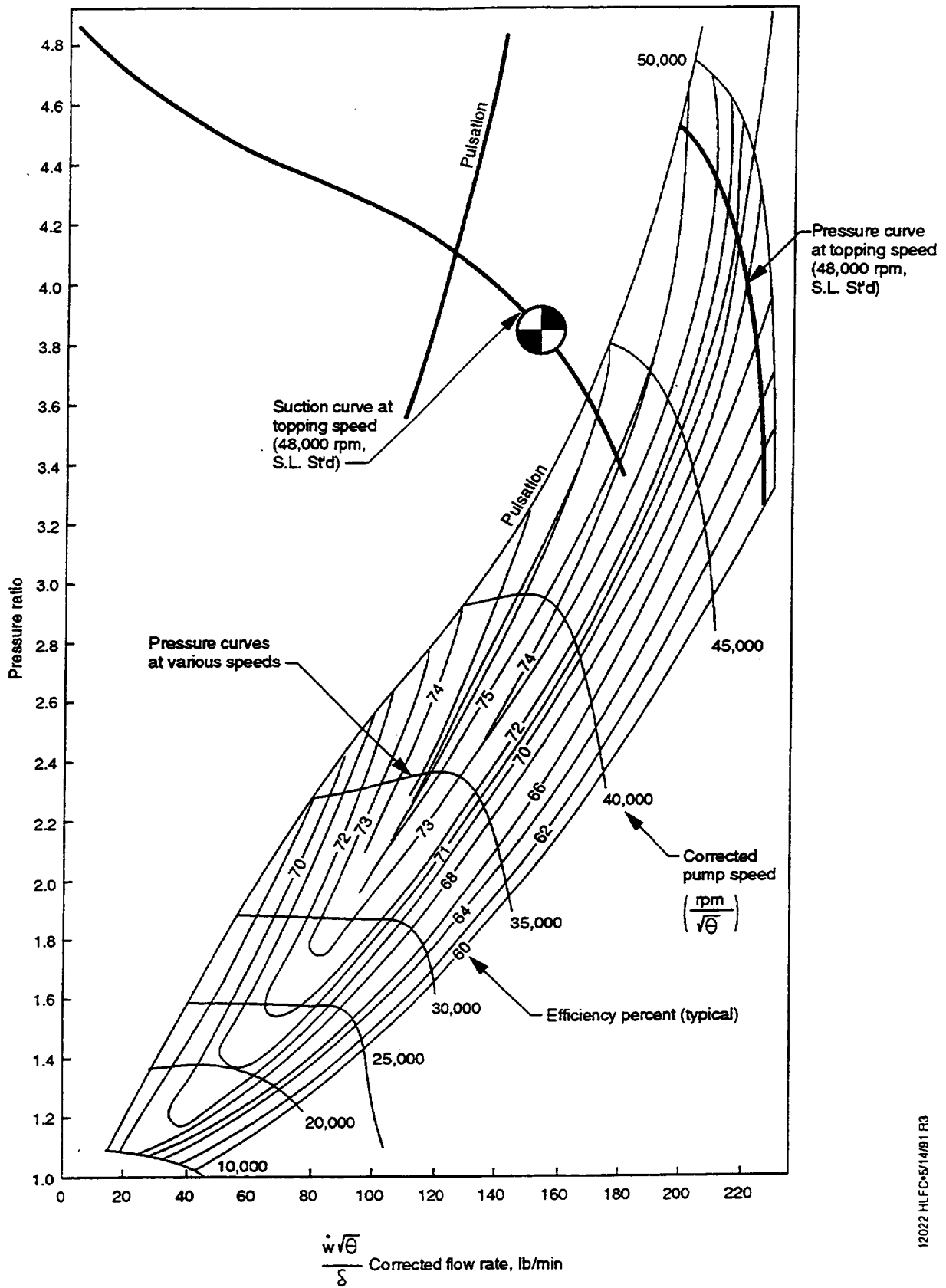


Figure 4.3-2. Turbocompressor Map

#### 4.4 FLUTES AND SUCTION PANEL

The basic flute design philosophy was to provide a constant internal pressure by following isobars in the CF control area, while maintaining a spacing that prevented outflow. In the TS control area the pressure gradients were small but the contours were irregular. So to obtain the constant internal (flute) pressure, the porosity was varied while the spacing of the flutes was held constant. The layout of these flutes is shown in figure 4.4-1.

The additional requirement on the flute design was of spanwise continuity. Any barrier to flow within the flute would produce unacceptable steps in the local  $c_q$  that could have been detrimental. The method of spanwise flute pressure control therefore depended on matching pressure gradients generated by internal flow to the changes in external pressure and flow requirements that occurred in the off-design conditions.

A method for analyzing collector ducts with large numbers of tributary flows was developed by Haerter (ref. 3). His procedure was used to analyze HLFC flute flow, and laboratory tests of candidate flute designs were found to give good agreement with that model (fig. 4.4-2). (Details of the flute flow calculations are presented in appendix C.)

The flute flow model was combined with the exponent/constant method of representing the flow resistance of perforated skin (sec. 4.5) and with standard duct friction terms to construct flow networks to analyze off-design conditions (fig. 4.4-3). The variation in flow through the skin was predicted for the flutes exposed to the largest spreads of external pressure for lift coefficients from 0.45 to 0.60. The worst case flute was number 15, located in the aft (TS control) zone. Flapper valve adjustment was able to maintain adequate suction uniformity (fig. 4.4-4). Over 85% of the span,  $c_q$  was essentially constant and the deviation elsewhere was acceptable.

The isobar variation in the forward (CF control) zone with changing  $C_L$  was much less drastic. In fact, very little valve adjustment was required to compensate for this effect. To illustrate this, figure 4.4-5 shows the performance of a small flute designed for  $C_L = 0.5$  but exposed to the pressures corresponding to  $C_L = 0.4$  and 0.6. Because the flute may fall into a different part of the suction requirement curve, the overall suction level may be adjusted.

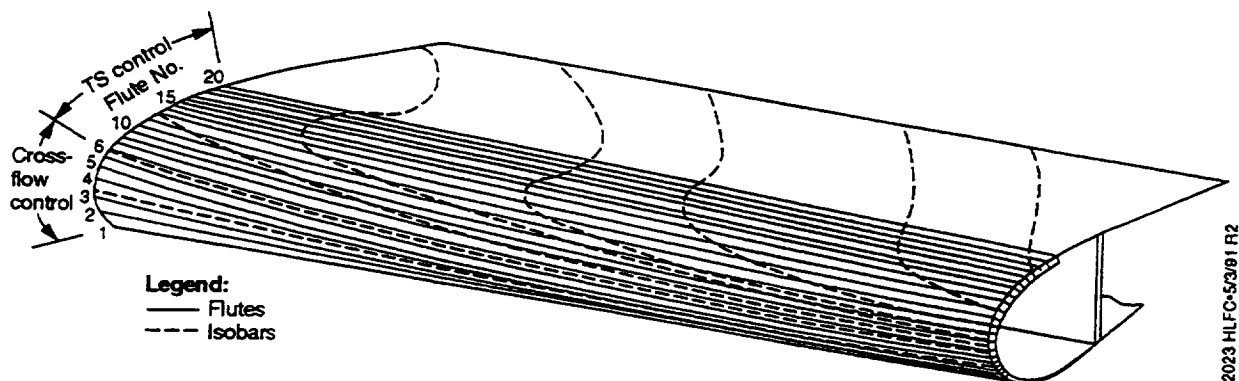
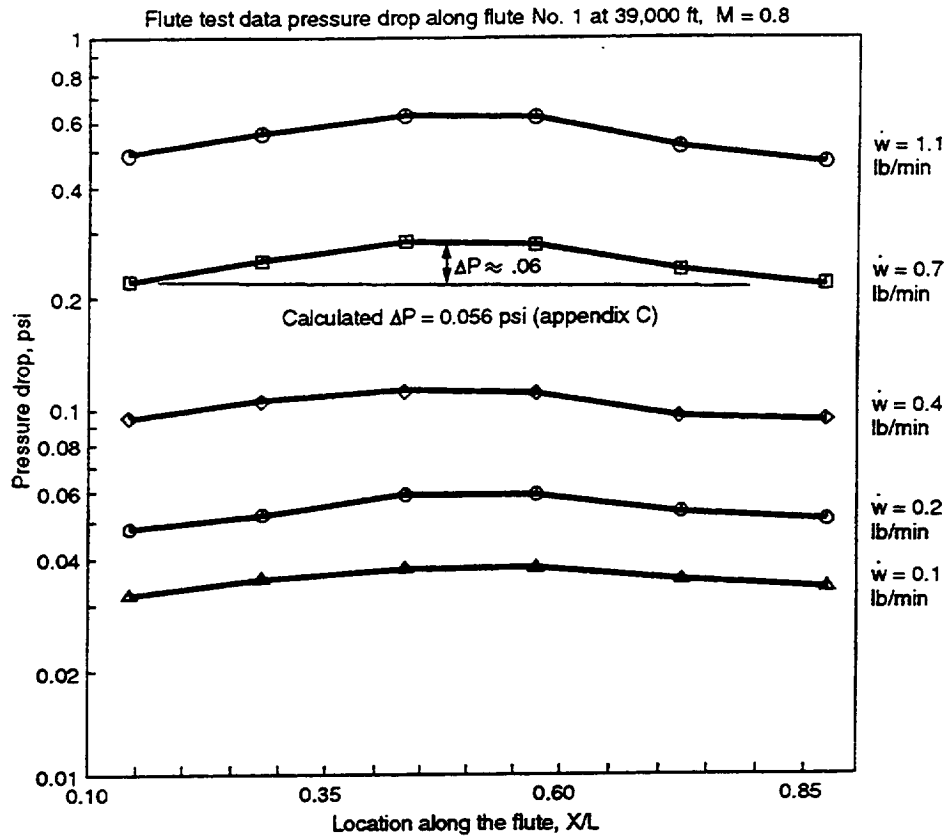


Figure 4.4-1. Flute Layout and Isobar Location



12024 HLF-C-5/17/81 R3

Figure 4.4-2. Theoretical Flute Pressure and Measured Drops

#### 4.4.1 FLUTE WIDTH SELECTION

The practical  $c_q'$  was previously depicted as a bar graph (fig. 3.2-2). The  $c_q'$  actually varies across the width of the flute because of the external pressure gradient; the upstream edge of the flute is exposed to a higher static pressure than the downstream edge. Sufficient flow resistance through the perforated skin to avoid outflow and flatten the upper line while not exceeding system capacity due to pressure loss was ensured by the proper selection of hole spacing, hole diameter, and flute width. Figure 4.4-6 shows how this  $c_q'$  variation changed with hole spacing. Note the reverse flow threshold for 0.00326 lb/s and the 0.003-in-diameter hole that occurs at a spacing of 0.017 in.

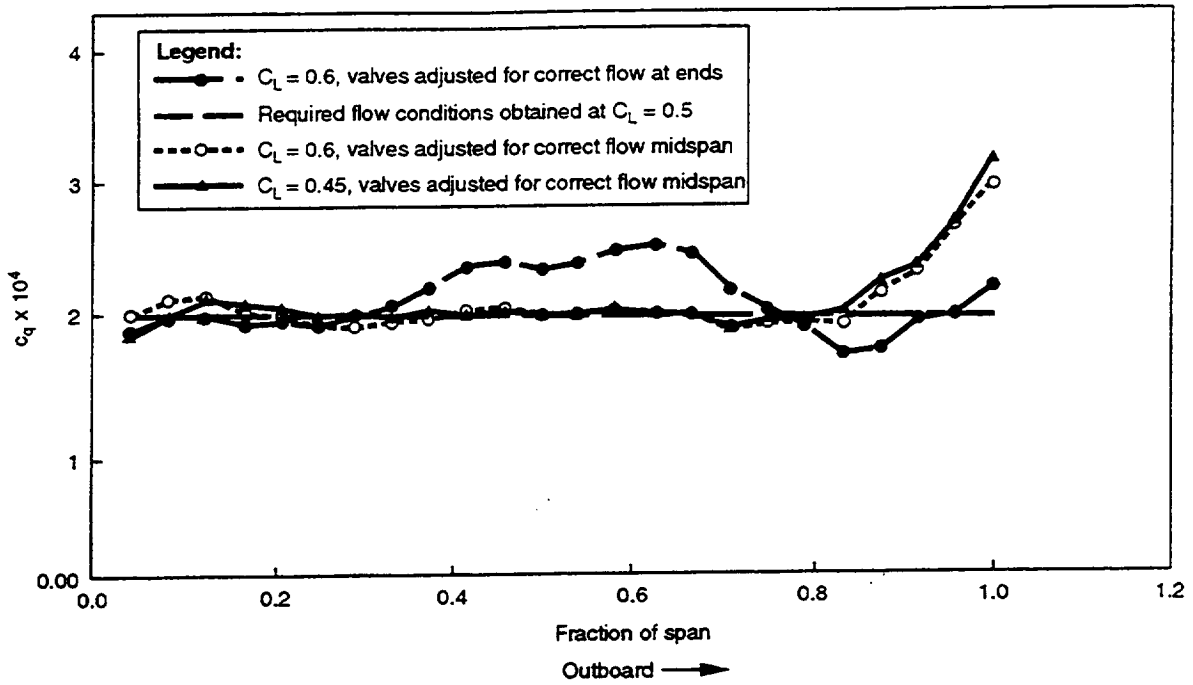
The flow into a flute on the threshold of reverse flow at its downstream edge was expressed in terms of the flute width  $w_F$ , the external pressure  $P$ , and the external pressure gradient  $dP/ds$ . In the next section the flow per hole will be represented by an expression of the form

$$\dot{m}_H = kP(\Delta P)^b,$$

where  $\Delta P$  is the pressure difference across the skin. Setting  $\Delta P = 0$  at the downstream edge and integrating across the flute, the minimum acceptable mass flow per unit span for the flute was

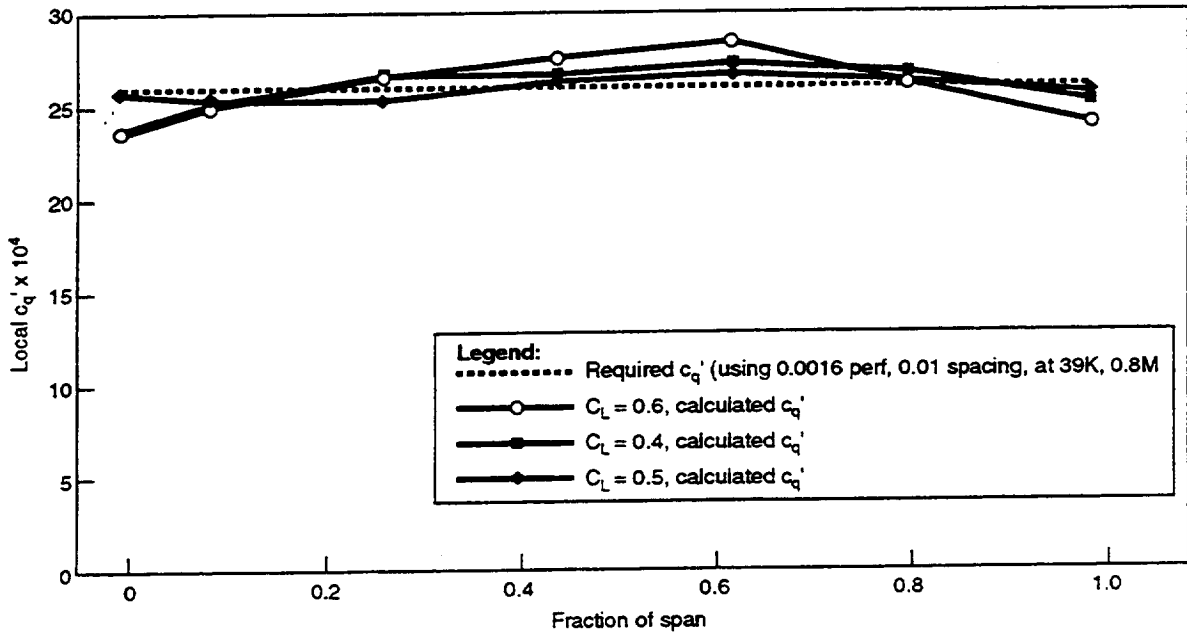
$$\frac{d\dot{m}_F}{ds} = Nk \left| \frac{dP}{ds} \right|^b \left[ \frac{w_F^{b+1}}{b+1} P_o - \frac{w_F^{b+2}}{(b+1)(b+2)} \left| \frac{dP}{ds} \right| \right]$$





12026 HILFC-5/3/81 R2

Figure 4.4-4. Flow Versus Span, 0.5  $C_L$  Design Case



12027a HILFC-6/14/81 R2

Figure 4.4-5. Effect of  $C_L$  on Suction Distribution, Flute 2 (CF Control Zone)

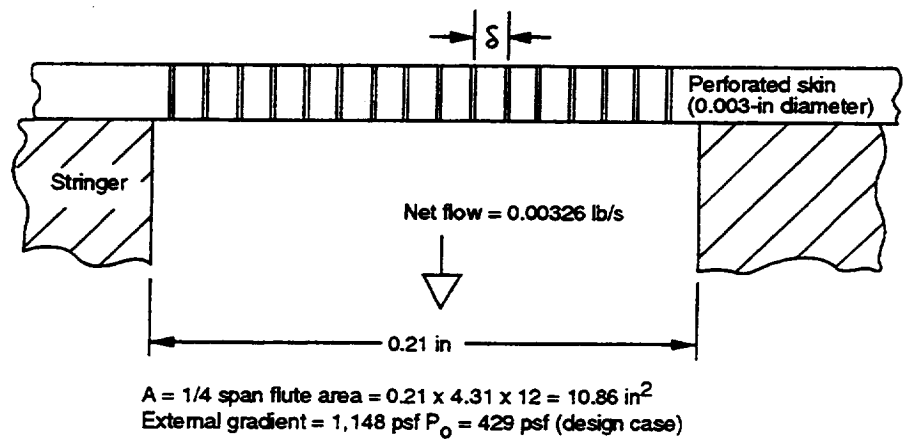
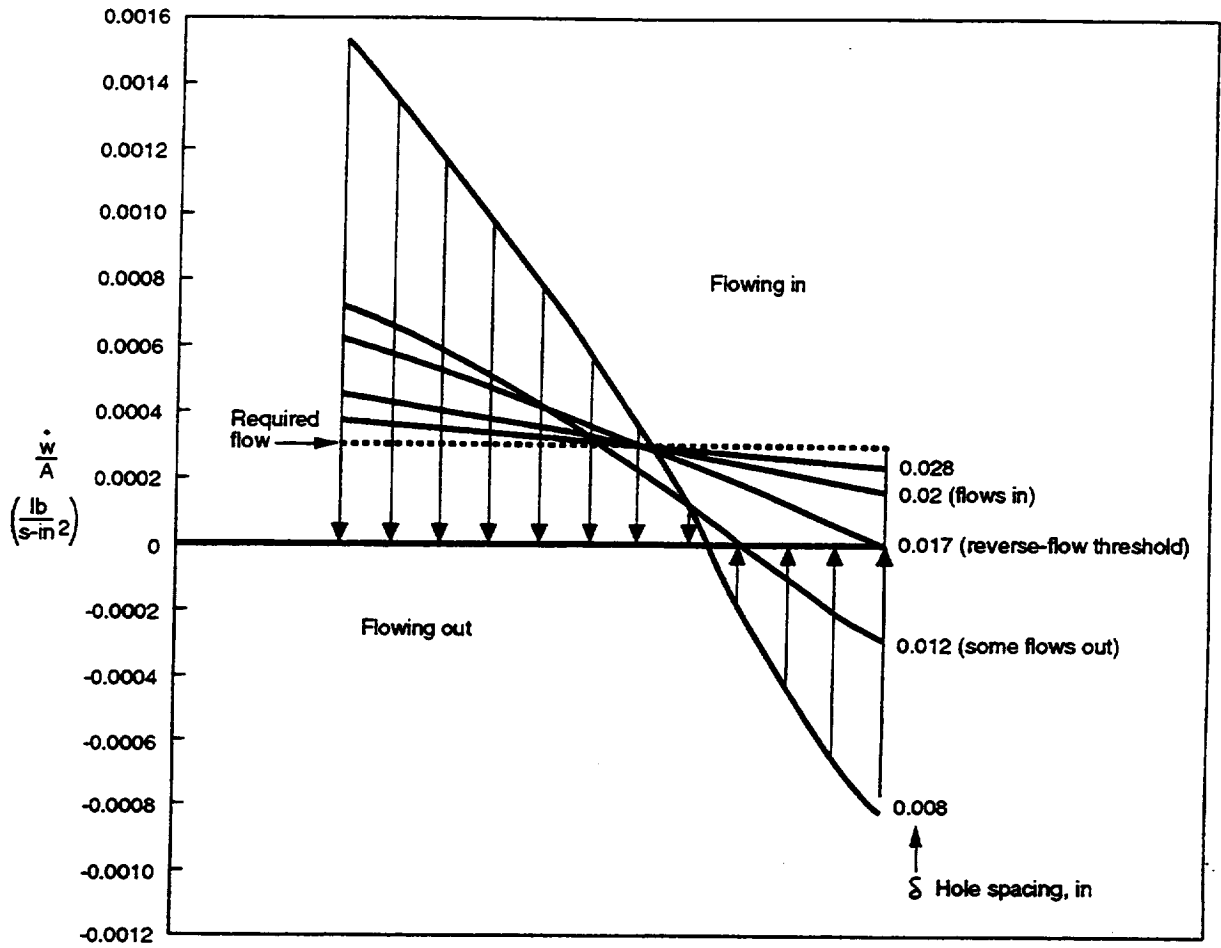
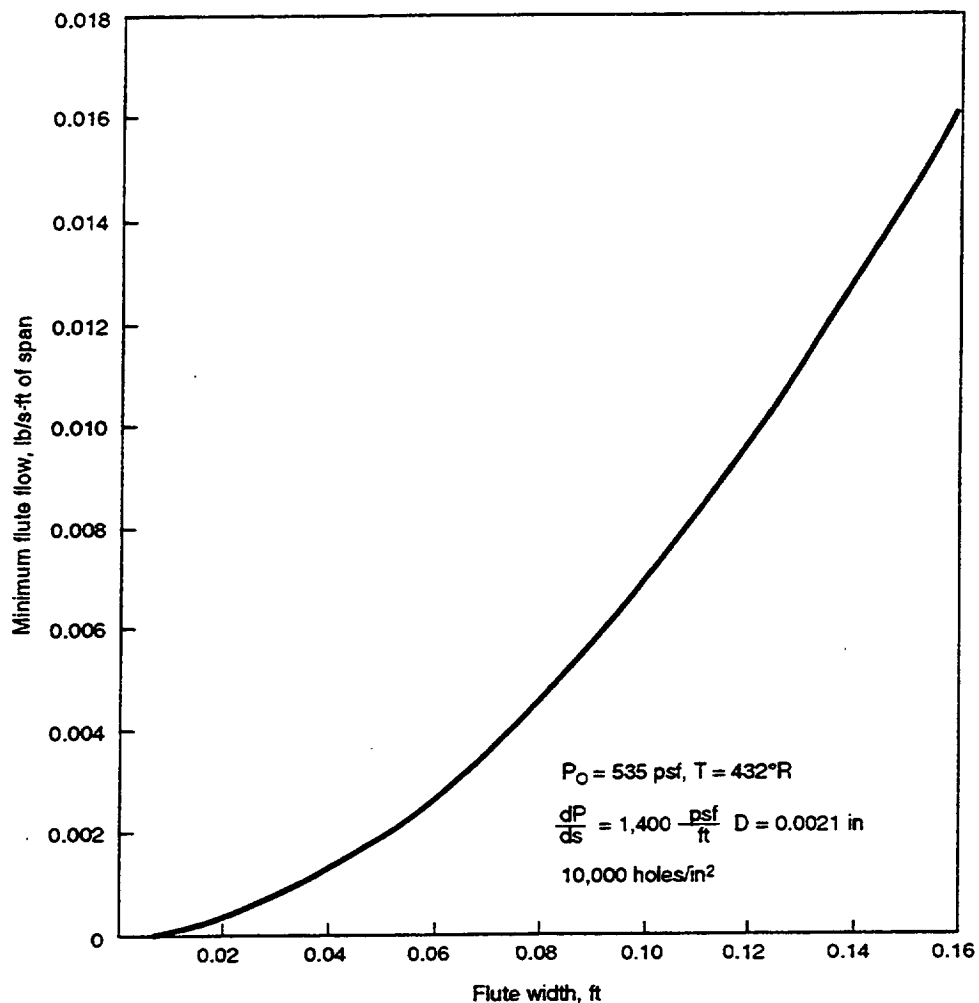


Figure 4.4-6. Distribution of  $c_q'$  Across Flute at a Constant Flow for Various Hole Spacings ( $\delta$ )

12028 HLFC-6/17/91 R2

where  $P_0$  was the exterior pressure at the upstream edge of the flute and  $N$  was the number of holes per unit area. Given a mass flow requirement, this relationship established the maximum flute width. Figure 4.4-7 shows an example for an early candidate design using 0.002-in-diameter holes at 0.01-in spacing.



12030 HLC-5/14/91 R3

Figure 4.4-7. Flow at Flute Reverse-Flow Threshold

The constant of proportionality in the hole flow formula is very sensitive to hole diameter, because both area and viscous friction losses are affected. Using the above analysis for a series of hole sizes, a plot like that shown in figure 4.4-8 was constructed to show the effect of hole diameter on minimum flute spacing. In this case it was assumed that stringers block the holes over 45% of the skin area. The example given shows that for 0.0016-in-diameter holes, a maximum flute spacing of 0.45 in is indicated.

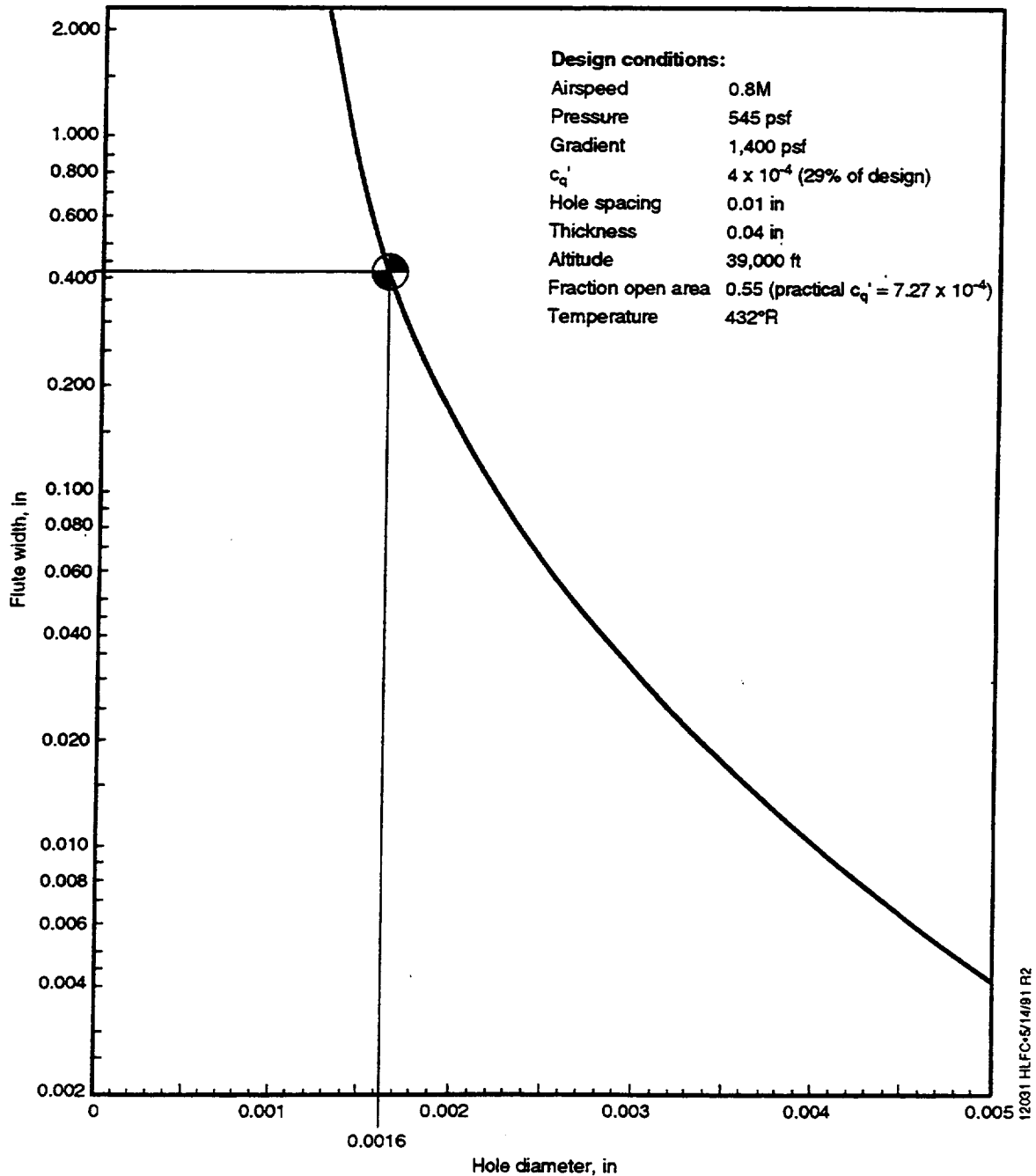


Figure 4.4-8. Effect of Hole Diameter on Minimum Flute Spacing

After the flute width was established, analysis showed that the use of simple rectangular stringers could produce high spanwise pressure gradients in the flutes with the highest  $c_q'$  (flutes 2, 3, and 4). To reduce this effect, these flutes were enlarged as shown in figure 4.4-9. This reduced the typical flute velocity from 130 to 95 ft/s. Also, the collector locations were spaced evenly along the span. Together, these changes reduced the spanwise pressure drop along the flute from 44.1 psf to 7.7 psf. (Referring to fig. 4.2-1, the anticipated skin pressure drop is 455 to 325, or 130, psf for flute 3. The pressure change of 7.7 psf will generate a 5.9% change in  $c_q'$  along this span.)

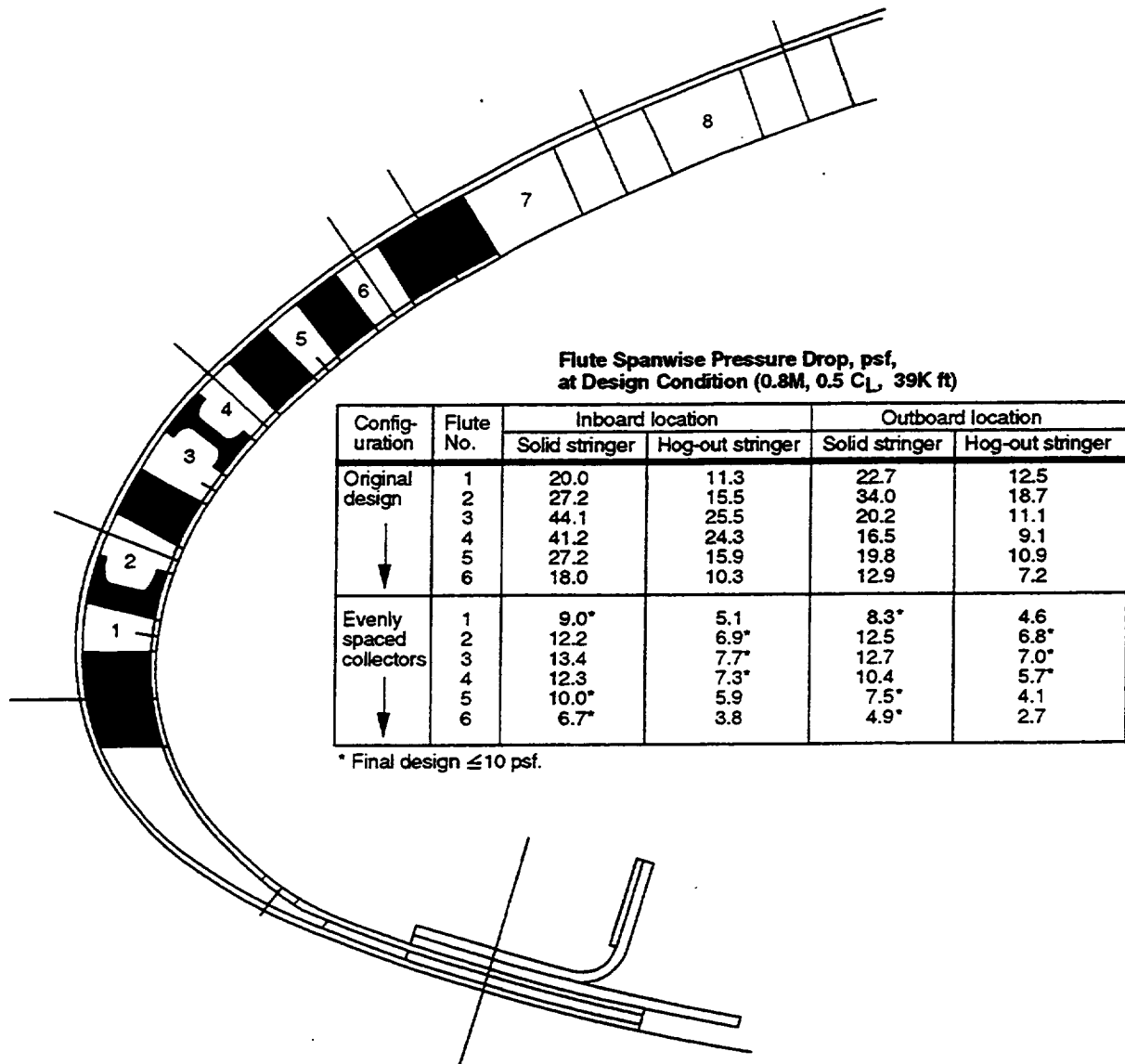


Figure 4.4-9. Flutes Enlarged To Reduce Spanwise  $\Delta P$

#### 4.4.2 Skin Porosity

When the stringers (and flutes) follow isobars, the practical  $c_q'$  depends on flute pressure. Within this area, constant skin porosity was used. The first six flutes follow isobars and have a design porosity using 0.0016-in-diameter holes at 0.01 in spacing.

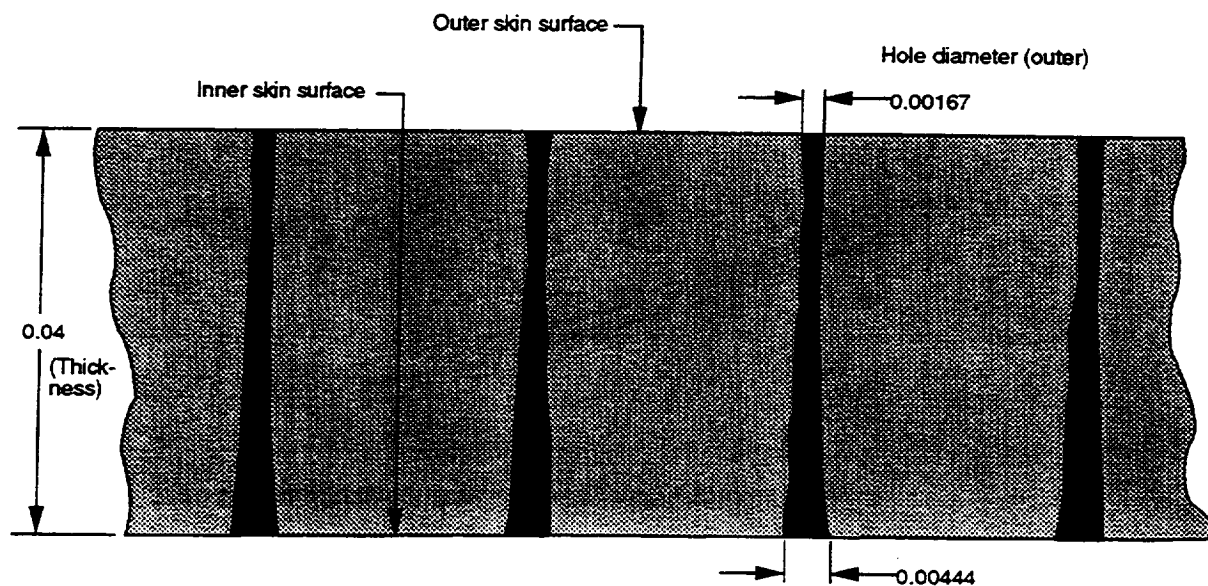
In the TS control zone, the stringers were evenly spaced. Because the isobars were not, the external pressures over the flutes varied considerably. There were 14 of these flutes in the aft zone and each one had a variable porosity associated with it. Because the required suction rates in the aft zone were much reduced relative to the forward high-suction zone, aerodynamic roughness (ref. 4) allowed larger hole diameter and spacing, which reduced drilling costs. The design porosity used 0.0023-in-diameter holes with a spacing that varied between 0.015 and 0.029 in.

The flow characteristics for these small, laser-drilled holes were approximated by a superposed incompressible friction term and a compressible flow term based on the minimum diameter.

The laser-drilled holes were typically tapered inward (fig. 4.4-10). This provided the advantage of avoiding blockage due to the wedging of particles when the smallest area faces outward. One disadvantage was that it complicated the flow analysis.

The flow regime that governs the hole flow was classified as laminar and compressible. The three methods that have been used to model the flow characteristics were—

- a. Simple Incompressible. Ignore the compressibility; find an equivalent (empirical) hole diameter that performs as tested within a limited range.
- b. Equivalent Orifice and Tube. The friction term was modeled by an incompressible tube, using an equivalent diameter and actual length (material thickness). The compressible term was modeled by using the actual minimum diameter multiplied by a discharge coefficient.



The taper profile was obtained by a rubber casting of perforations.

Figure 4.4-10. Laser-Drilled Holes

c. Adiabatic Tapered Tube. Using numerical integration techniques, the losses along the hole were computed with compressible expressions for area, velocity, Mach number, and friction factor.

These three methods are illustrated in figure 4.4-11. Model 3 was used to generate the complete flow versus  $\Delta P$  curve for the design flight condition.

An explicit expression for  $\dot{w}$  and  $\Delta P$  was required for flow analysis. To accomplish this, a curve of the form

$$\dot{w}_H = kP(\Delta P)^b$$

was fitted to the adiabatic tapered tube model in the region of interest.\* Figure 4.4-12 shows how these curves account for the friction/compressibility effects.

Once the relationship of the effective diameter to actual diameter is determined, it may be used for a range of hole sizes. The scaling ability is shown in figure 4.4-13 as a comparison of the output from the numerical integration code "ABDTDIF.BAS" (app. D) to actual test data.

An interesting diffuser effect occurs in the holes that have a slight taper angle such as these. As air travels inward along the taper, the flow is "attached" to the wall and the static pressure rises in the normal flow direction and falls in the reverse flow direction. This results in less flow resistance in the suction direction. Figure 4.4-14 shows the theoretical pressures along a tapered hole in the two flow directions, as computed using the "ADBTSTC.BAS" code (app. E).

If the taper angle is large, as in other drilling methods, or the Reynolds number is large enough to bring on transition and flow separation, the diffuser effect does not occur. Some electron-beam-drilled holes actually behave in the reverse.

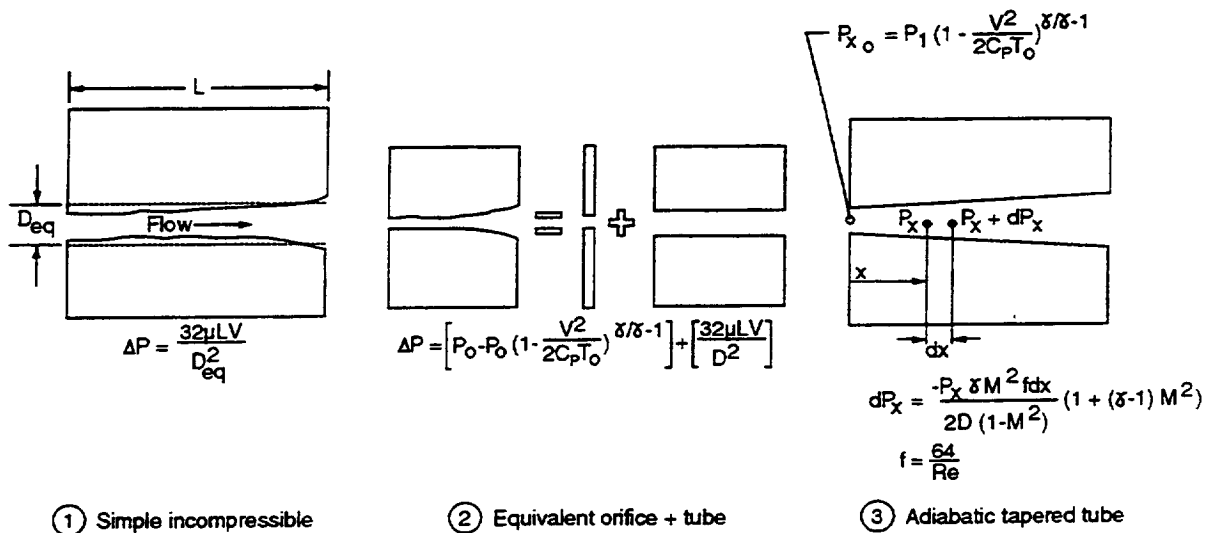


Figure 4.4-11. Flow Models Used for Perforation Analysis

\*Coefficient k has the dimensions  $(\text{lbm/s})/(\text{lb/ft}^2)^{1+b}$ .

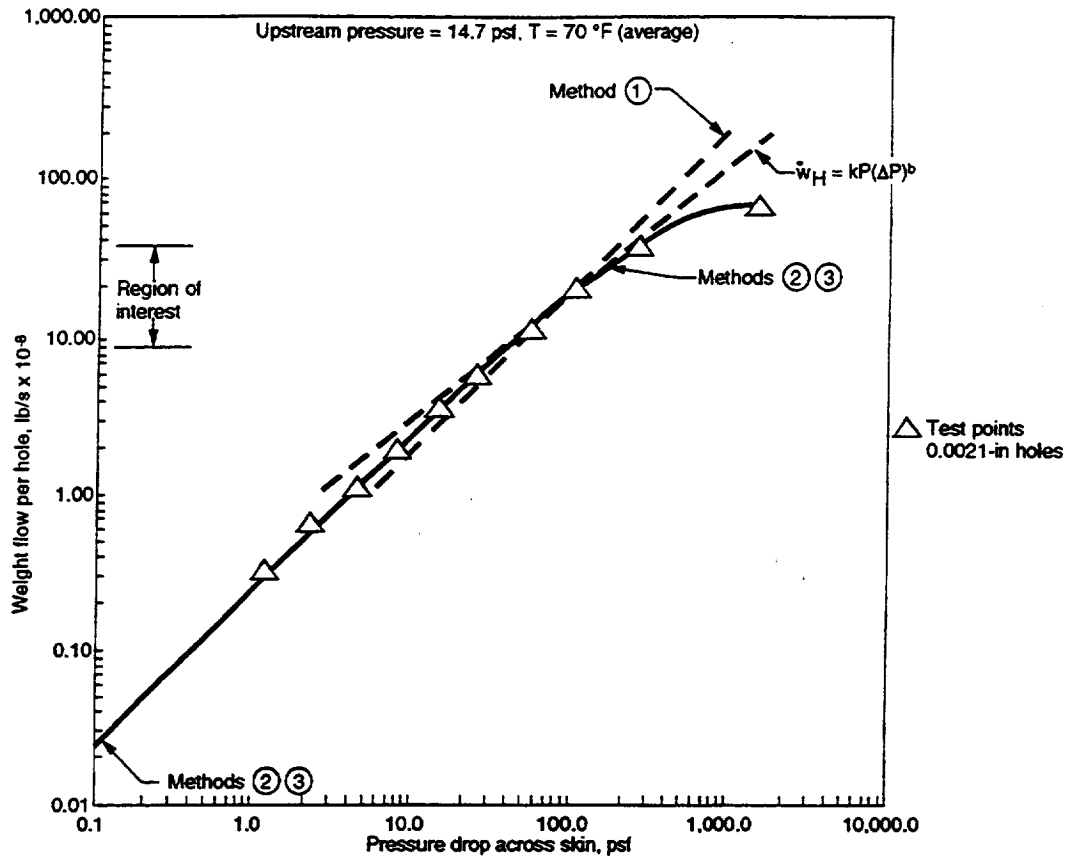


Figure 4.4-12. Methods of Modeling Flow Through Laser-Drilled Holes

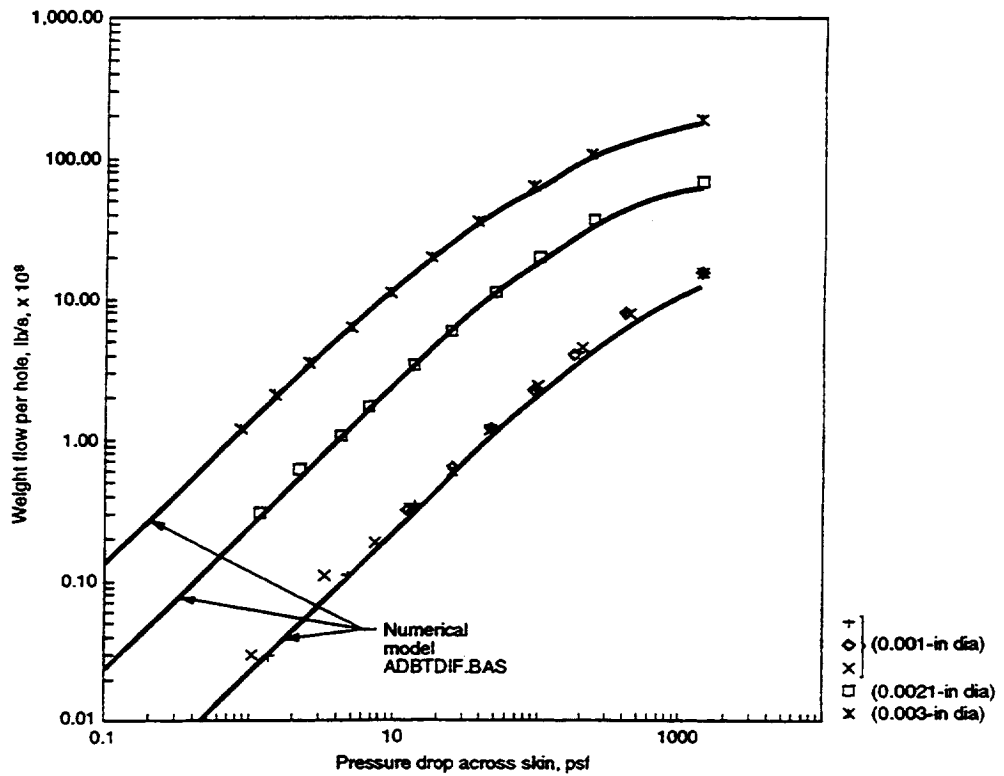
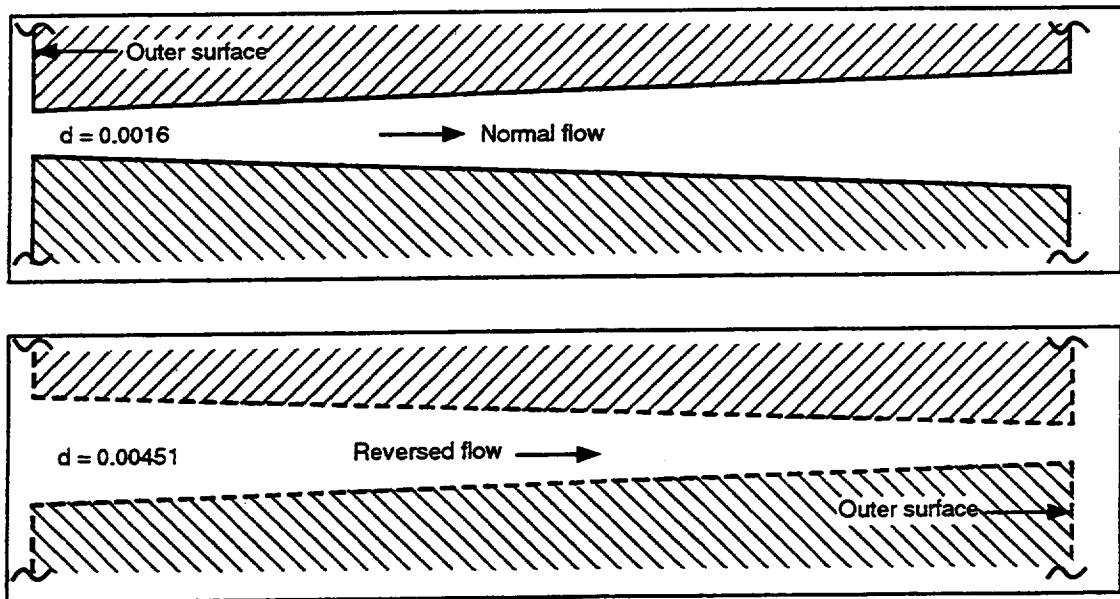
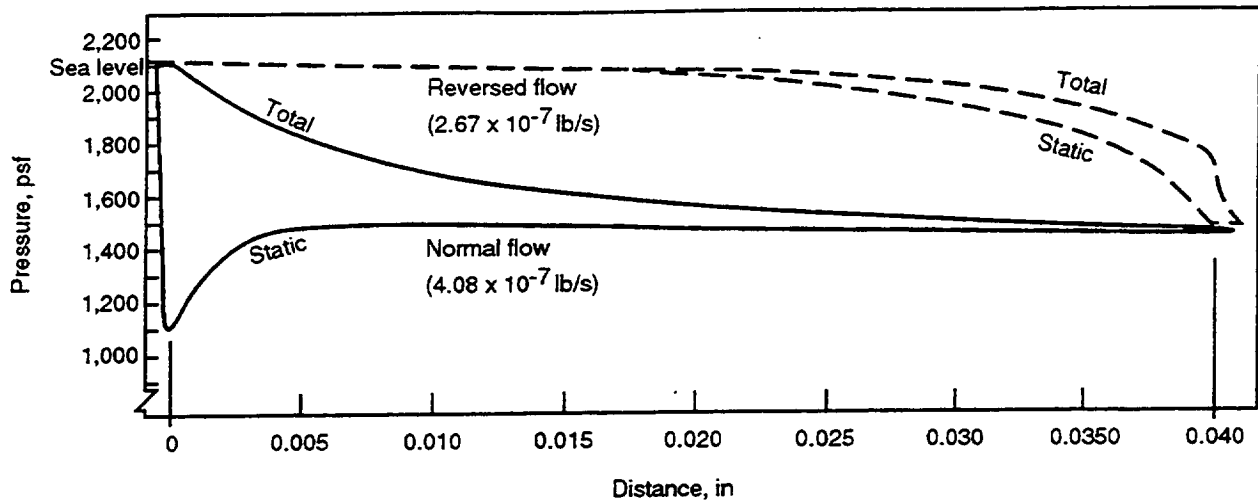


Figure 4.4-13. Computed and Measured Pressure Drop for Three Hole Diameters



12037-C 6/3/92

Figure 4.4-14. Diffuser Recovery Effect of a Laser-Drilled Hole

The two hole sizes selected for the suction panel design were as follows (fig. 4.4-15):

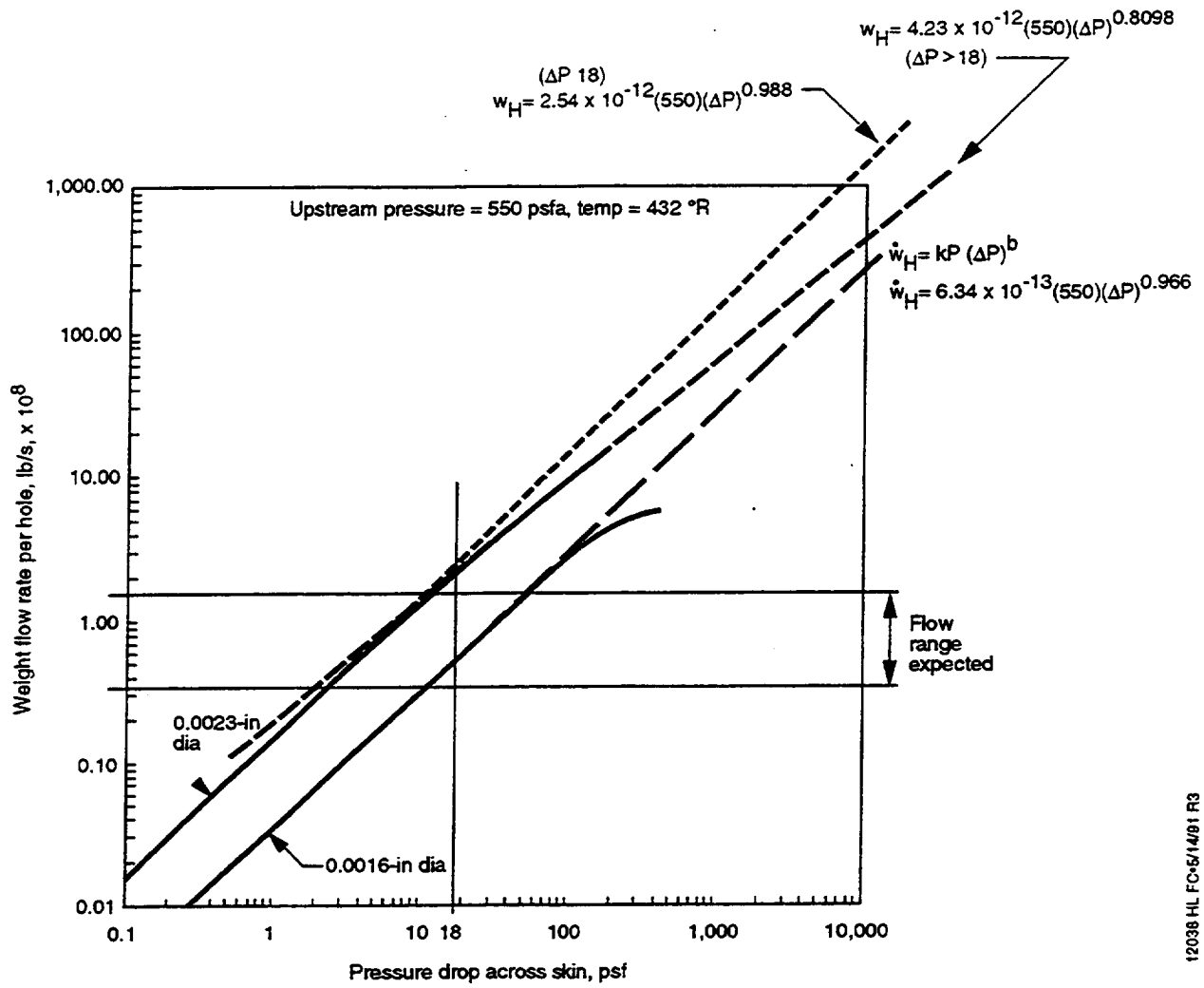
For crossflow control:

|                                   |   |
|-----------------------------------|---|
| Inlet diameter                    | 0.0016 in   |
| Exit diameter                     | 0.00416 in  |
| Hole spacing                      | 0.010 in  |
| Flow constant at design condition | $k = 6.34 \times 10^{-13}$                                    |
| Exponent at design condition      | $b = 0.966$   |
| Flow range expected               | $3 \times 10^{-9} < \dot{w}_H < 1.3 \times 10^{-8}$ lb/s/hole |

For TS control:

|                                   |   |
|-----------------------------------|---|
| Inlet diameter                    | 0.0023 in   |
| Exit diameter                     | 0.00598 in  |
| Hole spacing                      | $0.015 \leq d \leq 0.029$ (variable)                        |
| Flow constant at design condition | $k = 2.54 \times 10^{-12}$ ( $\Delta P \leq 18$ psf)        |
| Flow constant at design condition | $k = 4.23 \times 10^{-12}$ ( $\Delta P > 18$ psf)           |
| Exponent at design condition      | $b = 0.988$ ( $\Delta P \leq 18$ psf)                       |
| Exponent at design condition      | $b = 0.8098$ ( $\Delta P > 18$ psf)                         |
| Flow range expected               | $2 \times 10^{-9} < \dot{w}_H < 7 \times 10^{-9}$ lb/s/hole |

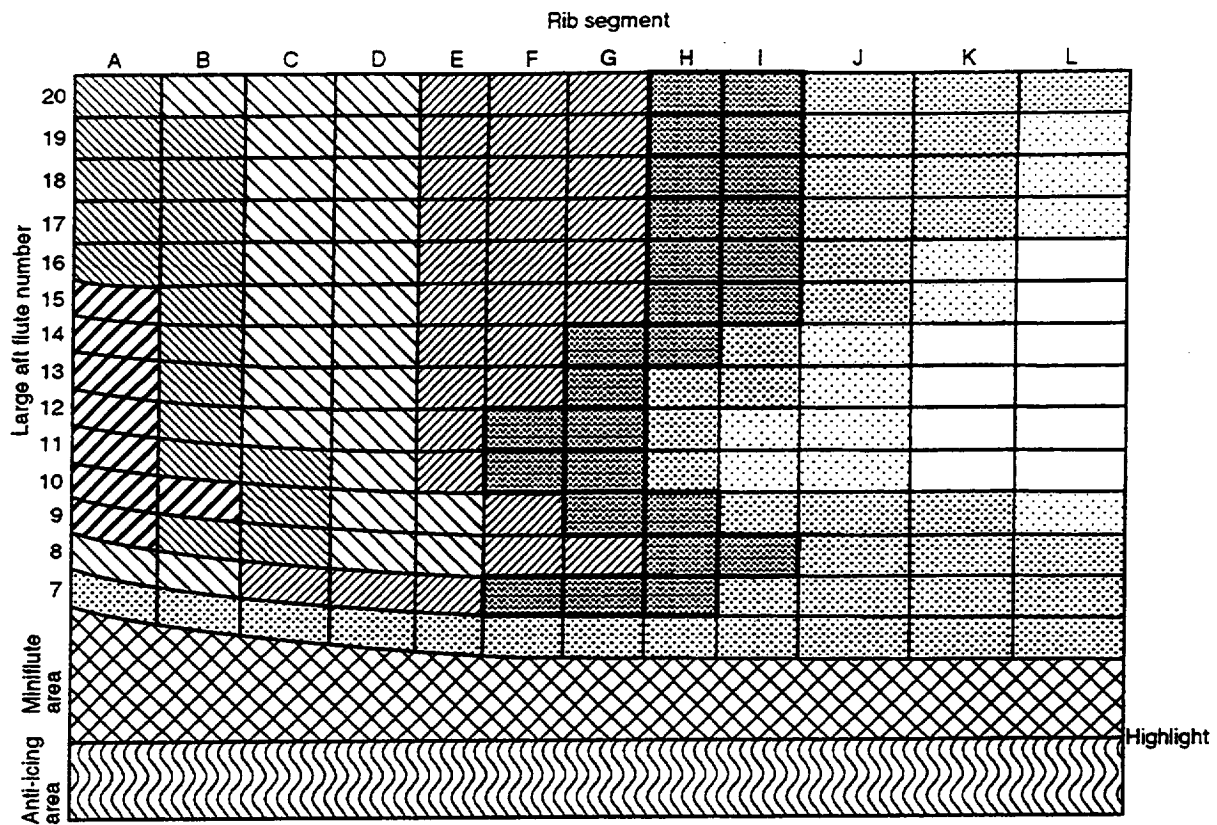
For the 14 flutes in the TS control zone, the span was divided into 12 sections (defined by air load rib and hinge rib locations). The external pressure, percent open area, area of segment, and design flute pressure were computed for each section. Based on these conditions, an ideal hole spacing was computed that would provide the correct  $c_q'$  (fig. 4.4-16). It was determined by the manufacturer of laser-drilled material that the positional drilling accuracy was  $\pm 0.001$  in. The design of the perforation pattern was resolved into the 0.002-in increments dictated by the drilling accuracy (fig. 4.4-17). The effect on  $c_q'$  is shown in figure 4.4-18.



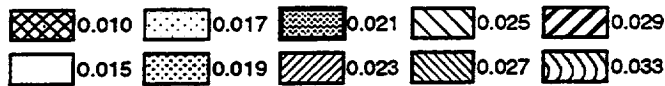
12038 HL FC-5/14/81 R3

Figure 4.4-15. Flow Characteristics for the Two Hole Sizes Used (at Design Conditions)





**Hole Spacing:**



**Note:** Using 0.0023-in-diameter holes, except the 0.01 hole spacing, which has a 0.0016-in diameter.

12040-HLFC-5/14/91 R3

*Figure 4.4-17. Outer Skin Perforation Pattern*

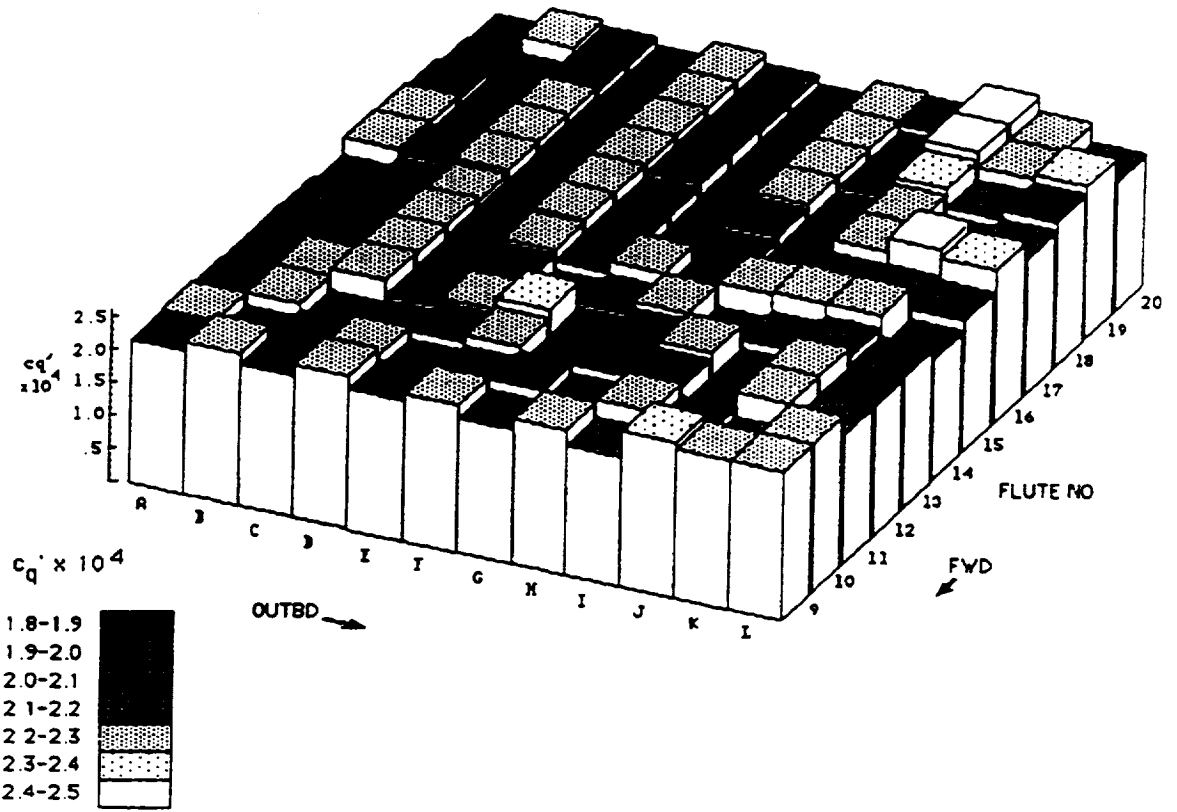


Figure 4.4-18. Variation of  $c_q'$  Due To Perforation Pattern Steps

## 5.0 HARDWARE DESIGN

### 5.1 REQUIREMENTS

The suction system had to provide an adequate source of suction for the wing test panel.

The suction rate and suction distribution had to be remotely controllable from the aircraft cabin.

The resulting ducting system had to contain provisions for anti-icing and purging of the perforated leading-edge skin.

The wing portion of the ducting system had to fit entirely within the wing leading edge. The pump section of the ducting system, together with the pump, had to fit inside a special fairing located under the port wing and behind the port engine nacelle.

It was a design goal to keep the maximum Mach number in the ducts below 0.3. The ducting minimum bend radius was to be 3 diameters.

Careful attention was required to minimize leakage and to avoid internal features that might cause separation or perturbations in the airflow.

The suction system had to be designed so that it could be installed in or removed from a structurally completed wing leading edge.

The entire suction system had to be supported to withstand the flight loads defined in volume III.

As far as possible, the suction system employed standard design practice and standard components to achieve minimum cost and technical risk.

### 5.2 SYSTEM ARRANGEMENT

To fit a system of this complexity into such a tight envelope (see figs. 5.2-1, -2, and -3), standard practice would include building a mockup to permit some preassembly and fit checking before manufacture of the final hardware. However, in an experimental program that planned only one set of hardware, the construction of a mockup would almost double the suction system manufacturing task. Therefore, a decision was made at the beginning of this program to employ a new three-dimensional CAD system, CATIA, for development of an "electronic mockup." This decision was a good one; during the suction system installation only one significant interference was discovered.

The CAD approach to design provided two additional benefits:

- a. An enhanced ability to respond to design change suggestions, which resulted in a superior end product.
- b. The opportunity to generate 3D datasets that were used to machine complex contours in various components, saving considerable time in drafting, machining, and inspection.

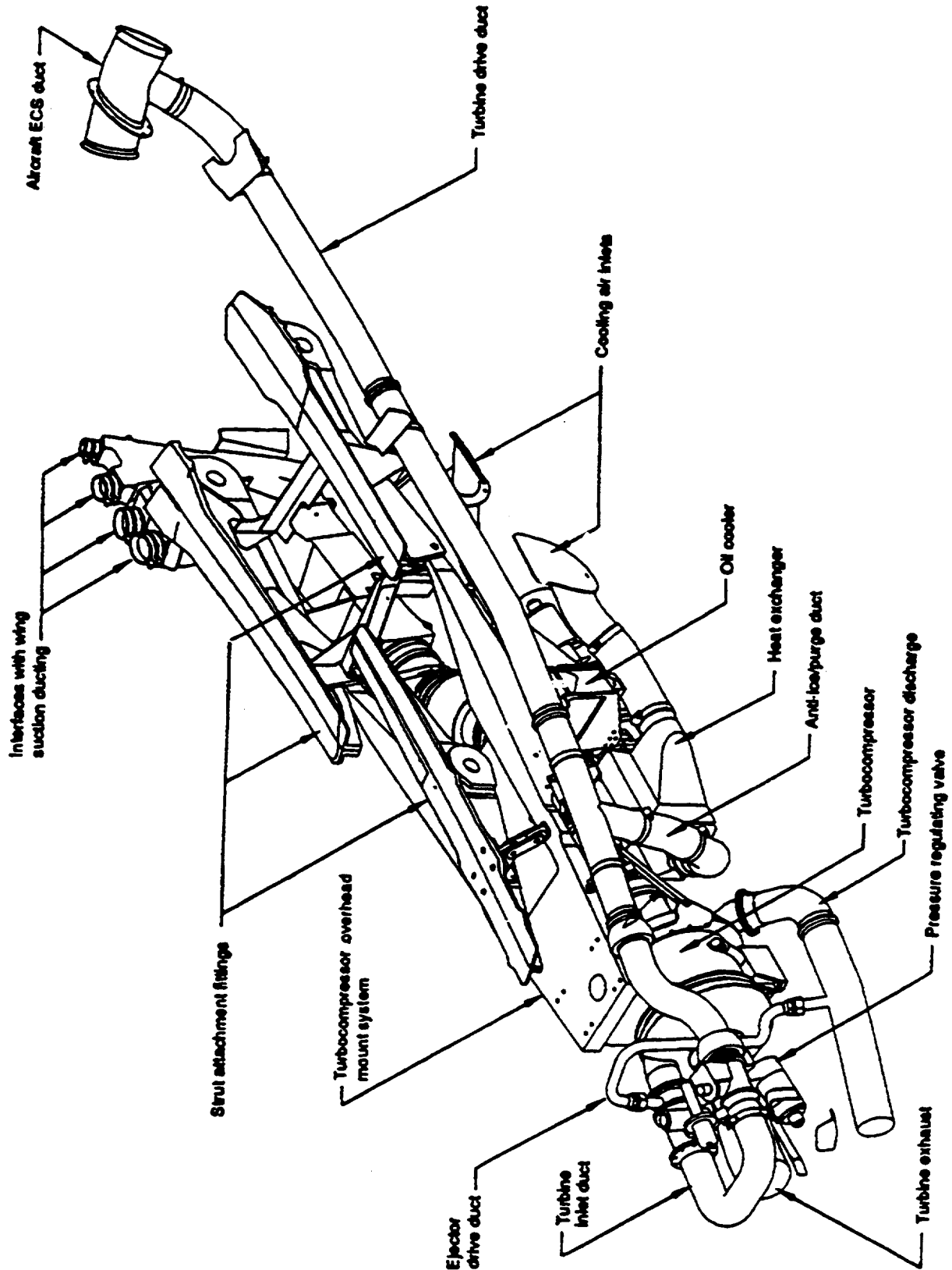


Figure 5.2-1. Turbocompressor Installation (Viewed From Inboard Side)

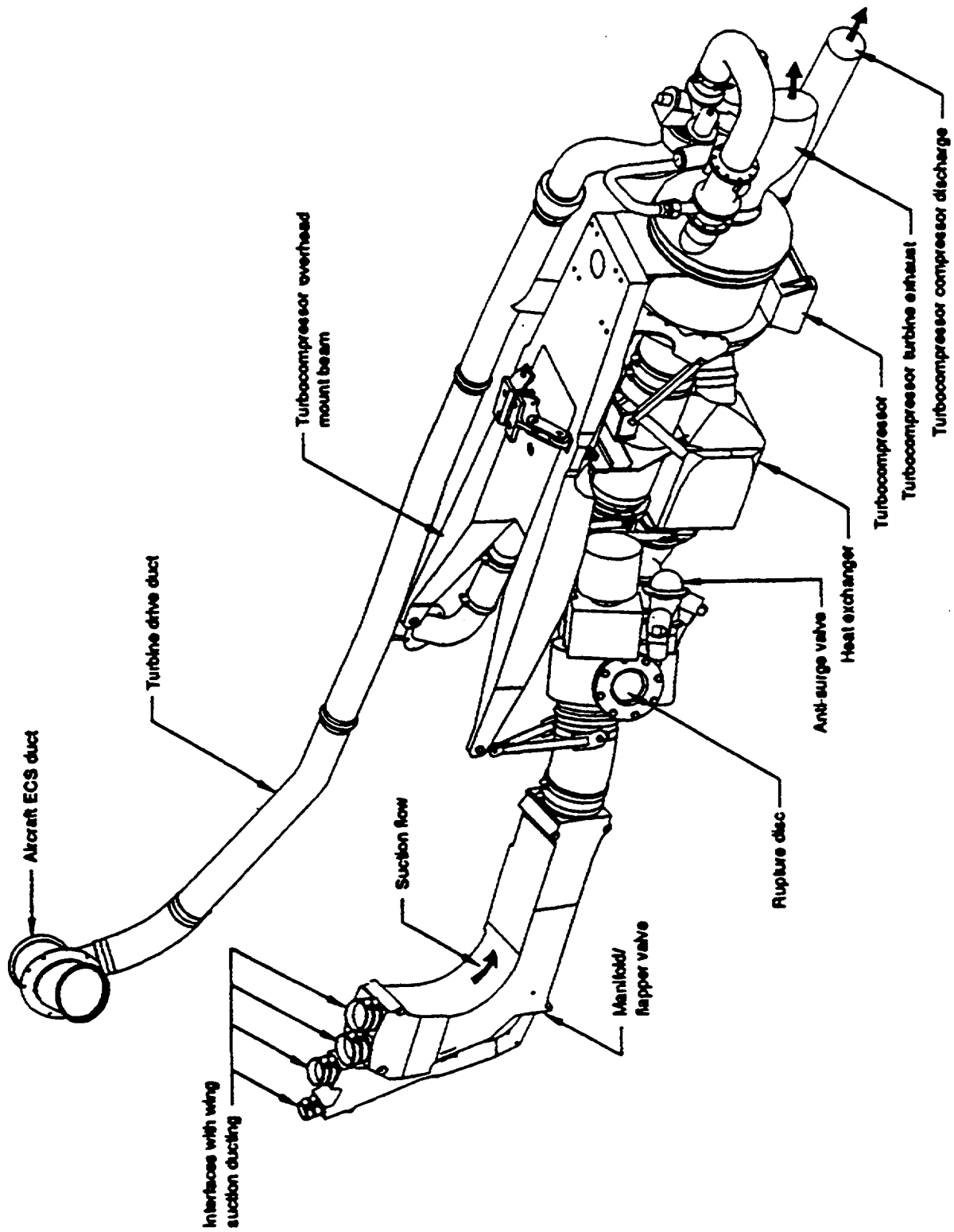


Figure 5.2-2. Turbocompressor Installation (Viewed From Outboard Side)

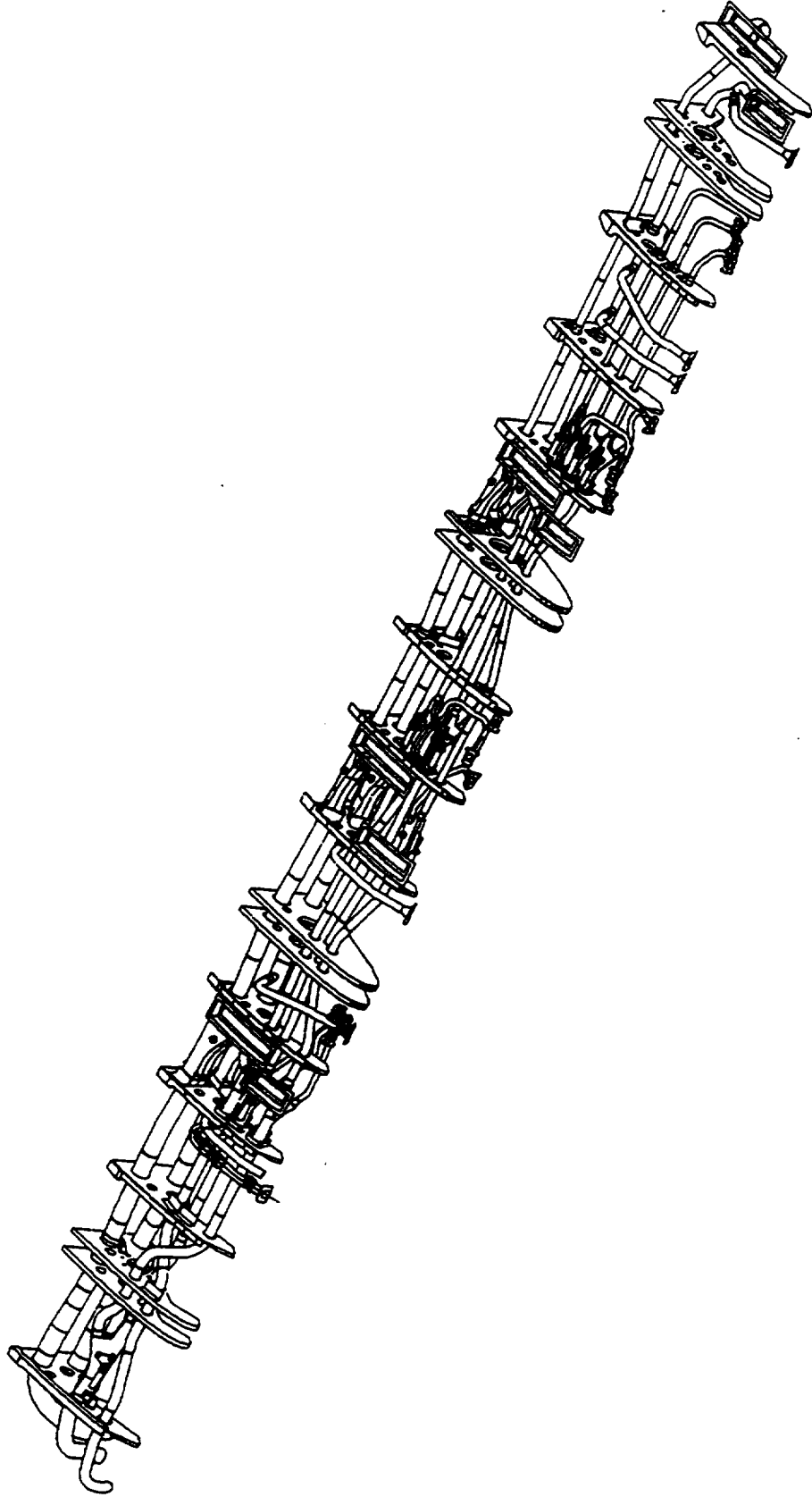


Figure 5.2-3. General Arrangement of Wing Suction System

The low-pressure, low temperature duty of the suction system suggested the use of aluminum, wherever possible, for valves and ducting and also allowed the use of rubber sleeves and hose clamps to connect the various components (fig. 5.2-4).

Only in the turbocompressor drive ducting (450°F and 45 psig) was it necessary to use other materials such as Inconel and stainless steel, although, in some cases, the availability of certain standard parts (e.g., duct flanges, valves, couplings, etc.) made it cost effective to use something other than aluminum.

The suction system schematic diagram (fig. 4.1-2) shows the major role that valves played in this experiment. While this was anticipated from the beginning, what did come as a surprise was the degree to which each valve had to be custom designed because of its peculiar function, operating parameters, or space limitations. Although considerable effort was expended in searching the market, no commercial, off-the-shelf valve was obtainable that would fit the available space and do the job.

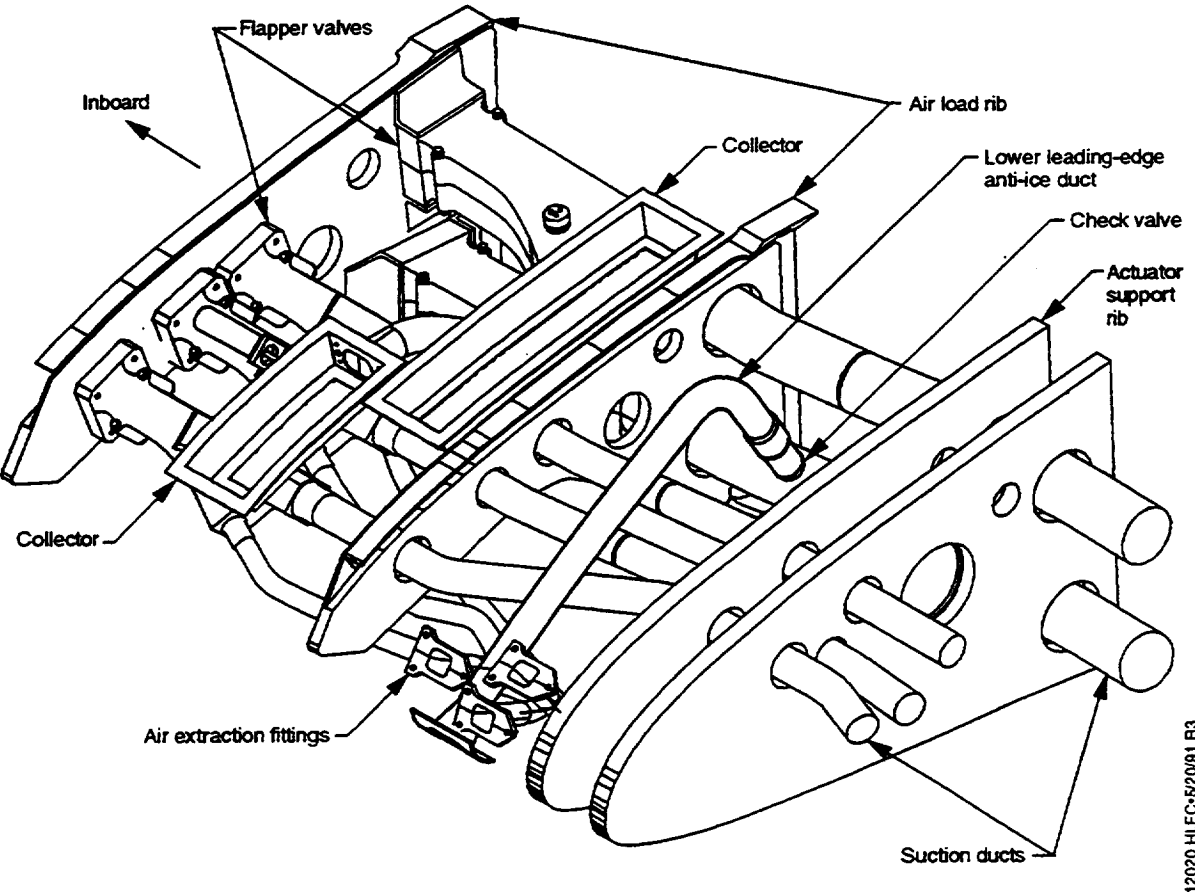


Figure 5.2-4. Typical Wing Leading-Edge Bay (Krueger Flap Drive Not Shown)

## 5.3 SPECIAL FEATURES

A number of components designed for the HLFC suction system are complex enough to warrant discussion.

### 5.3.1 Flapper Valves

A flapper valve is a Y duct in which a pivoted flap located at the intersection of two passages can rotate and alter the area ratio of the two throats (figs. 5.3-1 and 5.3-2). For this program it was necessary that each valve be remotely controllable, so each flap was driven through a worm-gear arrangement by a reversible trim motor. In addition, it was necessary during flight testing to be aware of flap position, so each valve was equipped with a linkage-driven potentiometer that reported the angular position of each flap. For each location in the system, each valve and each valve port had to be sized to match the adjoining, circular cross-section ducting. However, the flap needed a constant-width passage in which to operate. The resulting design had an inner flowpath that transitioned from circular at each of the three ports to rectangular at the intersection. In addition, there was a requirement to diffuse each entry passage so that a corresponding acceleration could be introduced where flow mixing occurred. Therefore the resulting inner contour was complex and not easy to define or machine in conventional terms; but it was well suited to the 3D electronic dataset referred to in section 5.2.

### 5.3.2 Check Valves

The suction system schematic diagram shows two check valves in the wing. Because of special requirements and space limitations, it was necessary to design two custom valves for this program. The first valve (fig. 5.3-3) was a conventional spring-loaded valve which allowed de-icing and purging of the lower leading edge while preventing suction flow from that region. The second valve (fig. 5.3-4) was installed to prevent a major loss of anti-ice or purge air through the outboard section of the test panel and yet offer minimum obstruction to the suction flow. This was accomplished by installing a thin, circular flap in a curved duct and pivoting the flap off center so that the flap trailed in the suction flow but slammed shut against a stop during purge or anti-ice operations.

### 5.3.3 Pressure Regulating Valve

There were two pressure regulating and shutoff valves (PRSOV) in the system: one in the turbocompressor turbine drive duct and the other in the anti-ice/purge duct. In each application it was necessary to modify a production valve so that the regulated pressure could be remotely adjusted

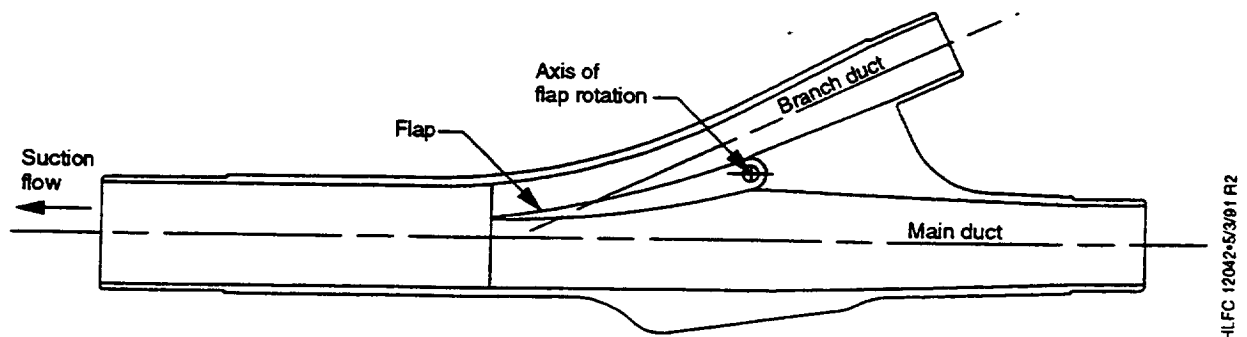
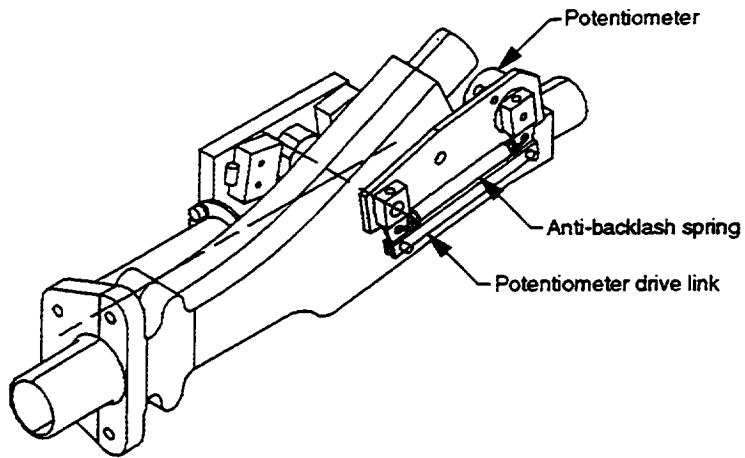
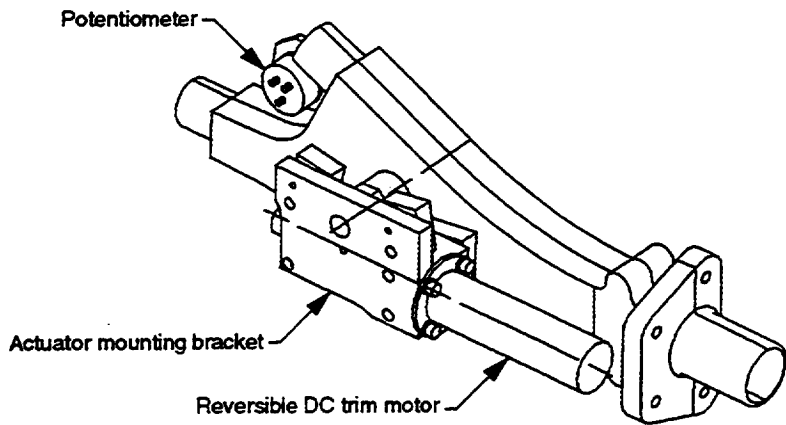


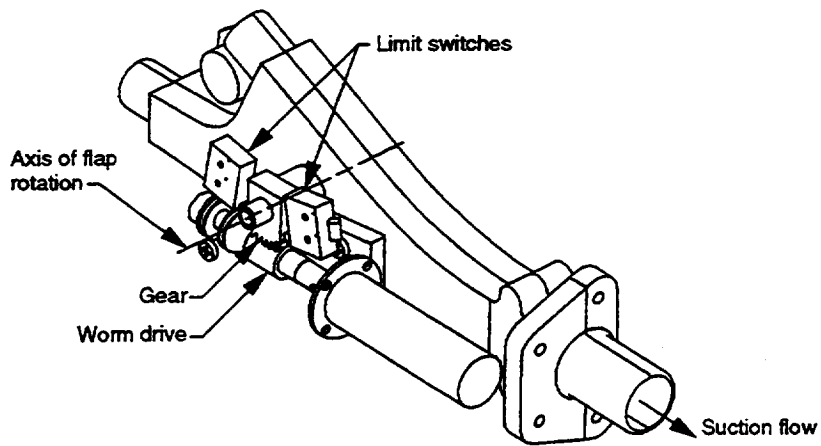
Figure 5.3-1. Typical Flapper Valve Arrangement



**View Showing Potentiometer for Position Indication**



**View Showing Flap Drive Actuator**



**View Showing Flap Drive Internal Components**

*Figure 5.3-2. Flapper Valve Drive and Position Indication*

HLFC 12042a/5/3/01 R1

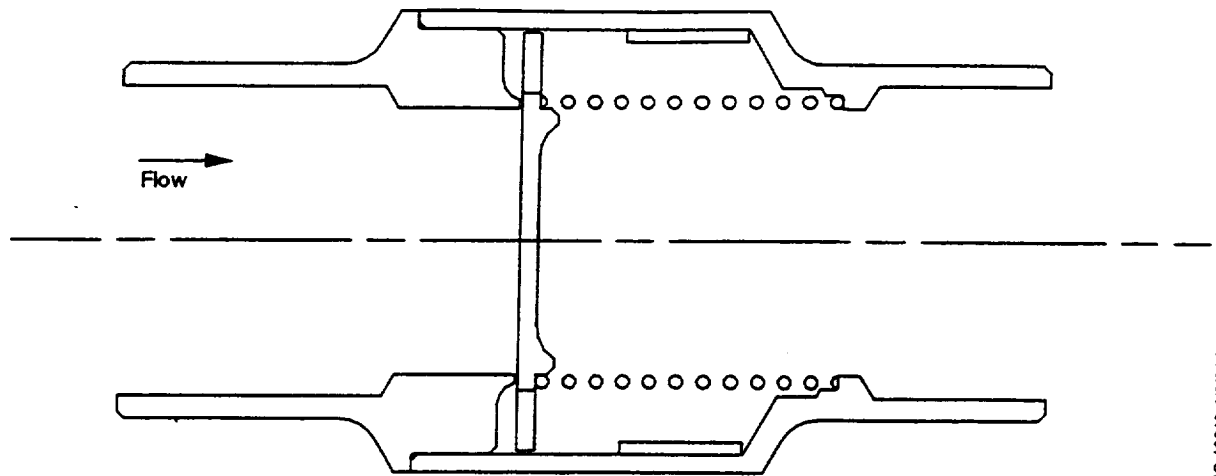


Figure 5.3-3. Anti-Ice Check Valve

HLFC 12043-1/9/01 R0

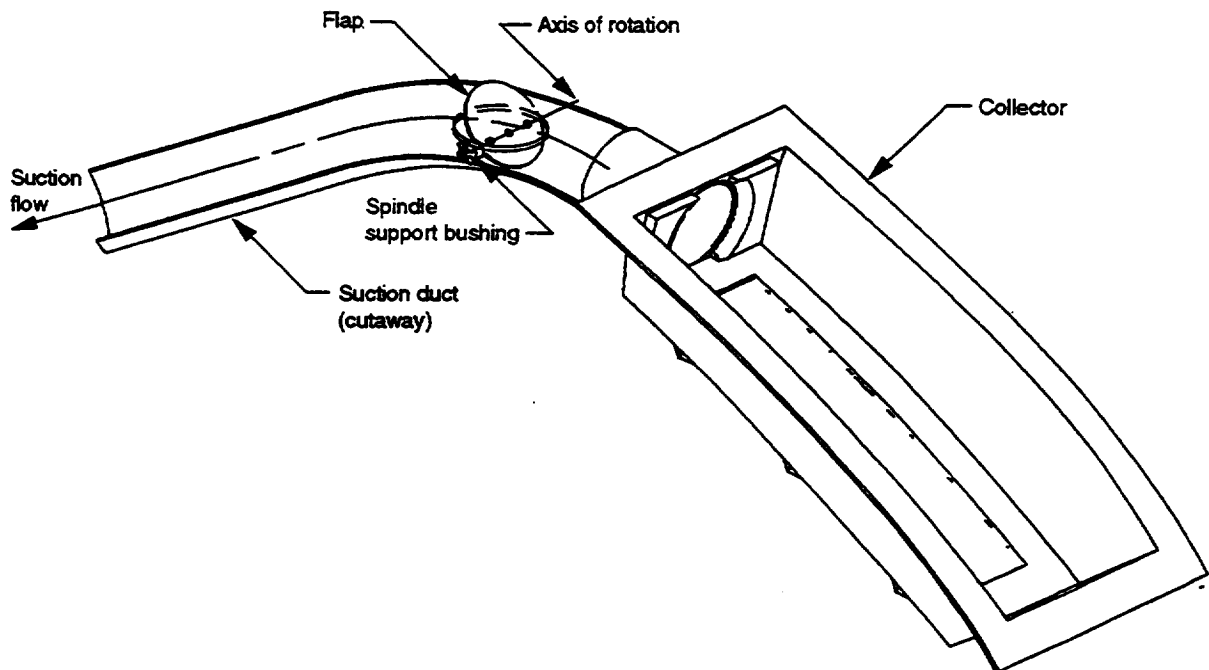


Figure 5.3-4. Check Valve

HLFC 12044-5/6/01 R1

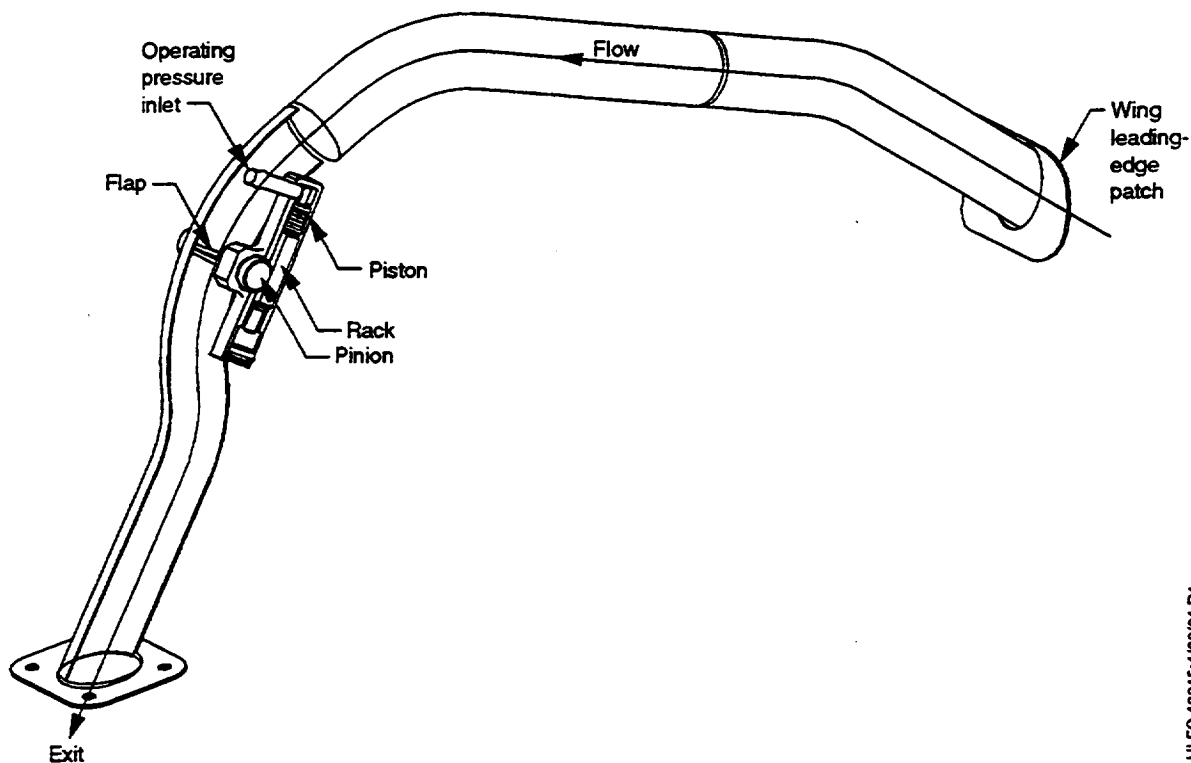
from the cabin. This was accomplished by mounting a reversible trim motor on the pilot valve load spring and providing stops so that a maximum pressure could not be exceeded.

With the first modified PRSOV in the system, it was possible to regulate the overall suction rate by controlling turbocompressor speed, thus avoiding the need for an ambient air vent valve. The second modified PRSOV allowed the operator to purge the system at a low level (1 to 3 psi) and to introduce the anti-ice air gradually to protect instrumentation in the ducting.

### 5.3.4 Shutoff Valve

This valve is found in the attachment-line flow control duct (fig. 5.3-5) where its function was to prevent the escape of warm air during anti-ice/purge functions. The shutoff valve was normally

spring-loaded closed, and was pneumatically energized to the open position by the turbocompressor start solenoid (i.e., at the beginning of each turbocompressor run). At turbocompressor shutdown the valve automatically returned to the closed position, where it was ready for purge or anti-ice functions. The valve itself consisted of a circular flap mounted on a spindle that penetrated the duct diametrically. One end of the spindle carried a pinion gear that engaged a spring-loaded, piston-driven rack. The whole mechanism was contained in an aluminum housing welded to the duct.



HLFC 12046-130/81 R1

Figure 5.3-5. Attachment-Line Flow Control Duct and Shutoff Valve

### 5.3.5 Plenum

Figure 4.1-2 shows there was a need to intersect the suction system ducting with the anti-ice/purge ducting so that the suction system could be subjected to backflow. Also, at low-flow conditions in the suction mode, provisions had to be made to introduce ambient air into the suction pump inlet through two antisurge valves.

Figure 5.3-6 shows a plenum designed to meet these requirements and also provide system overpressure protection by means of a rupture disk. Antisurge air was introduced through an annulus at the outside diameter of the main duct, thus avoiding the duct blockage of previous designs.

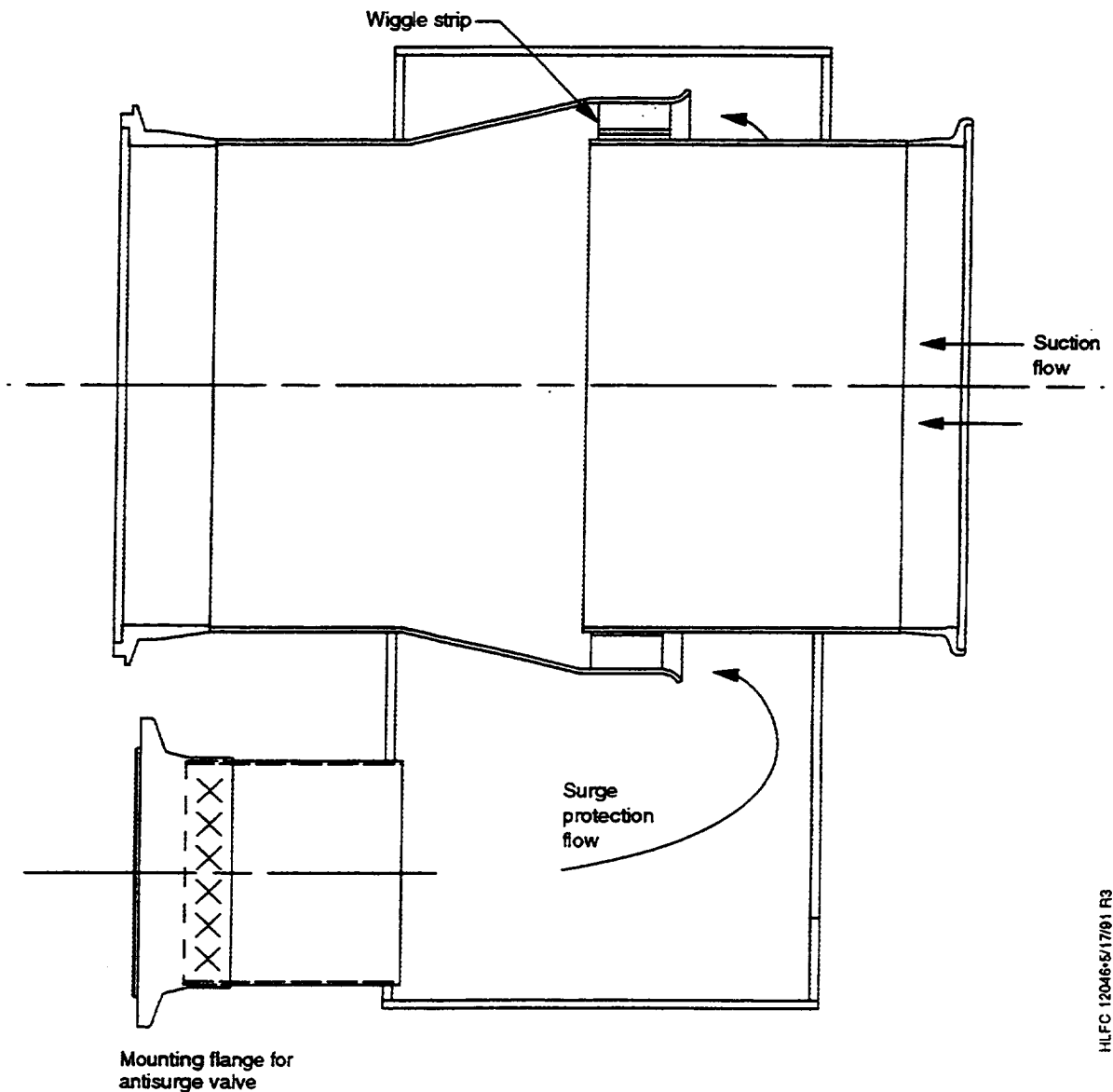


Figure 5.3-6. Plenum Assembly

HLFC 12046-6/1701 R3

### 5.3.6 Muffler

Immediately upstream of the turbocompressor inlet was an acoustically treated section of ducting. It was designed to attenuate high-frequency noise generated by the turbocompressor wheel that could have caused propagation upstream and disturbance of the wing boundary layer.

Figure 5.3-7 shows the construction details of the muffler. The duct liner was a feltmetal cylinder backed by a honeycomb core, enclosed in a steel tube. The assembly was equipped with suitable flanges at each end.

### 5.3.7 Filter

The air supply for the anti-ice and purge functions was drawn from the aircraft environmental control system and was unfiltered at the extraction point. Therefore it was necessary to protect the leading-edge skin from particles that might have plugged the perforations. A 5- $\mu\text{m}$  filter was designed and installed as shown in figure 4.1-2.

A cross section through the filter assembly is shown in figure 5.3-8.

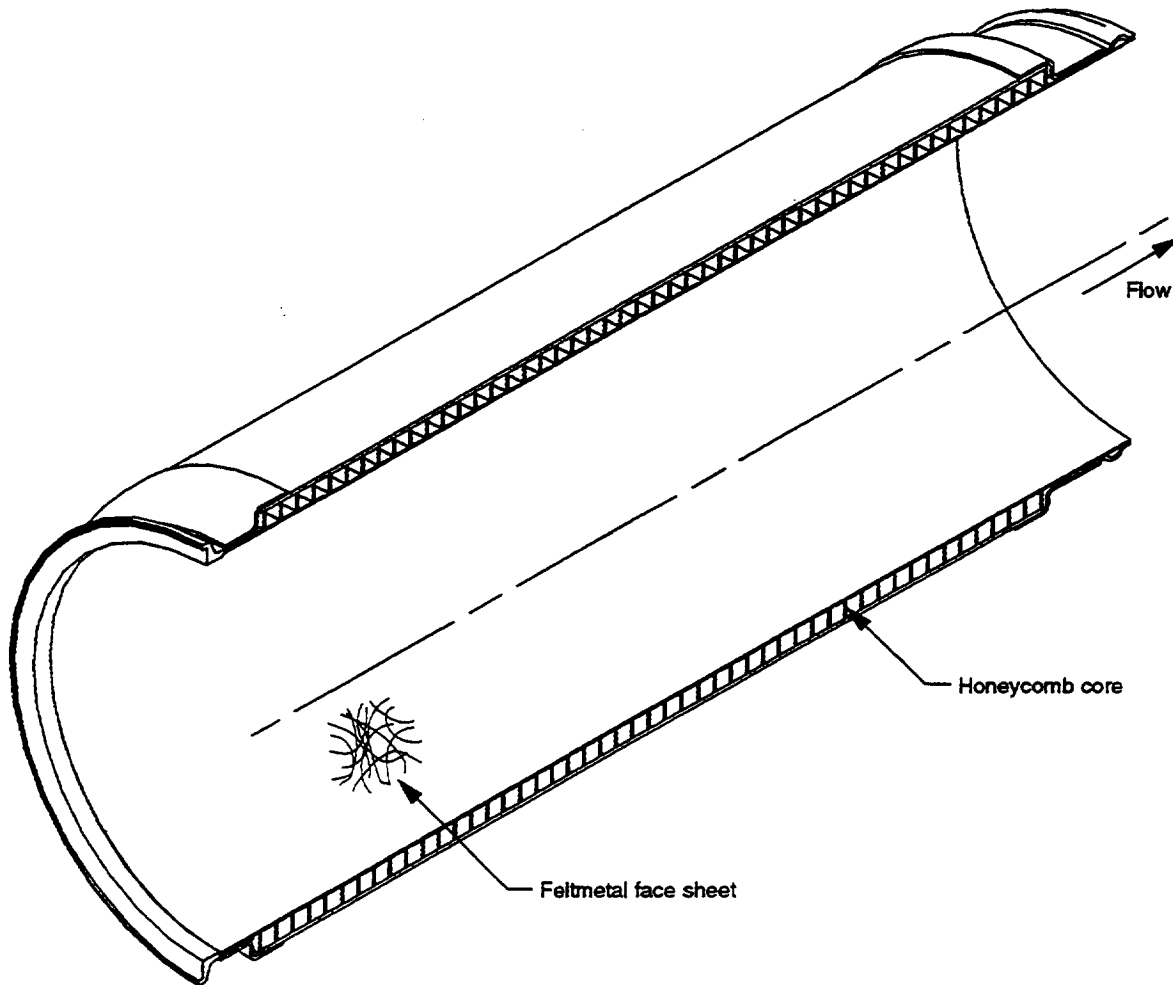
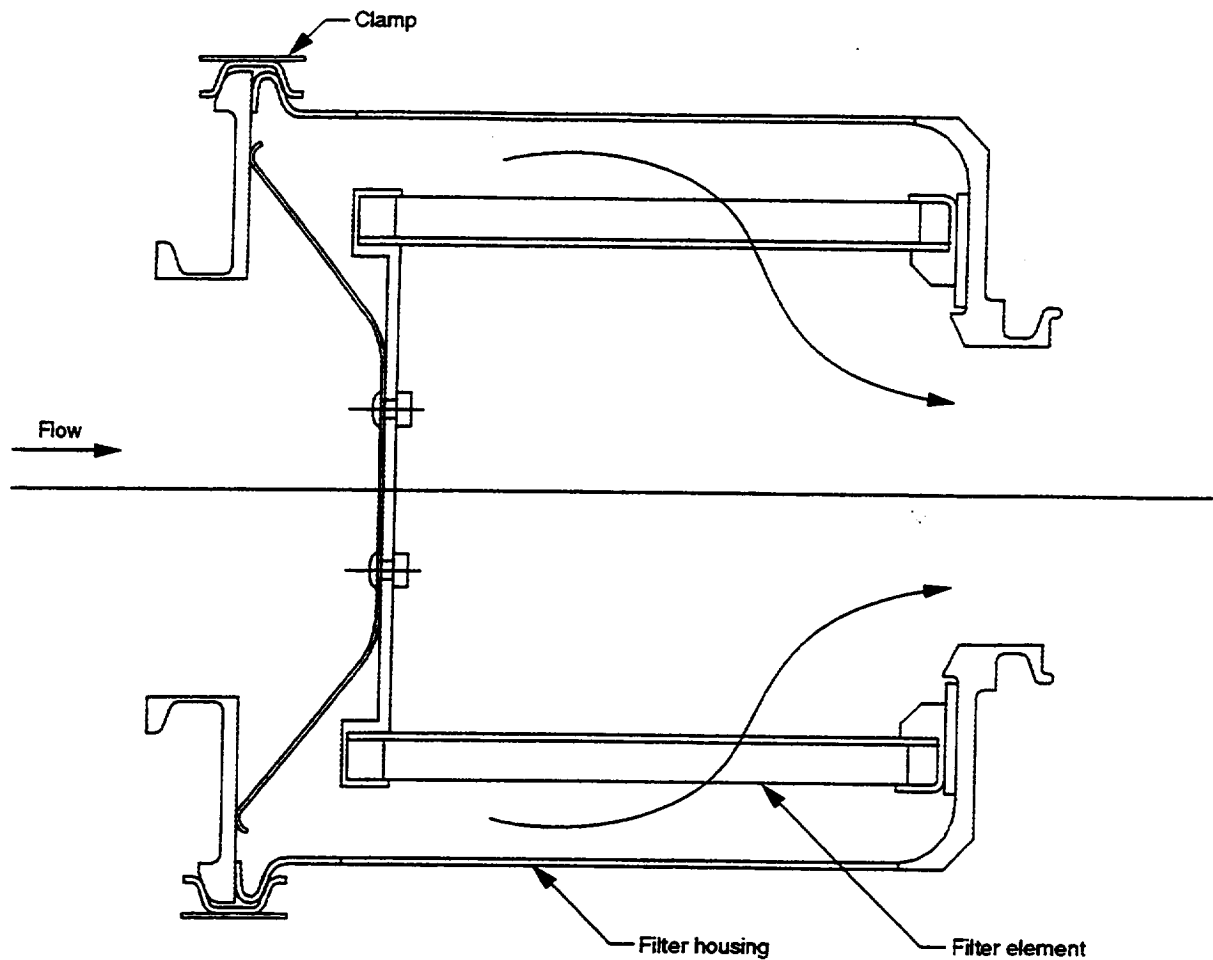


Figure 5.3-7. Muffler

HILFC 12047-5/8/81 R1



HLFC 12046-5/14/01 R2

Figure 5.3-8. Air Filter

#### 5.4 TURBOCOMPRESSOR MODIFICATIONS

As in previous programs, the suction source was a modified 707 turbocompressor furnished for this experiment by NASA.

Additional modifications for this installation included a new overhead mounting system, the provision of an isolation valve in front of the compressor inlet, and check valves near the surge valves to prevent the escape of warm air during the anti-ice/purge functions.

## 6.0 SUCTION CONTROL SCHEME

The suction system provided the flexibility and control required for a research program, but exceeded that considered necessary for production airplanes. To obtain the flexibility necessary for research, several redundant flow paths (i.e., flutes versus ducts) provided smooth spanwise  $c_q$  transitions, but they complicated the control.

The control scheme was based on pressure differentials between the flutes and the local external pressures. By monitoring and controlling these differentials,  $c_q$  was controlled.

### 6.1 SPANWISE CONTROL

For spanwise control, the pressures outside and inside the flute were displayed graphically on a system control panel, and only one flute associated with each of the five spanwise ducts was analyzed. Using the flapper valve numbering convention shown in figure 6.1-1, the spanwise control was obtained as follows (fig. 6.1-2):

- a. One flute for each of the spanwise ducts was selected for display (in this case the lowest pressure flute in each collector):

i.e.,

|          |              |
|----------|--------------|
| Flute 2  | Forward duct |
| Flute 4  | Second duct  |
| Flute 6  | Third duct   |
| Flute 11 | Fourth duct  |
| Flute 12 | Aft duct     |

- b. The static pressures outside the flutes, for the entire span, were displayed as lines. The horizontal axis was, therefore, the distance along the flute (repeated five times) while the vertical axis was the pressure or  $C_p$ .

- c. The internal pressures for the entire span of a given flute were displayed along the corresponding external pressure lines as circle symbols. (The lever and fulcrum symbols were not displayed on the control panel, but are shown in figure 6.1-2 to illustrate the interrelationships of the controls.)

i.e.,

|         |        |                             |
|---------|--------|-----------------------------|
| Flute 2 | Points | A, B, C, D                  |
|         |        | A—inboard flute pressure    |
|         |        | B, C—midspan flute pressure |
|         |        | D—outboard flute pressure   |
| Flute 1 | Points | M, N, O, P                  |
|         |        | M—inboard flute pressure    |
|         |        | N, O—midspan flute pressure |
|         |        | P—outboard flute pressure   |

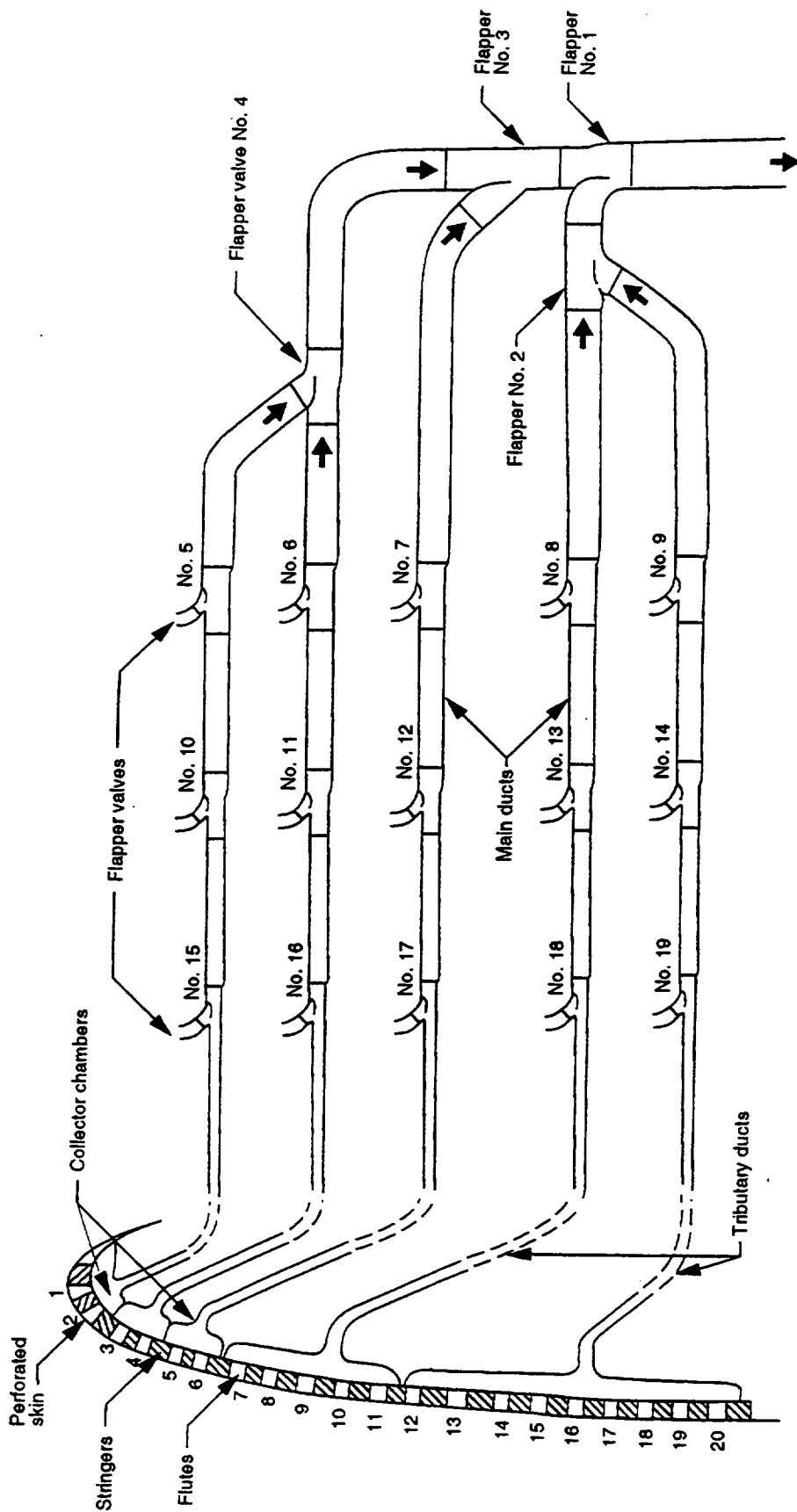


Figure 6.1-1. Flapper Valve Numbering Convention

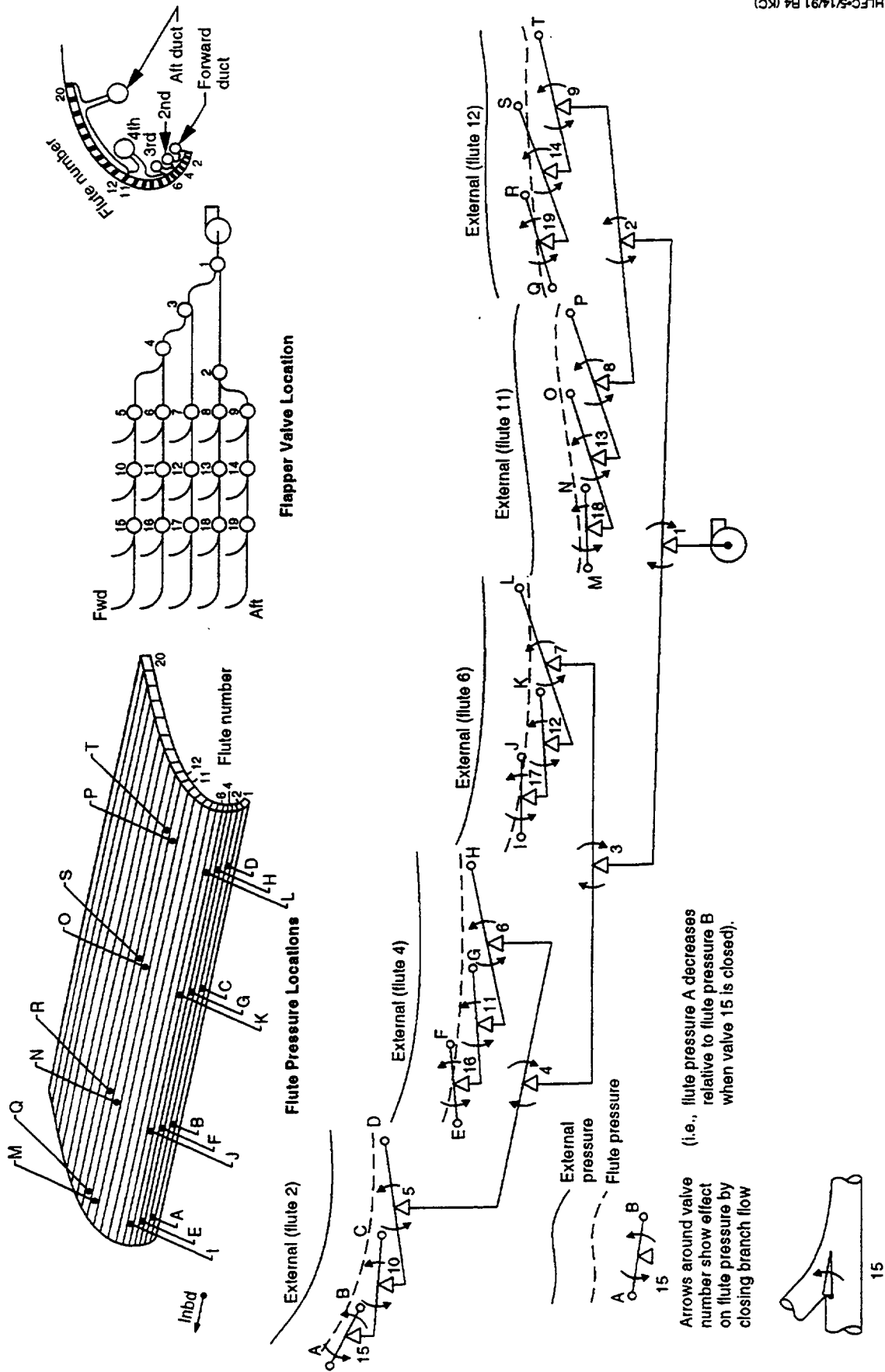


Figure 6.1-2. Overall System Control Method

The flute pressure required to obtain the correct  $c_q'$  is shown as a dashed line below the external pressure. This is a computed line based on  $c_q'$  required, external pressure, and skin porosity.

The flapper valves were manipulated to generate flute pressure gradients by diverting flow spanwise. The effect on the flute pressures was cumulative (i.e., valve 5 balanced flow between point D versus points A, B, C). Some examples are—

- a. By closing valve 15, flute pressure B increased relative to flute pressure A.
- b. By closing valve 7, flute pressure L increased relative to flute pressures I, J, K.
- c. By closing valve 1, flute pressures A, B, C, D, E, F, G, H, I, J, K, L, increased relative to flute pressures M, N, O, P, Q, R, S, T.
- d. The overall suction rate was varied by changing the compressor speed.
- e. The adjustments were continued until flute pressures A through T lay on their appropriate dashed lines (required flute pressures).

## **6.2 CHORDWISE ADJUSTMENT**

After the spanwise adjustments were complete, the streamwise adjustment was made. This adjustment was very coarse in flight but could be improved by on-the-ground metering screen replacement. The control logic was identical to that used in spanwise control (fig. 6.2-1).

Perhaps, in future applications, this process could be accomplished automatically (by computer) thereby optimizing system performance for all flight conditions.

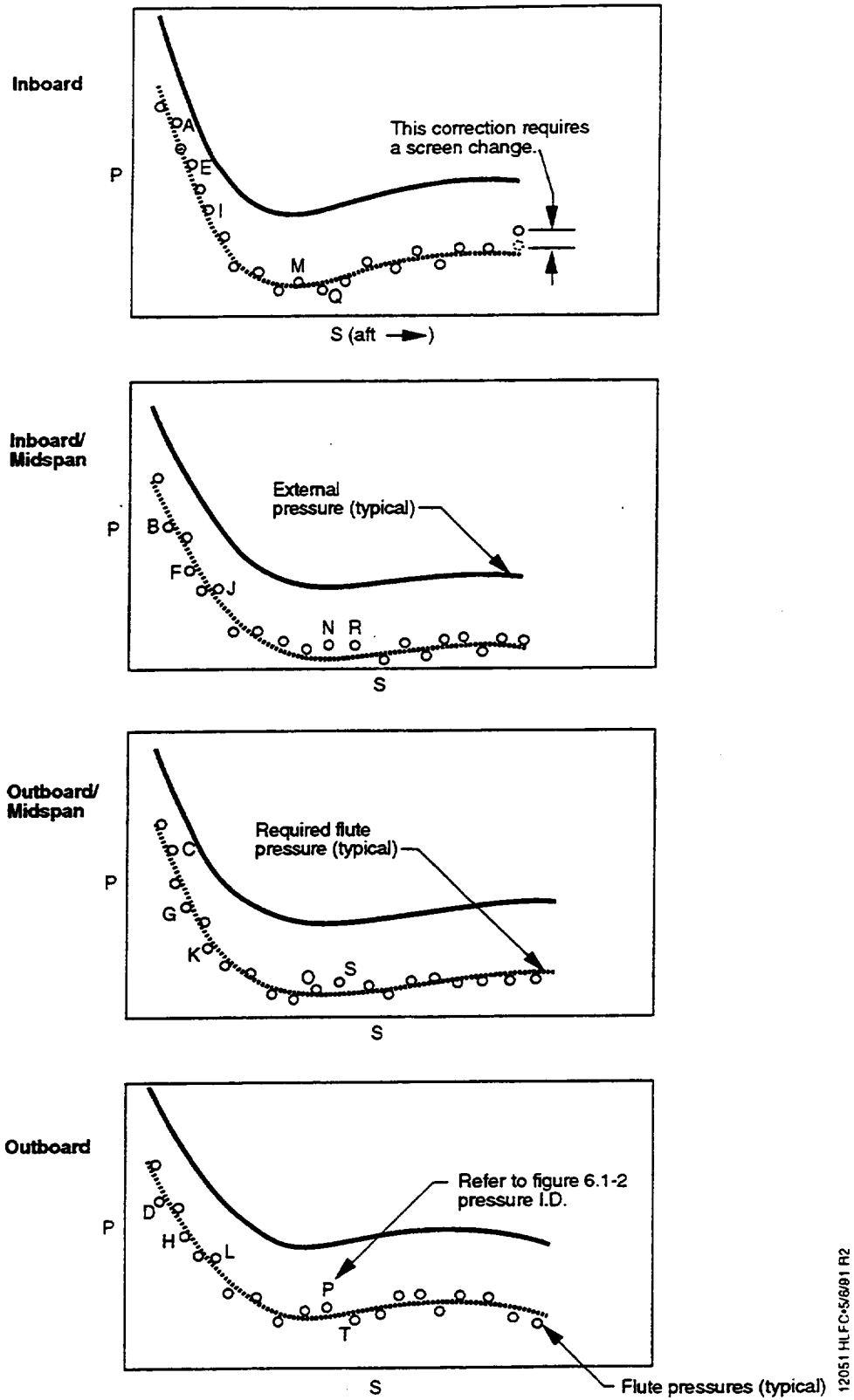


Figure 6.2-1. Streamwise Pressure Display

12051 HLC-5/8/81 R2

**This page intentionally left blank**

## 7.0 ANTI-ICE AND PURGE OPERATION

### 7.1 ANTI-ICE

During early Boeing feasibility studies, an innovative idea emerged: anti-icing by a reverse flow of hot air through the suction ducting. This scheme has the potential for greatly increased efficiency compared to the conventional approach of blowing hot air against the inside of the leading edge, for the following reasons:

- a. The skin is heated more efficiently because of the high heat transfer coefficients between the air and the inside surface of the perforations.
- b. The air emerging from the perforations is in direct contact with the ice, so virtually all the heat is available for melting the ice. In addition, blocking of the perforations by ice was not expected to be a concern in natural icing. Aerodynamically deposited ice was found to be naturally porous (ref. 4).
- c. Convective cooling of the skin is reduced by the insulating effect of the layer of warm air flowing back over the wing surface. While this effect is large for convective heating or cooling, it is relatively unimportant in the present application because the primary mode of heat transfer is by direct impingement of supercooled water droplets on the wing.

In the HLFC flight experiment, the performance of the anti-ice system was compromised significantly by limitations that arose during the design. In particular the structural adhesive temperature limit of 240°F required the addition of a heat exchanger that reduced the total amount of airflow that could be obtained. As actually manufactured the experimental system was less powerful than that of a production 757. Fortunately, the limitations of the experimental system can be overcome in production.

#### 7.1.1 External Heat Loads

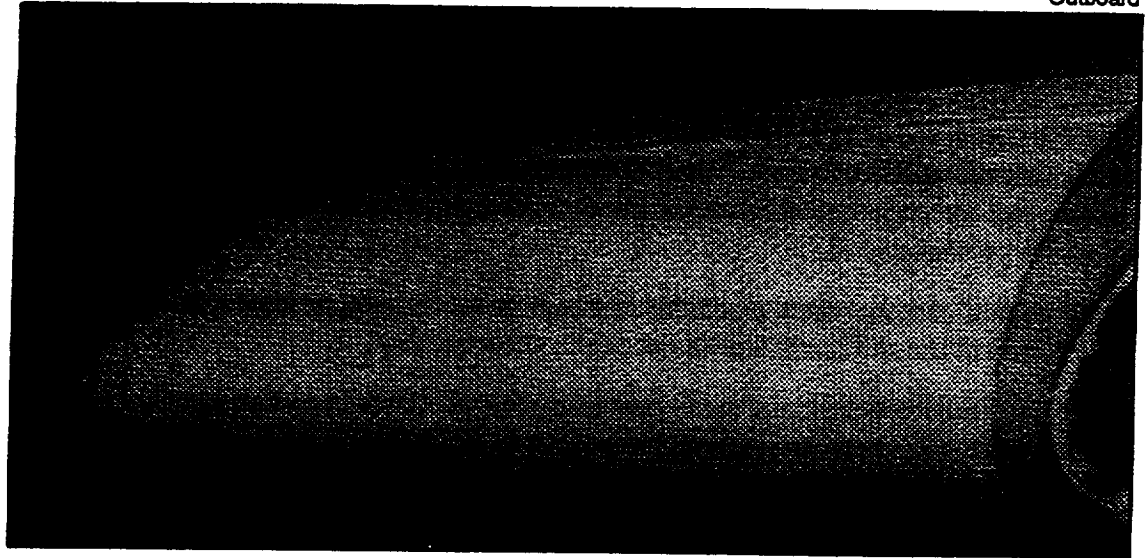
The wing anti-ice system provided sufficient heat to prevent the formation of ice on the leading edge. Ice formation was limited to an area near the stagnation line where the angle of incidence was sufficiently near normal that the supercooled droplets attached. Droplets with incidence angles less than this simply passed by. This incidence angle was found to be between 24 and 37 deg in icing tunnel tests (app. F) with perforated material (fig. 7.1-1). The lowest incidence angle, 24 deg, corresponded to a surface distance of 5 in and a projected distance of approximately 3.5 in above the stagnation line. The distance below the stagnation line was shorter (projecting approximately 1.5 in) and it was determined by the practical limits imposed by the Krueger flap and mechanism. By using this distance of 3.5 and 1.5 in vertically and a projected span distance of approximately 15 ft horizontally, an area was obtained that, when swept through a volume of given droplet concentration, produced the ice loading.

$$Q_{ICE} = \beta A_P \gamma_\infty V_\infty c \Delta T_W \quad \text{running wet}$$

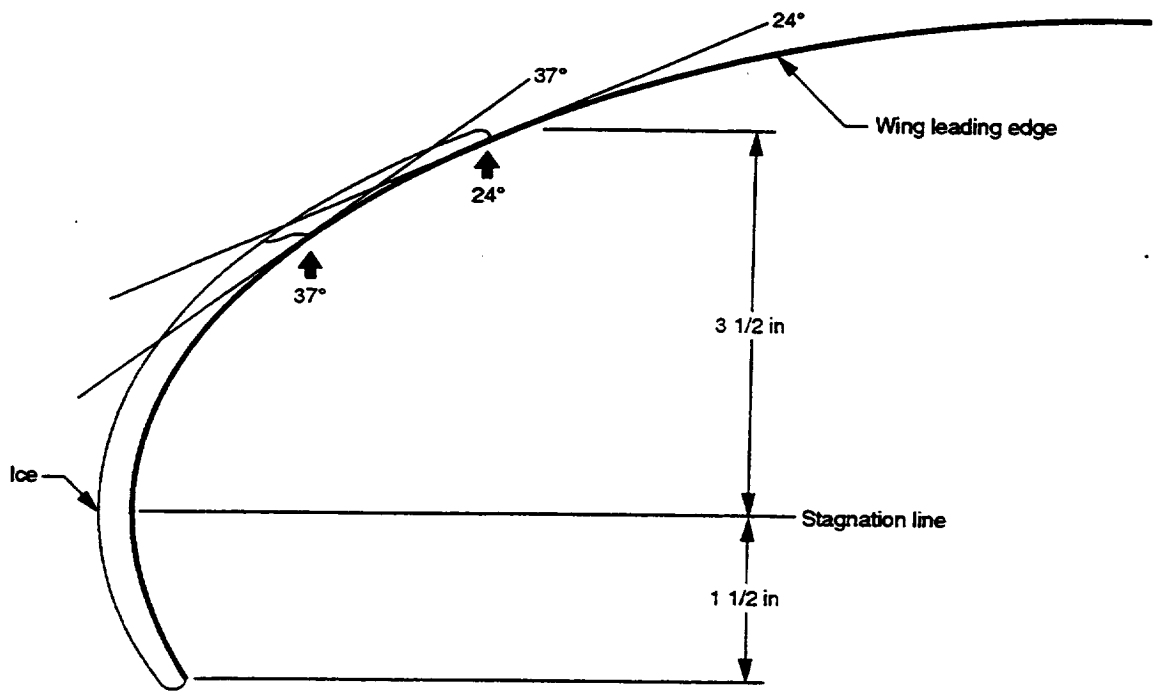
$$Q_{ICE} = \beta A_P \gamma_\infty V_\infty (c \Delta T_E + h_{fg}) \quad \text{evaporative}$$

Inboard

Outboard



Icing Tunnel Photograph (After 180 sec)



Area of Predominant Icing

Figure 7.1-1. Icing Tunnel Test

12052 H.L.F.C.-5/9/81 R2

The running-wet loading was applied to the surface below the stagnation line where runback was not detrimental to performance. All the ice had to be evaporated above the attachment line because any runback would have refrozen on the upper surface and caused laminar transition later in cruise.

An impingement efficiency ( $\beta$ ) of 32% had been derived from previous icing tests (ref. 5) using a relationship of the normal velocity component and the vertical distance from the attachment line.

Another heating load encountered during the anti-ice operation was convection. Convective heat transfer coefficients for surfaces with transpiration are modified by the insulating effect of the air exiting the surface (ref. 6). Good approximations of this effect have been obtained using boundary layer growth mixed with transpiration flow to obtain the boundary layer temperature. From this an effective heat transfer coefficient and resultant heat loss is obtained (fig. 7.1-2).

$$Q_{CONV} = h_{eff} A_S (T_S - T_{AW})$$

After ignoring structural conduction, the last heat load to consider was due to radiation, which was approximated as follows:

$$Q_{RAD} = \sigma A_S \varepsilon (T_S^4 - T_{\infty}^4).$$

The total heating load for the maximum icing condition is then

$$Q_T = Q_{ICE} + Q_{CONV} + Q_{RAD}.$$

For the present design condition,  $Q_T$  is 146,240 BTU/hr. (See app. G for details of calculation.)

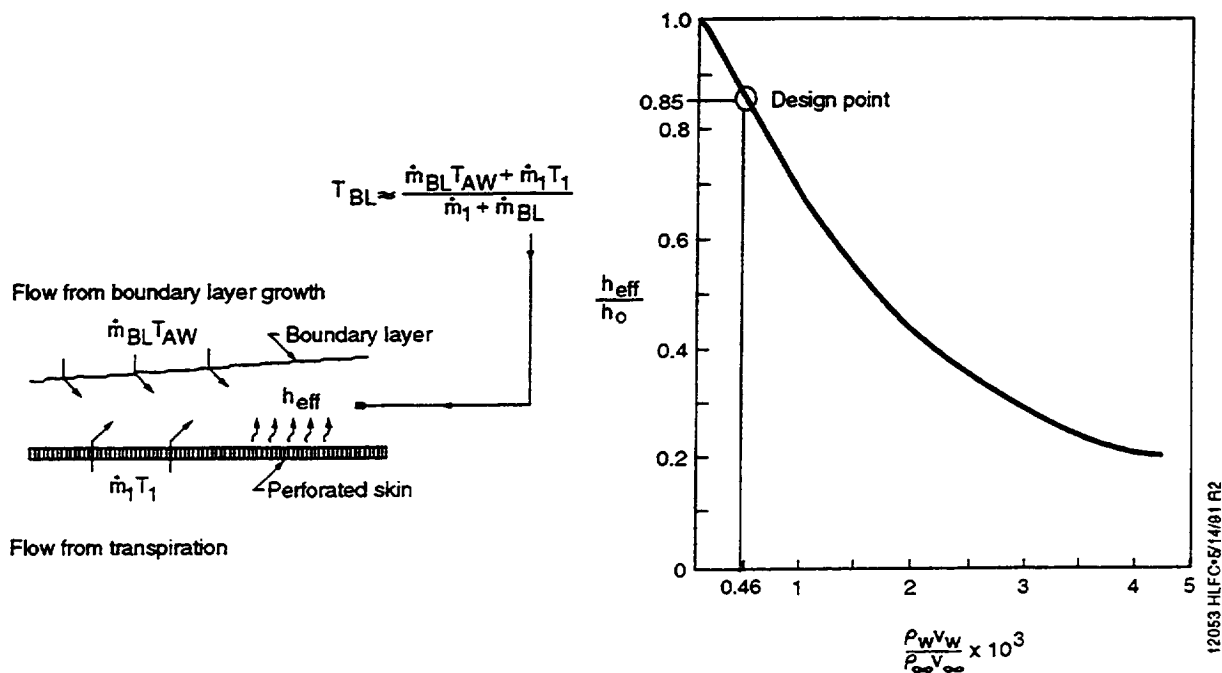


Figure 7.1-2. Reduction in Heat Transfer Rate Due To Fluid Injection (Air to Air)

### 7.1.2 System Performance

Normally engine bleed air is used as the heat source during the de-ice operation. The air is hot (300° to 400°F), so a relatively small amount is required.

$$\dot{w} = \frac{QT}{C_p \Delta T}$$

$$\dot{w} = \frac{146,240}{(0.24)(350 - 185)}$$

$$\dot{w} = 3,693 \text{ lb/hr (61.5 lb/min)}$$

However, the HLFC leading-edge temperature had to be limited to 240°F because of thermal stress and adhesive limitations. Therefore, a larger amount of air was needed.

$$\dot{w}_{\text{NEEDED}} = \frac{(146,240/60)}{(0.24)(240 - 185)} = 184.6 \text{ lb/min (using 240°F air)}$$

A comparison of a conventional anti-icing system and the transpiration system used in this program is shown in figure 7.1-3. The heating capacity for the transpiration system is considerably below that required for an evaporative system (fig. 7.1-4). Presently, the combination of these factors have reduced the system capacity to approximately 0.06 inches of ice per 5 min (running wet). Explanation of these factors follows.

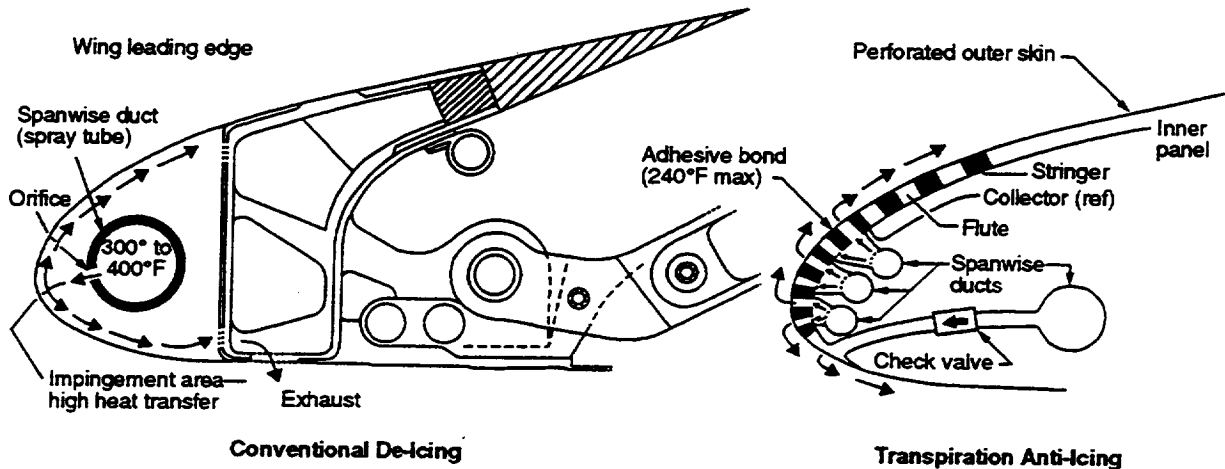


Figure 7.1-3. Comparison of Ice Protection Methods

12054 HLFC-5/20/91 R2

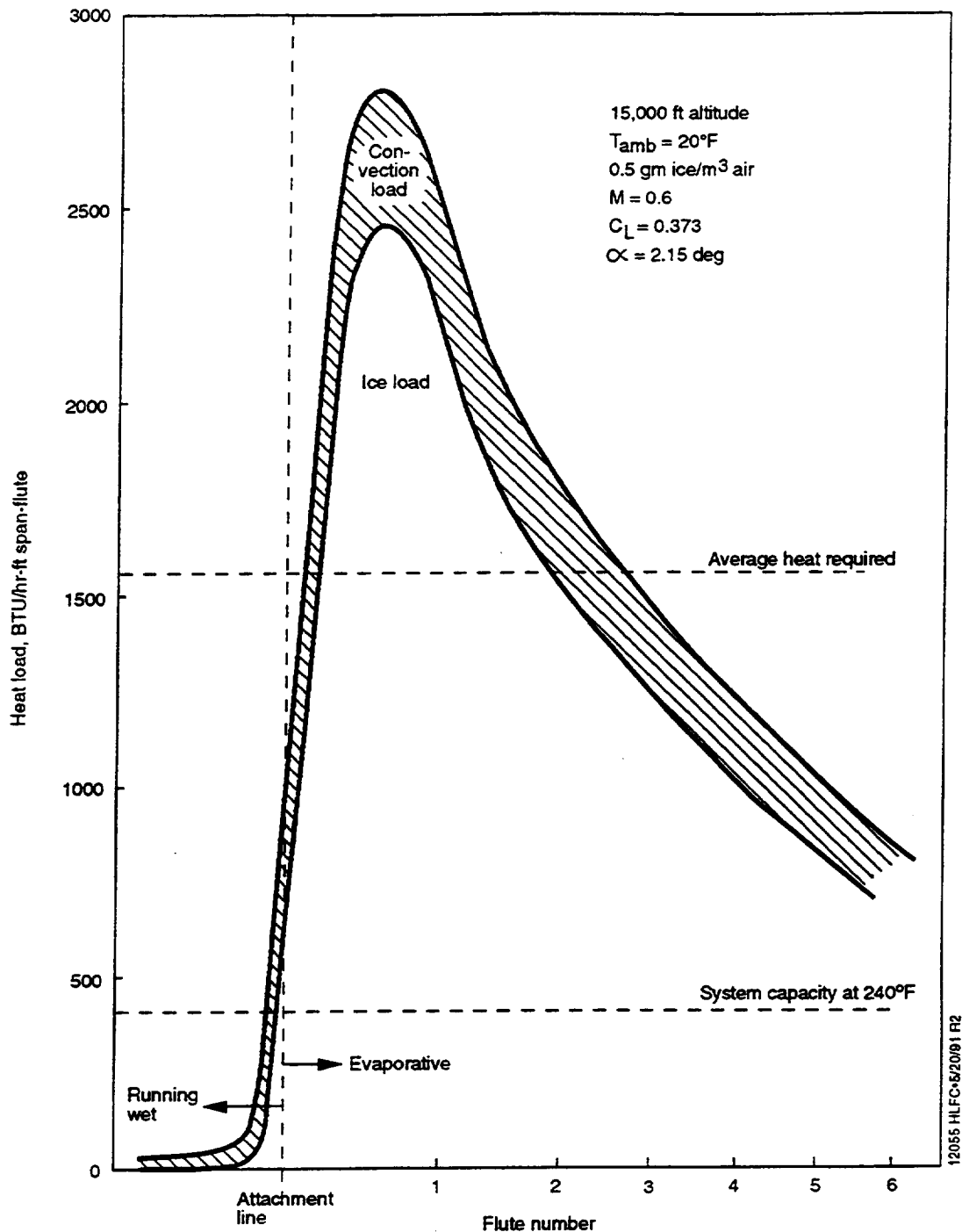


Figure 7.1-4. Flute Thermal Load at Maximum Icing Conditions

**Bondline Temperature.** Finite difference heat transfer modeling was conducted for the anti-ice conditions for airspeed and ambient temperature without ice loading to simulate the worst case anti-icing bond temperature (fig. 7.1-5). The maximum allowable bond temperature ( $240^{\circ}\text{F}$ ) was attained using  $300^{\circ}\text{F}$  air. The allowable stress temperature is based on adhesive stress levels between the stringers and skin. The adhesive used in the bonding process had this strength-versus-temperature limitation. The other, higher temperature adhesives evaluated for this program were not satisfactory for reasons of insufficient lay-up tackiness or melt flow.

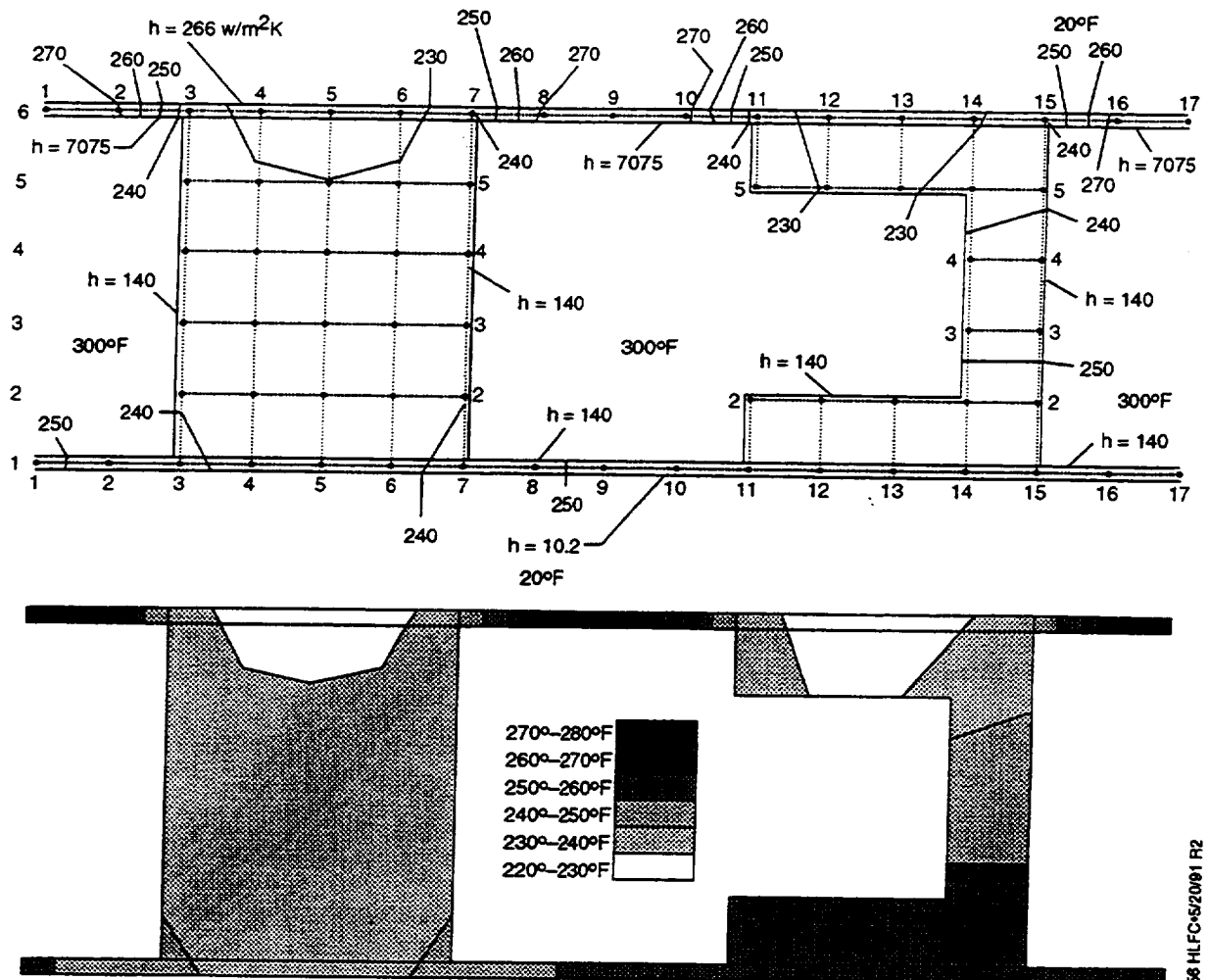


Figure 7.1-5. Flute Temperature Distribution (Anti-Icing Conditions)

The temperatures depended on external flow conditions. Under static or low-speed conditions higher temperatures would occur (figs. 7.1-6 and -7). It was not considered feasible to provide a sufficient number of temperature sensors to ensure that no part of the system exceeded the allowable temperature unless the air temperature itself was limited to 240°F. Therefore a heat exchanger was added to reduce the bleed air to this temperature.

**Heat Exchanger Performance.** The largest heat exchanger that could fit into the strut fairing could only provide limited cooling capacity. Based on this space availability, the AiResearch precooler model 182400-1-1 was selected. The core dimensions for this unit were approximately 10 by 6 by 8 in.

The purpose of this heat exchanger was to reduce the engine bleed air temperature to safe levels at the stringer and skin bond when the system was in the purge or anti-ice mode.

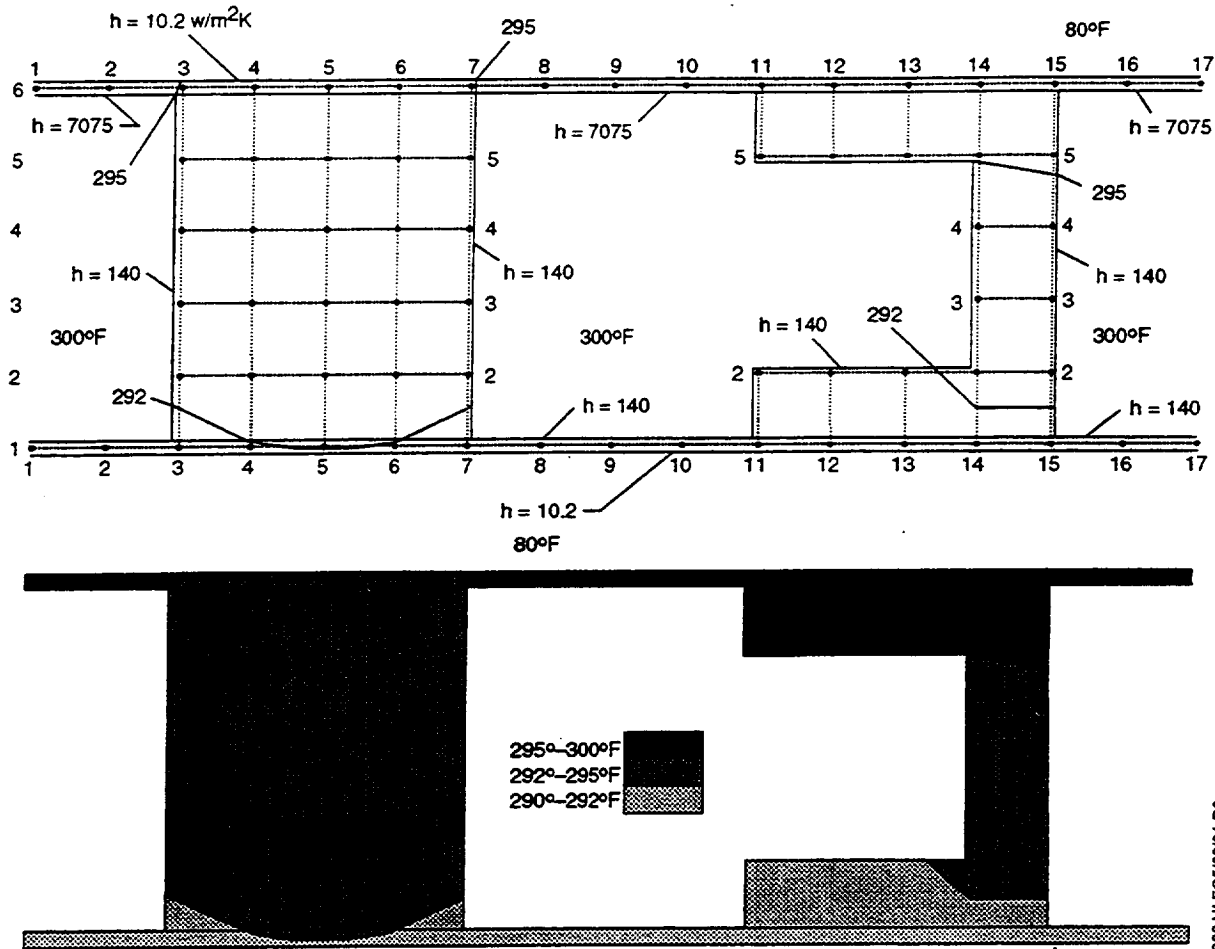


Figure 7.1-6. Flute Temperature Distribution (Still, on the Ground)

The heat sink for reducing the bleed air temperature was freestream ram air at the following nominal design conditions:

$$P_{\infty} = 1,057 \text{ psf}$$

$$\text{ALT} = 18,000 \text{ ft}$$

$$T_{\infty} = 20^{\circ}\text{F}$$

$$M = 0.4.$$

At these conditions the heat exchanger was capable of providing approximately 50 lb/min for purge or anti-ice. This was far short of the 185 lb/min required for an evaporative anti-ice system. Appendix E contains the heat exchanger calculations that predicted the maximum flow rate.

**Effect of Metering Screen.** The flutes that shared a common collector but were exposed to an external pressure gradient required flow balancing screens between the higher pressure flutes and the collectors (air extraction fittings). During suction the screens were sized to produce the desired flow

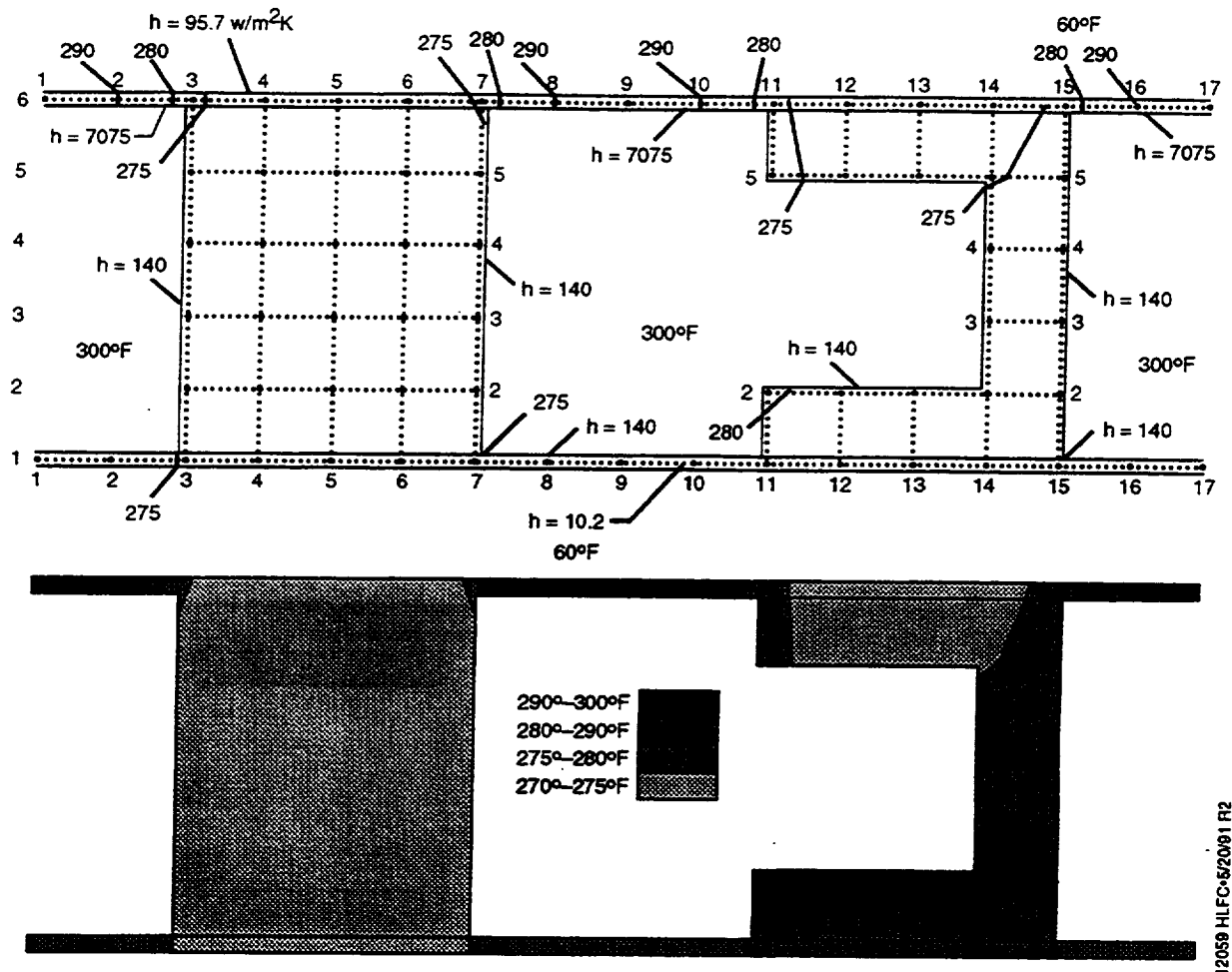


Figure 7.1-7. Flute Temperature Distribution (Normal Takeoff Purge)

by restricting flow at areas of locally high external pressure (fig. 7.1-8).

The consequence of using metering screens is that, during anti-ice or reverse flow, the screens restrict the flow in the region where it is most needed. In other words, compensating for the external pressure gradient during blowing requires that screened and open flutes be switched during suction to obtain balanced flow.

The anti-icing flow through the flutes that have screens is so low that freestream recirculation within the flute, due to external pressure gradients, will probably nullify any heating effect and drop the skin temperature to near the local boundary layer temperature.

**Spanwise Temperature Distribution.** The average distance between collectors was approximately 4 ft. This required some anti-ice air to traverse a considerable spanwise distance before exiting through the perforations in the skin. Heat was lost to the structure and atmosphere in the process, lowering the flute temperature.

Figure 7.1-9 shows the system temperature at the onset of icing. Note how the spanwise temperature change was most dramatic along the flutes.

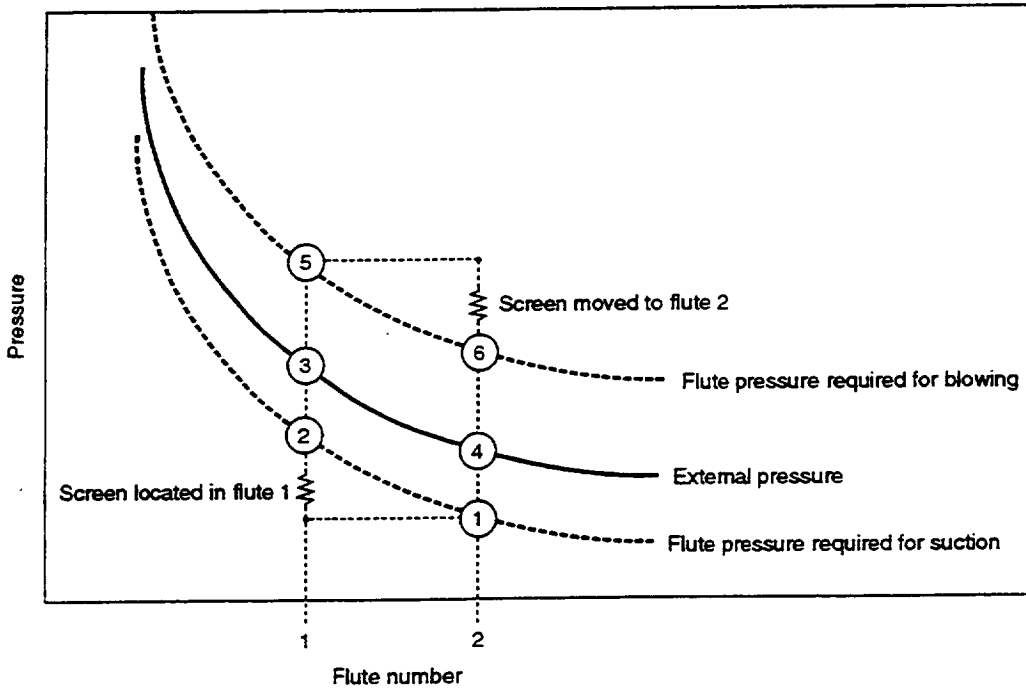
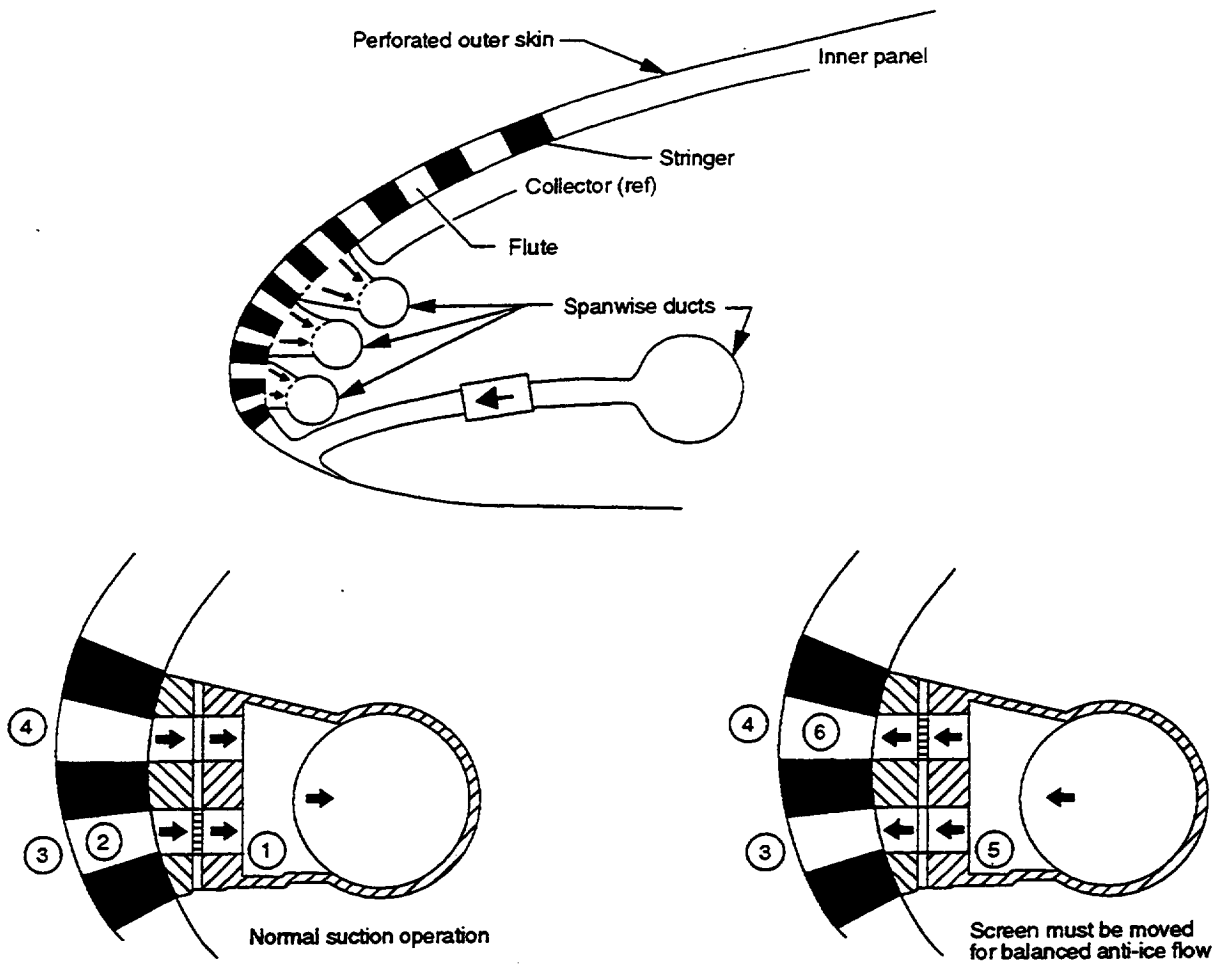


Figure 7.1-8. Metering Screen Location Required for Suction Versus Anti-Ice

12058 HLFC-52001 R3 (KC)

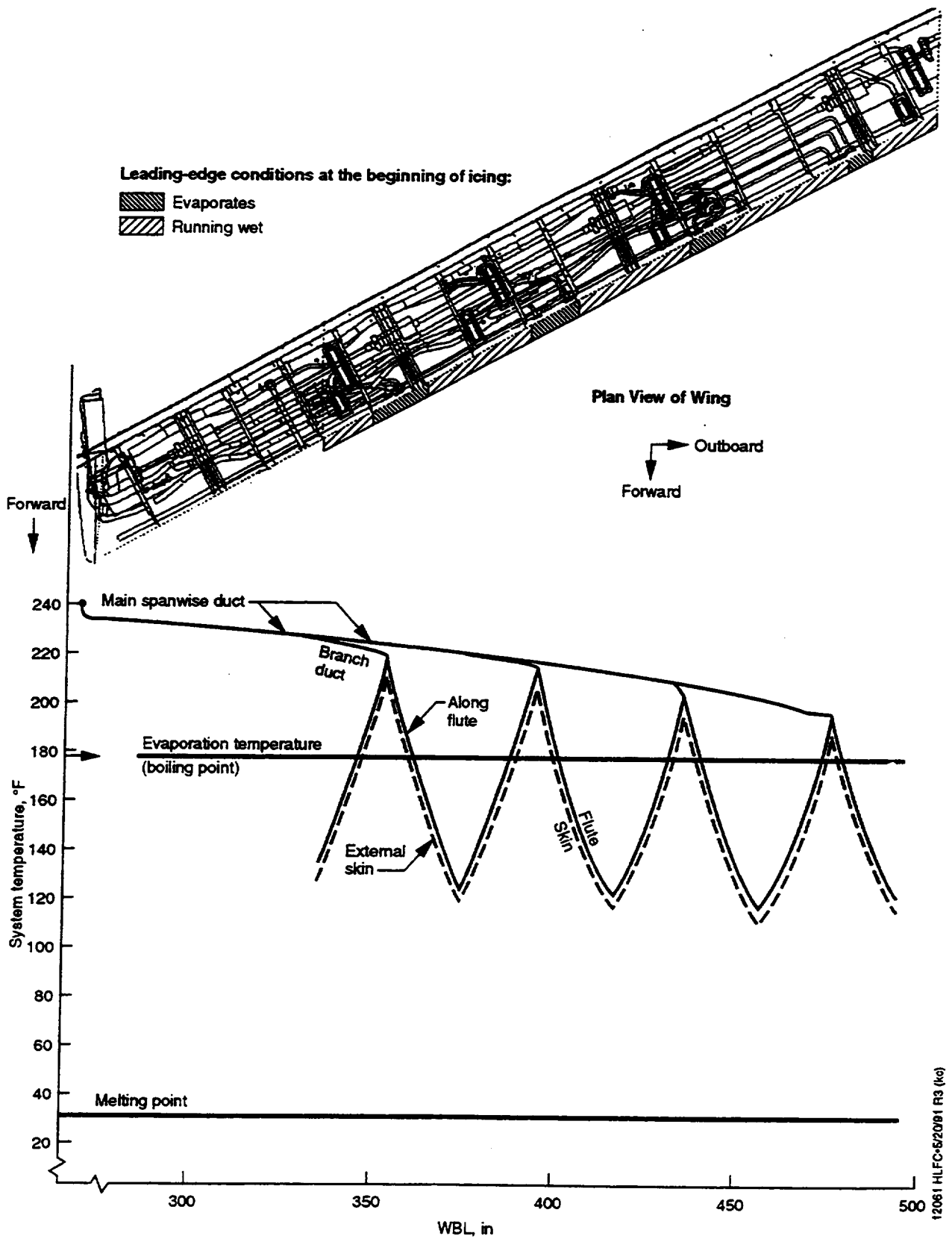


Figure 7.1-9. Air Temperature During Anti-Ice (No Ice Load)

External surface temperatures are further degraded by the changes in icing rates. Figure 7.1-10 shows the theoretical system temperatures with ice loading and figure 7.1-11 shows the ice buildup anticipated at various ice loads.

## 7.2 PURGE

Water from rain or condensation occasionally collected in the system. To remove this water, airflow was reversed in a manner similar to the anti-icing operation. The important factor in purging was not the heat flux but rather the pressure drop across the skin. The pressure drove water from the holes and out into the freestream. Therefore, this operation had to be done in above-freezing temperatures to avoid runback ice.

Tests have shown that the pressure required to purge could be as high as 1 psig (ref. 4). Assuming a worst case set of conditions, the pressure required to overcome surface tension is

$$\Delta P = \frac{2\gamma_{ST}}{r} \cos \theta$$

$$\Delta P = 150 \text{ psf (1.04 psig)} \quad \gamma_{ST} = 0.005 \text{ lb/ft (water) surface tension}$$

$$\text{where } r = 6.67 \times 10^{-5} \text{ ft} \quad \theta = 0 \text{ (maximum condition wetting angle).}$$

Because the bleed airflow rate was limited, the purge operation had to be conducted sequentially. Starting with the forward duct, the system was cleared collector by collector until the aftmost section had been cleared. In this way no more than one spanwise duct at a time was pressurized and the heat exchanger capacity was not exceeded.

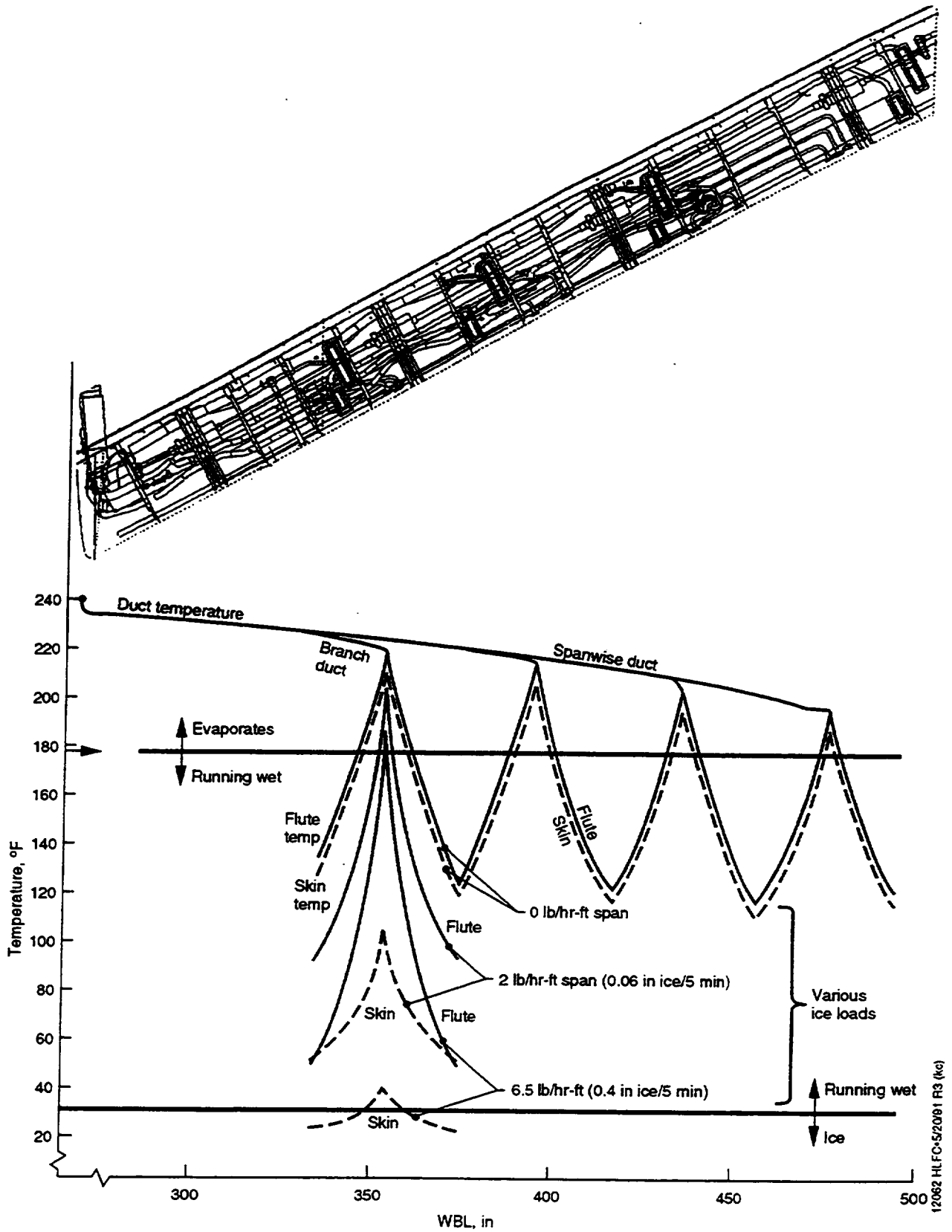


Figure 7.1-10. Effect of Icing Rates on Air Temperature During Anti-Icing

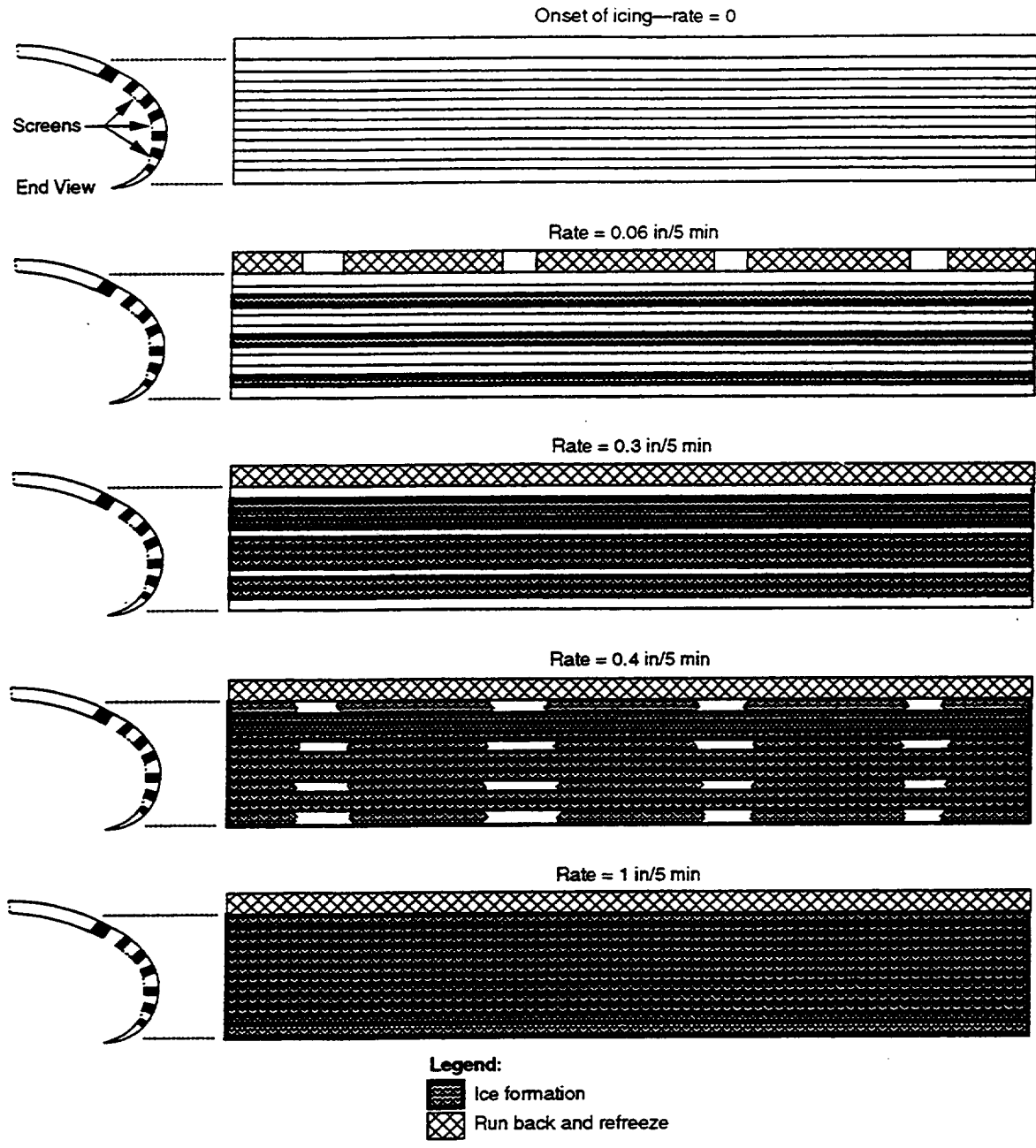


Figure 7.1-11. Theoretical Ice Formation at Various Icing Rates

12063 HLFC-16/20/01 R3

**This Page Intentionally Left Blank**

## 8.0 REFERENCES

- 1 Fischer, D. F., and M. C. Fischer, "The Development Flight Tests of the JetStar LFC Leading Edge Flight Test Experiment," NASA CP-2487, 1987.
- 2 Maddalon, D. V., and A. L. Braslow, "Simulated-Airline-Service Flight Tests of Laminar-Flow Control With Perforated-Surface Suction System," NASA TP2966, 1990.
- 3 Haerter, A. A., "Flow Distribution and Pressure Changes Along Slotted or Branched Ducts," A.S.H.R.A.E. Journal, January 1963.
- 4 Goldsmith, J., "Critical Laminar Suction Into an Isolated Hole of a Single Row of Holes," Northrop Report NA1-57-529 or BLC-45, February 1957
- 5 Bowden, D. T., "Investigation of Porous Gas-Heated Leading Edge Section for Icing Protection on a Delta Wing," NACA RM E54103, May 1954.
- 6 Leadon, B. M., and C.J. Scott, "Transpiration Cooling Experiments in a Turbulent Boundary Layer," *Journal of the Aeronautical Sciences*, August 1956.



## APPENDIX A. EQUATIONS USED IN DUCT ANALYSIS

Hole flow:

$$\dot{w}_H = K P_{EX} (\Delta P)^b$$

$K = 6.34 \times 10^{-13}$  for 0.0016 - in diameter, 0.04 - in thickness  
 $b = 0.966$  for 0.0016 - in diameter, 0.04 - in thickness  
 $\dot{w}_H =$  flow rate per hole (lb/sec/hole)  
 $K = 2.54 \times 10^{-12}$  for 0.0023 - in diameter, 0.04 in - thickness  
 $b = 0.988$  for 0.0023 - in diameter, 0.04 in - thickness  
 $P_{EX} =$  external surface static pressure, psf  
 $\Delta P =$  pressure drop across hole, psf

Flow through skin:

$$\dot{w}_H = \dot{w}_H N A = \dot{w}_H A / \delta^2 = \dot{w}_H b (\% \text{ open}) (L) / [\delta^2 (100)]$$

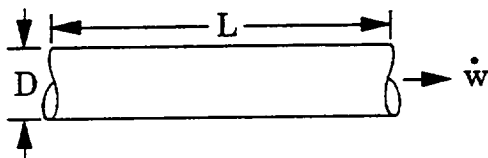
$\dot{w}_H =$  flow through surface (lb/sec)  
 $\dot{w}_H =$  flow rate per hole (lb/sec/ hole)  
 $N =$  number of holes per ft<sup>2</sup>  
 $A =$  area of surface, ft<sup>2</sup>  
 $b =$  flute pitch, ft  
 $L =$  flute length, ft; assume 1/4 of test panel span  
 $\% \text{ open} =$  flute open area / total area %  
 $\delta =$  hole spacing, ft

Duct friction factor (solved iteratively):

Duct resistance:

$$f = \left( \frac{1}{(-0.85859) \ln \left( \frac{12K}{3.7D} + \frac{2.51}{R_e \sqrt{f}} \right)} \right)^2$$

$$R_D = \left( \frac{\gamma_o}{\gamma} \right) K_R \frac{fL}{D^5}$$



$K =$  duct wall roughness (use 0.0001 ft)

$D =$  duct diameter, in

$R_e =$  Reynolds number

$\ln =$  natural log

$f =$  friction factor

$\gamma_o =$  ref density = 0.075 lb/ft<sup>3</sup>

$\gamma =$  actual density (lb/ft<sup>3</sup>)

$K_R =$  flow constant = 4.458

$L =$  duct length, ft

$D =$  duct diameter, in

$R_D =$  duct flow resistance

$$\frac{\text{"wc}}{(\text{lb/min})^2}$$

"wc = inches of water column pressure

$F =$  friction factor

Duct pressure drop:

$$\Delta P = \left( 144 \frac{\text{psf}}{\text{psi}} \right) \left( 0.0361 \frac{\text{psi}}{\text{"wc}} \right) R_D \dot{w}^2$$

$$R_D = \text{duct resistance} \left( \frac{\text{"wc}}{(\text{lb/min})^2} \right)$$

$\dot{w}$  = flow rate in duct (lb/min)

$\Delta P$  = psf

Expansion resistance:

$$R_{EX} = \left( \frac{\gamma_o}{\gamma} \right) \left[ 0.0052\theta + 0.0594(1 - e^{-0.2075\theta}) \right] \left( \frac{1}{D_1^4} - \frac{1}{D_2^4} \right)$$

$\gamma_o$  = ref density = 0.075 lb/ft<sup>3</sup>

$\gamma$  = actual density, lb/ft<sup>3</sup>

$\theta$  = angle of expansion deg (60 - deg max)

(if  $\theta > 60$  let  $\theta = 60$ )

$D_1$  = diameter at entrance, in

$D_2$  = diameter at exit, in

$$R_{EX} = \text{resistance of expansion} \left( \frac{\text{"wc}}{(\text{lb/min})^2} \right)$$

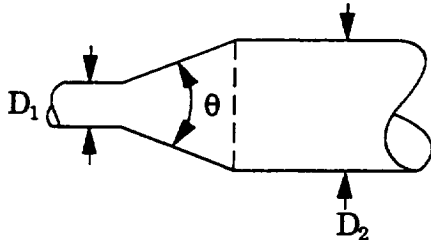
Expansion pressure drop:

$$\Delta P(\text{total}) = (144) (0.0361) R_{EX} \dot{w}^2$$

$$R_{EX} = \text{resistance of expansion} \left( \frac{\text{"wc}}{(\text{lb/min})^2} \right)$$

$\dot{w}$  = flow rate, lb/min

$\Delta P$  = pressure drop (total), psf



Elbow resistance:

$$R_{el} = \frac{\left[ 0.0234 + 0.3667e^{-4.61 \times 10^{-4} \left( \frac{\dot{w}}{D\mu} \right)^{0.779}} \right] \left[ 1 + 0.382 \left( 1 - e^{-4.59 \times 10^{-4} \left( \frac{\dot{w}}{D\mu} \right)} \right) \left( \left( \frac{R}{D} \right)^{-0.93935} - 0.36024 \right) \right]}{D^4} K_\theta$$

$$K_\theta = \text{Correction factor for angle} = \left[ 0.0158\theta^{0.91178} + 8.95 \times 10^{-6}\theta^2 \cos\left(\frac{\theta}{1.5}\right) \right]$$

$\theta$  = bend angle, deg

$\dot{w}$  = flow rate, lb/min

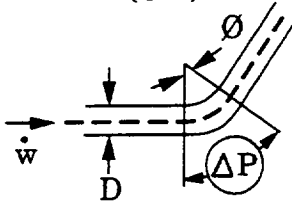
$D$  = diameter, in

$\mu$  = viscosity, lb - sec/ft<sup>2</sup>

$R$  = centerline bend radius

Duct pressure drop:

$$\Delta P = 144 \left( \frac{\text{psf}}{\text{psi}} \right) (0.0361) \left( \frac{\gamma_o}{\gamma} \right) R_{el} \dot{w}^2$$



$\gamma_o$  = ref density = 0.075 lb/ft<sup>3</sup>

$\gamma$  = actual density, lb/ft<sup>3</sup>

$\dot{w}$  = flow rate, lb/min

$\Delta P$  = pressure drop, psf

$R_{el}$  = elbow resistance  $\left( \frac{\text{"wc}}{(\text{lb/min})^2} \right)$

Valve resistance:

$$R_v = \frac{0.3719 K_v}{D^4}$$

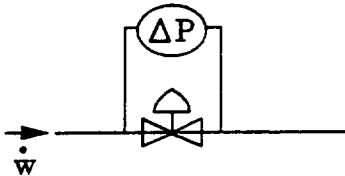
$K$  = valve loss coefficient

$D$  = valve size diameter, in

$R_v$  = valve resistance  $\left( \frac{\text{"wc}}{(\text{lb/min})^2} \right)$

Valve pressure drop:

$$\Delta P = 144 \left( \frac{\text{psf}}{\text{psi}} \right) \left( 0.0361 \frac{\text{psi}}{\text{"wc}} \right) \left( \frac{\gamma_o}{\gamma} \right) R_v \dot{w}^2$$



$\gamma_o$  = ref density = 0.075 lb/ft<sup>3</sup>

$\gamma$  = actual density, lb/ft<sup>3</sup>

$R_v$  = valve resistance  $\left( \frac{\text{"wc}}{(\text{lb/min})^2} \right)$

$\dot{w}$  = flow rate, lb/min

Orifice flow rate:

Subcritical:

$$\dot{w} = \frac{2.05 P_1 A C}{\sqrt{T_1}} \sqrt{\left( \frac{P_2}{P_1} \right)^{1.43} - \left( \frac{P_2}{P_1} \right)^{1.71}}$$

$P_1$  = upstream pressure, psf

$P_2$  = downstream pressure, psf

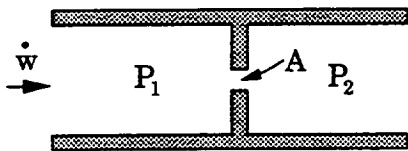
$A$  = area, ft<sup>2</sup>

$C$  = discharge coefficient = 0.65

$T_1$  = air temperature (total), °R

Critical: ( $P_2 \leq 0.528 P_1$ )

$$\dot{w} = \frac{0.525 P_1 A C}{\sqrt{T_1}}$$



Note: These equations were derived from "handbook" quality equations from many sources, or curve-fitted from datasets. The equations were then modified to use consistent units and placed in computer subroutines for access depending on geometry.



## APPENDIX B. "CORRECTED" FLOW PARAMETERS

The following are the turbocompressor conditions shown in section 4 and in figure 4.3-2. They have been included to illustrate the analytical method used for compressor sizing.

$$\begin{aligned} \dot{w} \frac{\sqrt{\theta_1}}{\delta_1} &= \frac{11.456\sqrt{0.8332}}{0.06889} \\ &= 151.76 \text{ lb/min} \\ &\text{(normalized compressor flow)} \end{aligned}$$

From figure 4.3-2:

$$\begin{aligned} \text{For } \dot{w} \frac{\sqrt{\theta_1}}{\delta_1} &= 151.76 \\ \frac{P_{2T}}{P_{1T}} &= 3.86 \text{ (available)} \end{aligned}$$

The required pressure ratio:

$$\left( \frac{P_{2T}}{P_{1T}} \right)_{\text{REQD}} = \frac{P_{\infty}}{P_{1T}} = \frac{411}{145.75} = 2.82$$

Because  $\frac{P_{2T}}{P_{1T}} > \left( \frac{P_{2T}}{P_{1T}} \right)_{\text{REQD}}$  the compressor capacity is acceptable.

$$\dot{w} = 11.4546 \text{ lb/min}$$

$$\theta_1 = \frac{T_1}{T_{\text{STD}}}$$

$$\theta_1 = \frac{432.43}{518.67}$$

$$\theta_1 = 0.08332$$

$$\delta_1 = \frac{P_{1T}}{P_{\text{STD}}}$$

$$\delta_1 = \frac{145.75}{2,116.22}$$

$$\delta_1 = 0.06889$$



## APPENDIX C. EXAMPLE FLUTE PRESSURE DROP CALCULATION

Haerter (ref. 3) analyzed pressure variations in ducts with large numbers of tributary flows. Assuming constant density and duct cross-sectional area, he integrates the momentum equation to obtain an expression for the pressure drop from a point where the average duct velocity is zero (i.e., halfway between collectors) to a point where the average duct velocity is  $V_1$ . For the case where the tributary flow is at right angles to the duct flow (so it contributes no momentum),

$$\Delta P = -(\rho/2) V_1^2 (f L/3D_H + 2)$$

where  $f$  is the friction coefficient,  $L$  is the length of the flow (one-half the distance between collectors, 2.2 ft), and  $D_H$  is the hydraulic diameter (four times duct area over perimeter). For the present case the mass flow is 0.362 lb/min and the duct area is 0.564 in<sup>2</sup>. For a temperature of 400 °R and a pressure of 238 lb/ft<sup>2</sup>, the density is 0.00035 slugs/ft<sup>3</sup>, leading to a flow velocity of 136.5 ft/s. The Reynolds number is about 7,500, giving a friction coefficient of 0.0345 for an assumed roughness of 0.00016 ft. The hydraulic diameter is 0.0514 ft.

Substitution into Haerter's formula gives  $\Delta P = -8.08$  psf (0.056 psi), a small enough change from the initial pressure to justify the assumption of incompressibility.



## APPENDIX D. HOLE FLOW PRESSURE DROP CODE "ADBTDIF.BAS"

Computer program ADBTDIF.BAS is used to predict the pressure drop through perforated material. Refer to section 4.4 and figures 4.4-12 and 4.4-13.

```
10 'ADBTDIF.BAS ADIABATIC DIFFERENTIAL MODEL
15 I = 1
20 D1 = .0021 * (.00255 / .0021) / 12
35 D2 = 2.6 * D1
37 CD = .7
38 D1 = CD * D1
40 CP = 6000
50 K = 1.4
60 TO = 432.432
70 R = 1716
80 THK = .04 / 12
90 PO = 550
100 X = 0
105 D = 41
110 G = 32.2
120 A = 3.14159 * D1 ^ 2 / 4
130 DX = .00002
140 INITIAL VALUES
141 IF (I = 1) THEN P1 = PO - 1
142 IF (I = 2) THEN P1 = PO - 5
143 IF (I = 3) THEN P1 = PO - 7
144 IF (I = 4) GOTO 550
145 I = I + 1
150 'INPUT "INPUT P1 THROAT PRESSURE PSF":P1
160 P = P1
170 V = (2 * CP * TO * (1 - (P1 / PO) ^ ((K - 1) / K))) ^ .5
175 V1 = V
180 T = TO * (P1 / PO) ^ ((K - 1) / K)
195 GAM = P * G / (R * T)
196 WH = GAM * A * V 'SIMPLIFIED
200 M = V / ((K * R * T) ^ .5)
204 MU = .317 * (T ^ 1.5) * (734.7 / (T + 216)) * 1E-10
206 RE = GAM * V * D / (G * MU)
208 F = 64 / RE
210 GAM = P * G / (R * T)
220 DIFFERENTIALS
230 DM = M * ((1 + .5 * (K - 1) * (M ^ 2)) / (1 - (M ^ 2))) * K * (M ^ 2) * F * DX / (2 * D)
240 M = M + DM
245 IF (M > 1) GOTO 500
250 DP = -P * ((1 + (K - 1) * (M ^ 2)) / (1 - (M ^ 2))) * K * (M ^ 2) * F + DX / (2 * D)
260 P = P + DP
270 DGAM = GAM * (-1 / (1 - (M ^ 2))) * K * (M ^ 2) * F * DX / (2 * D)
280 GAM = GAM + DGAM
290 DV = V * (1 / (1 - (M ^ 2))) * K * (M ^ 2) * F * DX / (2 * D)
300 V = V + DV
```

```

310 DT = -T * ( (M ^ 2) * (K - 1) / (1 - (M ^ 2)) ) * K * (M ^ 1) * F * DX / (2 * D)
320 T = T + DT
325 X = X + DX
327 Q = INT ( (X / THK) * 100)
330 PRINT "P="; P; " %DONE="; Q
340 IF (X > THK) GOTO 390
350 D = D1 + (D2 - D1) * X / THK
360 MU = .317 * (T ^ 1.5) * (734.7 / (T + 216)) * 1E-10
370 RE = GAM * V * D / (G * MU)
380 F = 64 / RE
385 GOTO 220
390 W = WH * (1 / .010 ^ 2)
400 LPRINT " "
405 LPRINT "HOLE DIAMETER="; O1 * 12 / CD; " INCH"
410 DELP = PO - P
420 PRINT "DELTA P="; DALP; " FLOW="; WJ; " ;B/SEC/HOLE"; " INITIAL P="; P1
421 LPRINT "DELTA P="; DALP; " FLOW="; WJ; " ;B/SEC/HOLE"; " INITIAL P="; P1
430 PRINT "      M="; M; " F="; "RE="; RE; " T="; T; " V="; V
431 LPRINT "      M="; M; " F="; "RE="; RE; " T="; T; " V="; V
432 GOTO 20
440 END

500 LPRINT "FLOW IS SONIC AT X="; X * 12; " INCH"
505 W = 3H * (1 / .01) ^ 2
506 LPRINT
507 DELP = PO = P
510 PRINT "DELTA P="; DALP; " FLOW="; WJ; " ;B/SEC/HOLE"; " INITIAL P="; P1
520 LPRINT "DELTA P="; DALP; " FLOW="; WJ; " ;B/SEC/HOLE"; " INITIAL P="; P1
530 PRINT "      M="; M; " F="; "RE="; RE; " T="; T; " V="; V
540 LPRINT "      M="; M; " F="; "RE="; RE; " T="; T; " V="; V
541 GOTO 20
550 END

```

## APPENDIX E. TAPERED HOLE FLOW PRESSURE DROP CODE "ADBTSTC.BAS"

Computer program ADBTSTC.BAS is used to predict the pressure drop through perforated material with static pressure recovery due to diffuser effect. Refer to section 4.4 and figure 4.4-13.

```

10 'ADBTSTC.BAS ADIABATIC DIFFERENTIAL MODEL-NO SEPARATION-CONSTANT TOTAL TEMP.
    STATIC MACH NO
12 ' AT DESIGN CONDITION
15 I = 1
20 D1 = .00167 / 12
35 42 = 2.7 * D1
37 CD = .74
38 D1 = CD * D1
39 D2 = CD * D2
40 CP = 6000
50 K = 1.4
60 TO = 432
70 R = 1716
80 THK = .04 / 12
90 PO = 550
100 X = 0
105 D = D1
110 G = 32.2
120 A = 3.14159 * D1 ^ 2 / 4
130 DX = .00004
140 'INITIAL VALUES
141 IF (I = 1) THEN P1 = PO - .001
142 IF (I = 2) THEN P1 = PO - .004
143 IF (I = 3) THEN P1 = PO - .01
144 IF (I = 4) THEN P1 = PO - .04
145 IF (I = 5) THEN P1 = PO - .1
146 IF (I = 6) THEN P1 = PO - .4
147 IF (I = 7) THEN P1 = PO - 1
148 IF (I = 8) THEN P1 = PO - 4
149 IF (I = 9) THEN P1 = PO - 10
150 IF (I = 10) THEN P1 = PO - 40
151 IF (I = 11) THEN P1 = PO - 70
152 IF (I = 12) GOTO 550
160 I = I + 1
170 V1 = (2 * CP TO * (1 - (P1 / PO) ^ ((K - 1) / K))) ^ .5
180 T1 = TO * (P1 / PO) ^ ((K - 1) / K)
182 PT = PO
184 TS = T1
186 PS = P1
188 WH = (PS * G / (R * TR) * (3.14159 * (D1 ^ 2) / 4) * V1
190 'LOOP 2
191 D = D1 + (D2 - D1) * X / THK
193 A = 3.14159 * (D ^ 2) / 4
195 GAM = PS * G / (R * TS)
204 MU = .317 * (TS ^ 1.5) * (734.7 / (TS + 216)) * 1E-10
205 V = WH / (GAM * A)
206 RE = GAM * V * D / (G * MU)

```

```

208 F = 64 / RE
210 DPT = F * DX * (V ^ 2) * GAM / (D * 2 * G)
220 PT = PT - DPT
230 C = (K * R * TS) ^ .5
240 M = V / C
245 IF (M > 1) GOTO 500
250 PS = PT / ((1 + (K - 1) * (M ^ 2) / 2) ^ (K / (K - 1)))
260 TS = TO / (1 + ((K - 1) / 2) * (M ^ 2))
270 PCT = (X / THK) * 100
325 X = X + DX
327 Q = INT ((X / THK) * 100)
330 PRINT "GAM="; GAM; " A="; A; " V="; V; " C="; C; " M="; M; "PS="; PS; " PT="; PT; " %DONE="; Q
340 PCT = (X / THK) GOTO 390
385 GOTO 190
390 W = WH * (1 / .01) ^ 2
395 X = 0
400 LPRINT "
405 LPRINT "HOLE DIAMETER="; D1 * 12 / CD; " INCH"
410 DELP = PO - PS
420 PRINT "DELTA P="; DELP; " FLOW="; WH; " LB/SEC/HOLE"; " INITIAL P="; P1
421 LPRINT "DELTA P="; DELP; " FLOW="; WH; " LB/SEC/HOLE"; " INITIAL P="; P1
430 PRINT "      M="; M; " F="; F; " RE="; RE; " TS="; TS; " V="; V
431 LPRINT "      M="; M; " F="; F; " RE="; RE; " TS="; TS; " V="; V
432 GOTO 140
440 END
500 LPRINT " "
501 LPRINT " "
502 LPRINT " FLOW IS SONIC AT X ="; X * 12; "; INCH"
505 W = WJH * (1 / .01) ^ 2
506 X = 0
507 DELP = PO - PS
510 PRINT "DELTA P="; DELP; " FLOW="; WH; " LB/SEC/HOLE"; " INITIAL P="; P1
520 LPRINT "DELTA P="; DELP; " FLOW="; WH; " LB/SEC/HOLE"; " INITIAL P="; P1
530 PRINT "      M="; M; " F="; F; " RE="; RE; " TS="; TS; " V="; V
540 LPRINT "      M="; M; " F="; F; " RE="; RE; " TS="; TS; " V="; V
541 GOTO 140
550 END

```

## APPENDIX F. ICING TUNNEL TEST OF HLFC TRANSPIRATION THERMAL ANTI-ICING (TAI)

### 1.0 MODEL DESCRIPTION

An existing 757 leading edge slat icing model was modified by addition of electron-beam (EB) perforated titanium outer skins and six simulated 0.6-in-wide suction flutes. Between flutes, 0.6-in strips, where stringers would have blocked the flow, were sealed with cured bonding material held in place by heavy gauge aluminum tape (fig. F-1). The slat represented a full-scale swept outboard leading edge, but the aft body was truncated to a model chord of 34.5 in. The perforated skin covered 10 in of the model's 16.25-in span. It was hand formed and fastened to stainless steel support ribs and to skin doublers at the aft edges by metal screws. Wood strips prevented TAI flow from reaching the skin aft of the simulated flutes (fig. F-2).

Two skins were tested:

- a. A piece of scrapped 0.040-in-thick skin from EB perforation tests, with 0.005-in holes spaced at 0.05 in.
- b. A 0.032-in-thick skin, provided by NASA, with 0.0039-in perforations at 0.032-in spacing.

The specimens were checked for perforation uniformity by placing photographic film on their back surfaces and exposing the fronts to a point light source. The "scrap" skin showed a substantial area of blocked holes, while the NASA specimen had only a few, randomly placed, "dry" holes.

The model was mounted horizontally at zero angle of attack in the Boeing Icing Research Tunnel. The TAI air was supplied at the inboard end of the model through a 0.5- by 7.2-in cutaway opening in the inboard end mounting rib. An exit plenum at the outboard end provided a bypass route for simulating higher velocity through the flutes. All internal joints were sealed with high-temperature RTV silicone rubber compound.

Instrumentation consisted of six skin thermocouples, one static pressure tap and air thermocouple in each plenum and calibrated flow tubes to measure supply and exit airflows. The tunnel was instrumented for liquid water content (LWC), and for tunnel air temperature and velocity. Droplet size and distribution were obtained from calibrated spray nozzles.

### 2.0 TEST CONDITIONS

Tests were run at 170 mph airspeed and 2,000 ft pressure altitude. Air temperatures were  $\pm 20^{\circ}\text{F}$ . Dry-air runs were made at both temperatures. Icing runs were made using 20- $\mu\text{m}$  droplets with 0.50 g/m<sup>3</sup> LWC at the higher temperature and 0.15 g/m<sup>3</sup> at the lower temperature. These are FAR Part 25 "maximum continuous" icing conditions.

**Perforated Panel**

Hole diameter  $\cong$  0.00394 in

Spacing  $\cong$  0.0315 in

No. of holes  $\cong$  1,008 in<sup>2</sup>

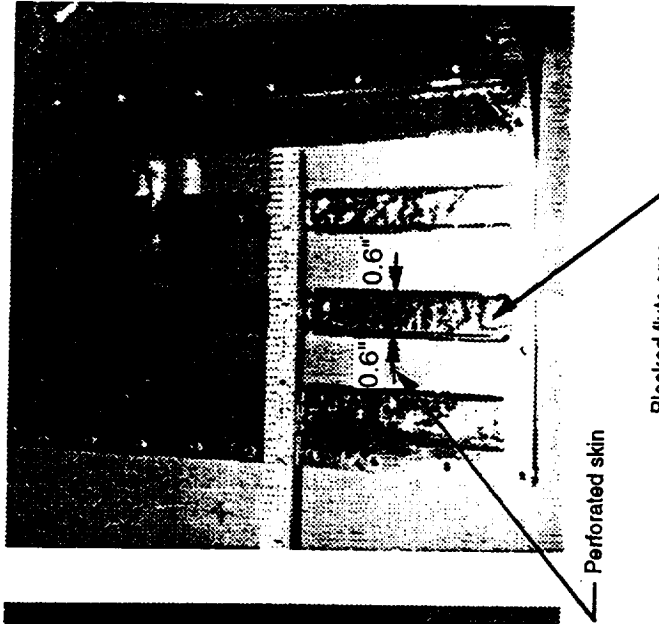
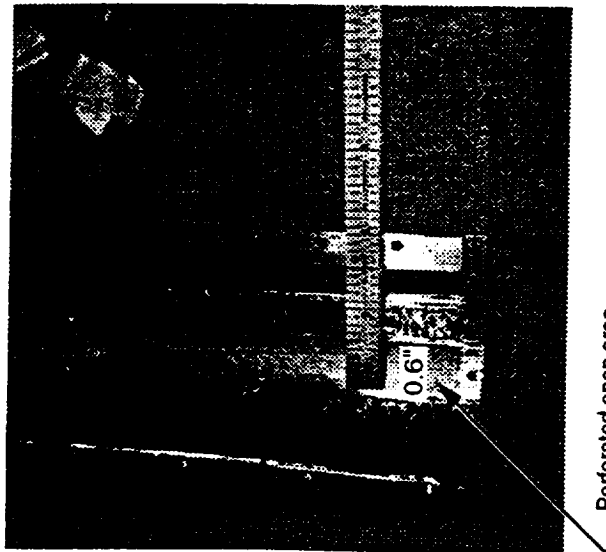


*Figure F-1. Proof-of-Concept Test Model*

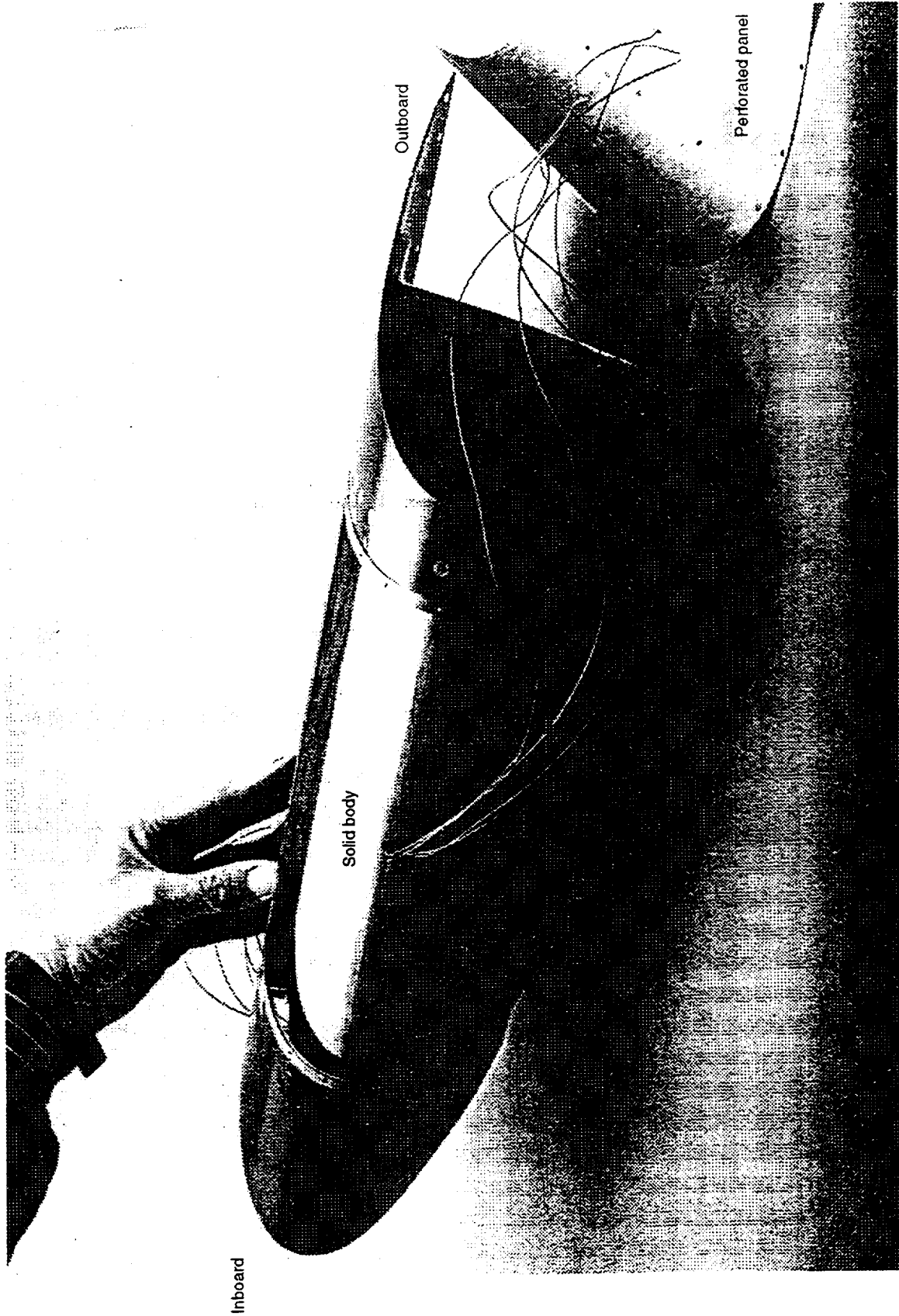


Figure F-2. Details of Test Model

### 3.0 RESULTS

Initial test runs were made using the 0.040-in skin. Because of the extensive dry-hole areas, there was considerable ice buildup on the outboard side, and the required airflow could only be reached at a pressure that caused leakage through the taped joints. It was concluded that results representative of a production skin could not be obtained with this sample. The remainder of the test was therefore run using the 0.032-in (NASA-owned) skin sample. The data presented below are for that skin only.

#### 3.1 Dry Air Tests

Figure F-3 shows skin temperatures measured at  $\pm 20^\circ\text{F}$  ambient air temperature and the design TAI airflow for the HLFC leading edge, 3 lb/min (3.6 lb/min/ft span). The TAI air supply temperatures were  $350^\circ\text{F}$  and  $200^\circ\text{F}$ . Data for "conventional" 757 and 767 TAI tests are shown for comparison. The HLFC transpiration flow system shows much less chordwise temperature variation. (The conventional TAI systems spray hot air onto the inside of the leading-edge skin from a supply tube. It impinges at the nose and flows aft, cooling as it goes.)

A heat balance analysis was done for the  $200^\circ\text{F}$  air supply (with bypass) cases, giving a heat transfer coefficient of  $10.2 \text{ BTU/hr/ft}^2 \text{ }^\circ\text{F}$  for the external flow over the upper surface. This compares with the  $24.3 \text{ BTU/hr/ft}^2 \text{ }^\circ\text{F}$  that could be expected for a nontranspiration surface. The 58% reduction is in good agreement with theory, and implies a potential TAI bleed flow requirement advantage for transpiration heating.

#### 3.2 Icing Tests

The  $350^\circ\text{F}$  air supply kept the leading edge essentially ice free and without runback in simulated FAR Part 25 maximum continuous icing at both ambient temperatures (fig. F-4). However, with the  $200^\circ\text{F}$  air supply, ice buildup was observed on areas where the flow was blocked by stringers, and runback freezing was observed aft of the heated sector (fig. F-5). This buildup continued for the duration of the run and did not shed. Figure F-6 shows skin temperatures for both ambient and both supply temperatures under dry air and wet conditions. For the  $350^\circ\text{F}$  supply, the wet-skin temperature approaches the dry value going downstream. This implies that the impinging moisture has mostly evaporated.

#### 3.3 De-Icing

To investigate the capability of the system to remove ice that has already accumulated, ice was allowed to build, with the TAI shut off, at  $-20^\circ\text{F}$  and  $0.15 \text{ g/m}^3$  LWC, to the point shown in figure 7.1-1. Some  $350^\circ\text{F}$  air was then provided, and it removed the ice from the perforated area in 3 min. This process was possible because of the porosity of ice formed by impingement of supercooled droplets. If the ice had solidly plugged the skin perforations, bleed flow would have been unable to reach the skin.

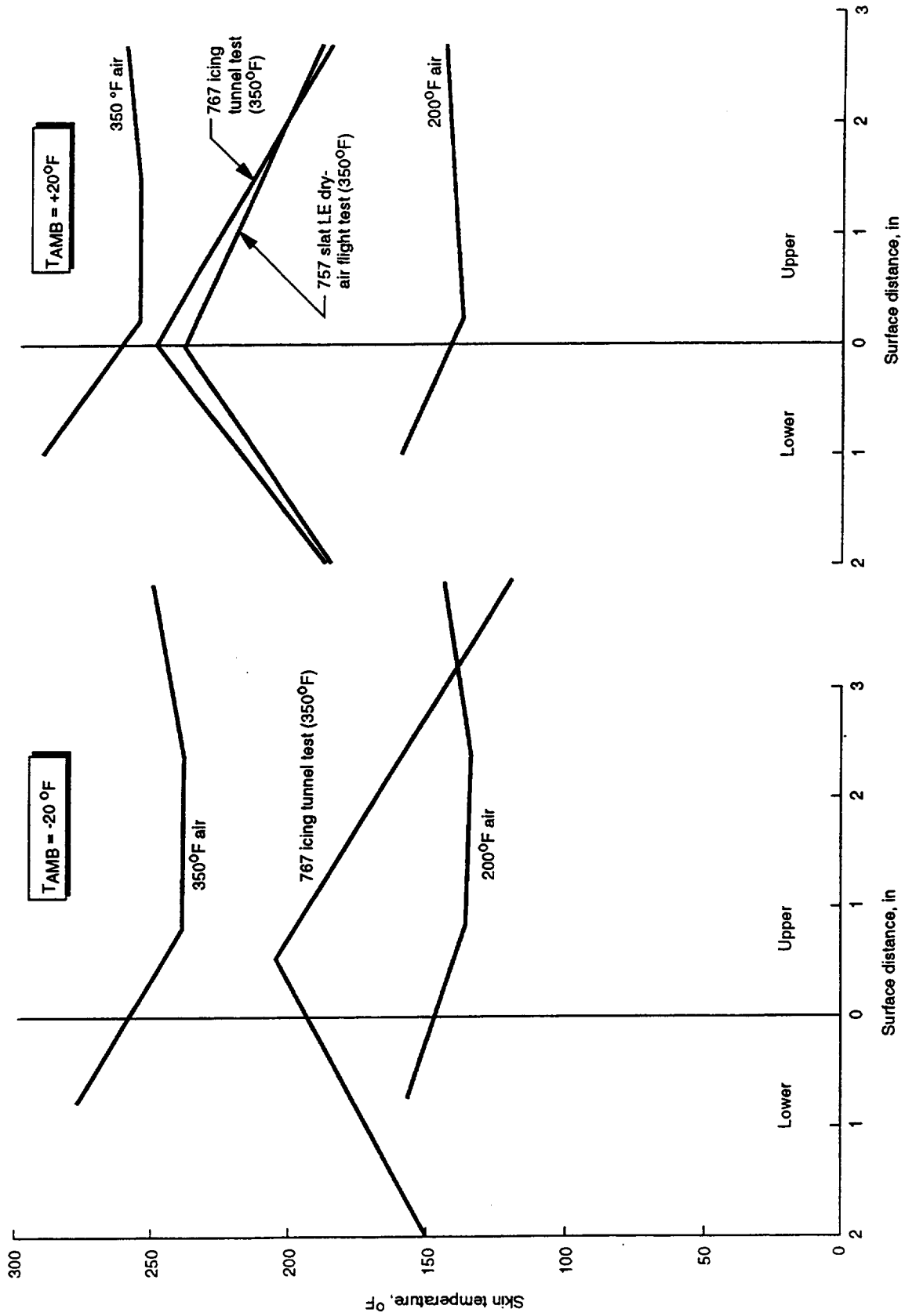
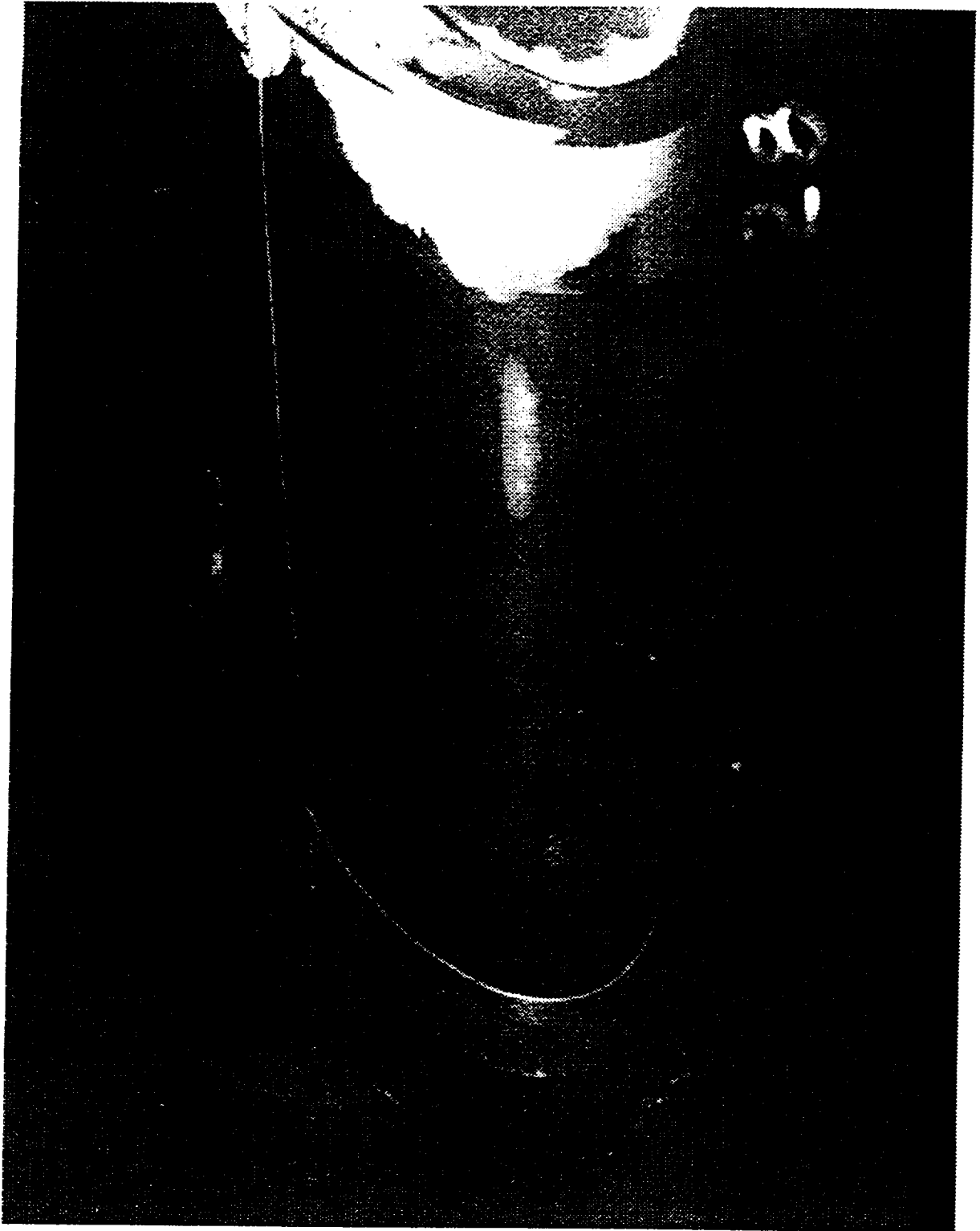
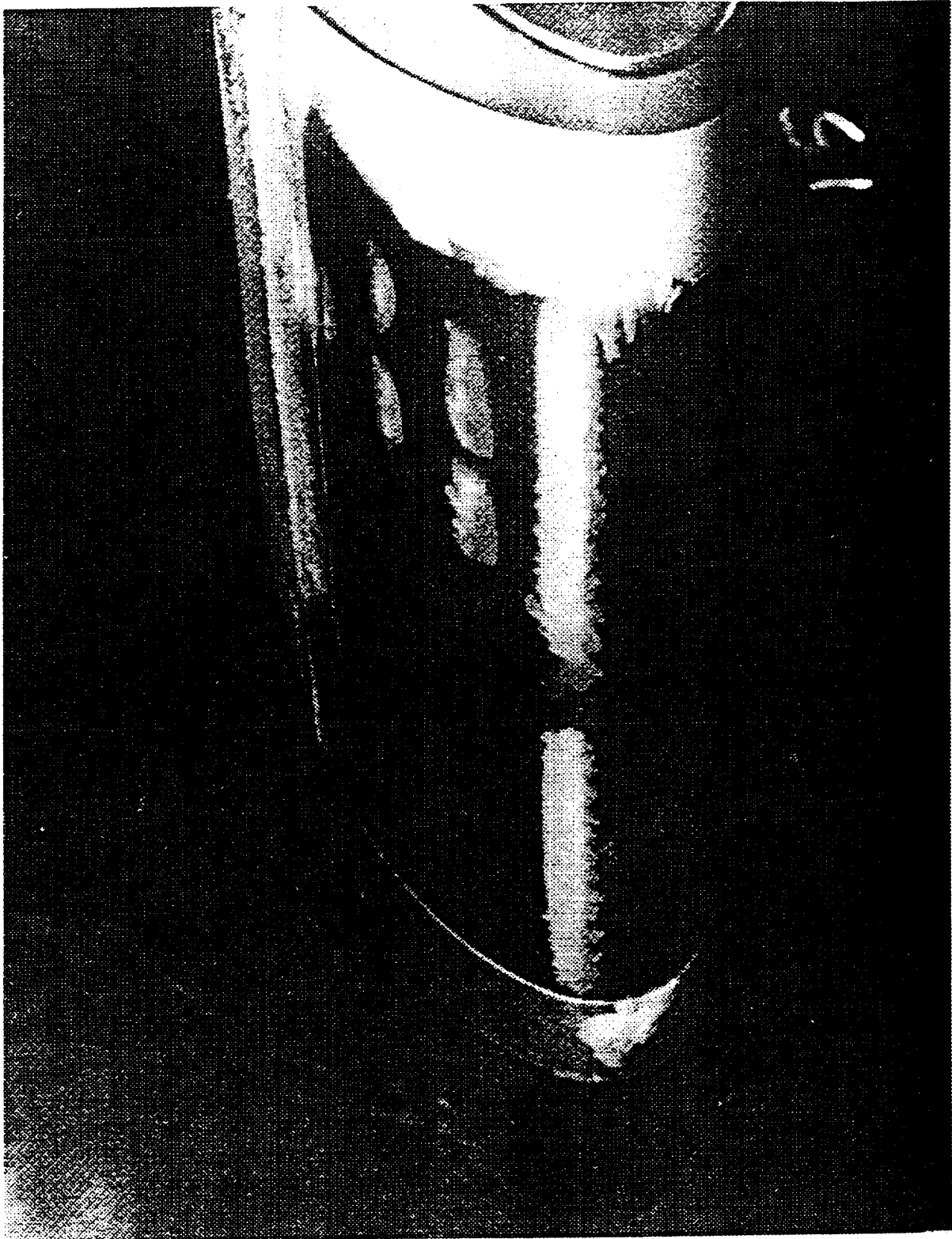


Figure F-3. Skin Temperatures in Dry-Air Tests of HLFC TAI System

HLFC 18-238-12064-5/17/91 R1



*Figure F-4. Leading Edge After 60 sec in FAA Maximum Continuous Icing With 350° F TAI Air, Ambient Air at -20° F*



*Figure F-5. Leading Edge After 60 sec in FAA Maximum Continuous Icing With 200°F TAI Air, Ambient Air at -20°F*

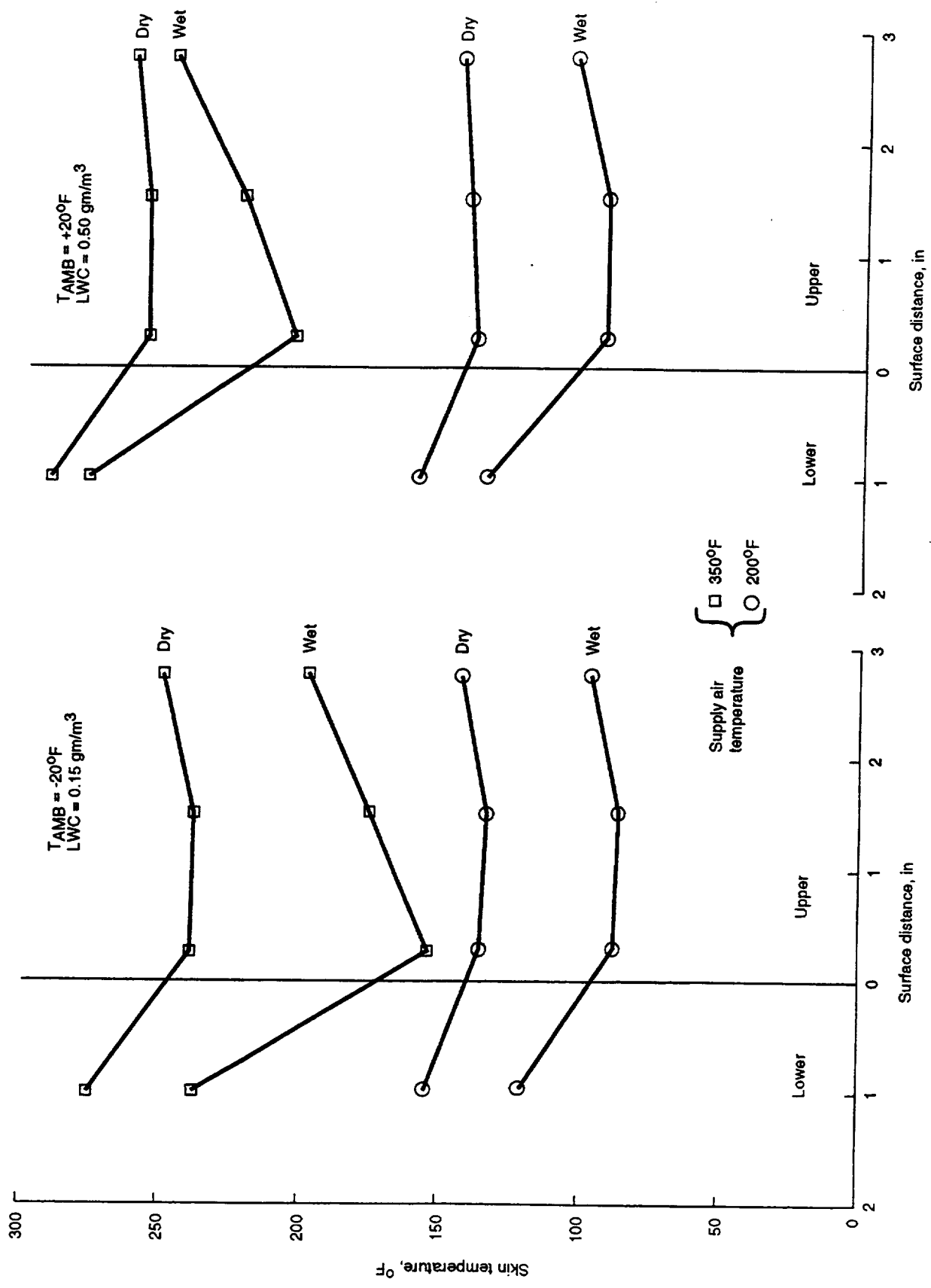


Figure F-6. Leading-Edge Temperatures With TAI in FAA Maximum Continuous Icing

## 4.0 CONCLUSIONS

The test program showed that—

- a. Thermal anti-icing by transpiration heating through a perforated skin designed for laminar flow control is feasible.
- b. TAI air bleed requirements may possibly be less for such a system than for a conventional internal flow arrangement, because transpiration reduces heat loss from the skin to the external airflow.



## APPENDIX G. LEADING EDGE HEATING LOAD AT ICING CONDITIONS

The following is an approximate heating load calculation for determining the heat required to melt ice that forms below the attachment line and evaporate ice that forms above the attachment line. The flight conditions are 15,000 ft altitude, 0.6 Mach, level flight, and  $3.12 \times 10^{-5}$  lb/ft<sup>3</sup> droplet concentration.

$$Q_T = Q_{ICE} + Q_{CONV} + Q_{RAD}$$

$$\begin{aligned} Q_{ICE} &= \beta A_p \gamma_\infty V_\infty (c \Delta T_E + h_{fg}) \\ &= (0.32) \left( \frac{3.5}{12} \times 15 \right) \left( \frac{3.12 \times 10^{-5} \text{ lb}}{\text{ft}^3 \text{ air}} \text{ ice} \right) (644) (1.0[185 - 20] + 987) \end{aligned}$$

$$Q_{ICE} = 32.4 \text{ BTU/sec (116,660 BTU/hr) evaporative above attachment line}$$

$$\begin{aligned} Q_{ICE} &= \beta A_p \gamma_\infty V_\infty (c \Delta T_w) \\ &= (0.32) \left( \frac{1.5}{12} \times 15 \right) \left( \frac{3.12 \times 10^{-5} \text{ lb}}{\text{ft}^3 \text{ air}} \text{ ice} \right) (644) (1.0[40 - 20]) \end{aligned}$$

$$Q_{ICE} = 0.241 \text{ BTU/sec (868 BTU/hr) running wet below attachment line}$$

$$\begin{aligned} Q_{CONV} &= h_{eff} A (T_s - T_{AW}) \\ &= (29.75) \left( \frac{5}{12} \times 17 \right) (185 - 50.9) \end{aligned}$$

$$Q_{CONV} = 28,259 \text{ BTU/hr} \quad \begin{array}{l} \text{above attachment line only since adiabatic wall} \\ T_{AW} = 50.9 \text{ }^\circ\text{F} > 40 \text{ }^\circ\text{F} \end{array}$$

$$\begin{aligned} Q_{RAD} &= \sigma A \epsilon (T_s^4 - T_\infty^4) \\ &= (1.713 \times 10^{-9}) \left( \frac{5}{12} \times 17 \right) (0.3) ((644.6)^4 - (479.6)^4) \end{aligned}$$

$$Q_{RAD} = 435.9 \text{ BTU/hr} \quad \text{evaporative above attachment line}$$

$$\begin{aligned} Q_{RAD} &= \sigma A \epsilon (T_s^4 - T_\infty^4) \\ &= (1.713 \times 10^{-9}) \left( \frac{2.5}{12} \times 17 \right) (0.3) ((499.6)^4 - (479.6)^4) \end{aligned}$$

$$Q_{RAD} = 17.1 \text{ BTU/hr} \quad \text{running wet below attachment line}$$

$$Q_T = (116,660 + 868) + 28,259 + (435.9 + 17.1)$$

$$Q_T = 146,240 \text{ BTU/hr}$$



## APPENDIX H. HEAT EXCHANGER SIZING CALCULATION

The following is a heat exchanger load calculation to determine the amount of air available for purge or anti-icing. It begins with the cooling side.

The pressure available to drive the cooling air through the heat exchanger is the difference between the total pressure at the inlet and the freestream static at the exit.

$$\begin{aligned} \Delta P &= P_T - P_\infty & P_T &= P_\infty \left( 1 + \frac{k-1}{2} M^2 \right)^{\frac{k}{k-1}} \\ &= 1,180.2 - 1057 & &= 1057 \left( 1 + \frac{1.4-1}{2} (0.4)^2 \right)^{\frac{1.4}{1.4-1}} \\ \Delta P &= 123.2 \text{ psf} & P_T &= 1,180.2 \text{ psf} \end{aligned}$$

Based on the heat exchanger loss coefficient of  $C = 225.64$  and assuming the heat exchanger is the predominant pressure loss, the cold side velocity is

$$\begin{aligned} V &= \left( \frac{2\Delta P}{C\rho_c} \right)^{\frac{1}{2}} & \rho_c &= \frac{P_T}{RT_T} & T_T &\equiv T_\infty \left( 1 + \frac{k-1}{2} M^2 \right) \\ V &= \left( \frac{2(123.2)}{225.64(0.001389)} \right)^{\frac{1}{2}} & \rho_c &= \frac{1,180.2}{1,716(495)} & T_T &\equiv T_\infty \left( 1 + \frac{1.4-1}{2} (0.4)^2 \right) \\ V &= 28.04 \text{ ft/s} & \rho_c &= 0.001389 \text{ slugs/ft}^3 & T_T &\equiv 495.0^\circ\text{R} (35.4^\circ\text{F}). \end{aligned}$$

The cold side flow rate is calculated and a guess of 50 lb/min is used on the hot side.

$$\begin{aligned} \dot{w}_c &= \rho_c gAV & \dot{w}_h &= 50 \text{ lb/min (guess)} \\ &= (0.001389)(32.2)(0.556)(28.04) \\ \dot{w}_c &= .6973 \text{ lb/sec} \\ \dot{w}_c &= 41.8 \text{ lb/min} \end{aligned}$$

Using the NTU method with a  $UA = 1,130$ , the heat exchanger effectiveness is:

$$\begin{aligned} NTU &= \frac{UA}{\dot{w}_c c_p} = \frac{1,130}{41.8(60)(0.24)} = 1.877 \\ Z &= \frac{\dot{w}_c c_p}{\dot{w}_h c_p} = \frac{41.8(0.24)(60)}{50(0.24)(60)} = \frac{601.92}{720} = 0.836 \\ \varepsilon &= \frac{1 - e^{-Z(1 - e^{-NTU})}}{Z} \\ &= \frac{1 - e^{-0.836(1 - e^{-1.877})}}{0.836} \\ \varepsilon &= 0.6069. \end{aligned}$$

This results in the following heat exchanger exit conditions:

$$\begin{aligned}
 T_{c1} &= T_{ci} + \frac{q\epsilon}{(\dot{w}_c c_p)} & q &= (\dot{w}_c c_p)(T_{hIN} - T_{cIN}) \\
 &= 35.4 + \frac{(249,556)(0.6069)}{601.92} & &= (601.92)(450 - 35.4) \\
 T_{c2} &= 287.0^\circ\text{F (cooling air exit)} & q &= 249,556 \text{ BTU/hr} \\
 T_{h2} &= T_{h1} - \frac{q\epsilon}{(\dot{w}_h c_p)} \\
 &= 450 - \frac{(249,556)(0.6069)}{720} \\
 T_{h2} &= 239.7^\circ\text{F (bleed air)}
 \end{aligned}$$

To summarize, the heat exchanger performance is

**Bleed air:**

|               |           |
|---------------|-----------|
| Flow rate     | 50 lb/min |
| Entering temp | 450°F     |
| Exiting temp  | 239.7°F   |

**Ram cooling air:**

|               |             |
|---------------|-------------|
| Flow rate     | 41.8 lb/min |
| Entering temp | 35.4°F      |
| Exiting temp  | 287°F       |



| REPORT DOCUMENTATION PAGE  |   |  | Form Approved<br>OMB No. 0704-0188   |  |
|--|---|--|--|--|
| Public reporting burden for this collection of information is estimated to average 1 hour per response, including the time for reviewing instructions, searching existing data sources, gathering and maintaining the data needed, and completing and reviewing the collection of information. Send comments regarding this burden estimate or any other aspect of this collection of information, including suggestions for reducing this burden, to Washington Headquarters Services, Directorate for Information Operations and Reports, 1215 Jefferson Davis Highway, Suite 1204, Arlington, VA 22202-4302, and to the Office of Management and Budget, Paperwork Reduction Project (0704-0188), Washington, DC 20503.   |   |  |  |  |
| 1. AGENCY USE ONLY (Leave blank)   |   | 2. REPORT DATE<br>April 1999                               | 3. REPORT TYPE AND DATES COVERED<br>Contractor Report                        |  |
| 4. TITLE AND SUBTITLE<br>High Reynolds Number Hybrid Laminar Flow Control (HLFC)<br>Flight Experiment<br>IV. Suction System Design and Manufacture   |   |  | 5. FUNDING NUMBERS<br><br>C NAS1-18574<br><br>WU 522-32-31-01                |  |
| 6. AUTHOR(S)<br>Boeing Commercial Airplane Group   |   |  |  |  |
| 7. PERFORMING ORGANIZATION NAME(S) AND ADDRESS(ES)<br><br>Boeing Commercial Airplane Group<br>P. O. Box 3707<br>Seattle, WA 98124-2207   |   |  | 8. PERFORMING ORGANIZATION<br>REPORT NUMBER                                  |  |
| 9. SPONSORING/MONITORING AGENCY NAME(S) AND ADDRESS(ES)<br><br>National Aeronautics and Space Administration<br>Langley Research Center<br>Hampton, VA 23681-2199  |   |  | 10. SPONSORING/MONITORING<br>AGENCY REPORT NUMBER<br><br>NASA/CR-1999-209326 |  |
| 11. SUPPLEMENTARY NOTES<br>Langley Technical Monitor: Fayette S. Collier, Jr.<br>Point of Contact: Ronald D. Joslin  |   |  |  |  |
| 12a. DISTRIBUTION/AVAILABILITY STATEMENT<br>Unclassified-Unlimited<br>Subject Category 02                      Distribution: Nonstandard<br>Availability: NASA CASI (301) 621-0390   |   |  | 12b. DISTRIBUTION CODE   |  |
| 13. ABSTRACT (Maximum 200 words)<br>This document describes the design of the leading edge suction system for flight demonstration of hybrid laminar flow control on the Boeing 757 airplane. The exterior pressures on the wing surface and the required suction quantity and distribution were determined in previous work. A system consisting of porous skin, sub-surface spanwise passages ("flutes"), pressure regulating screens and valves, collection fittings, ducts and a turbocompressor was defined to provide the required suction flow. Provisions were also made for flexible control of suction distribution and quantity for HLFC research purposes. Analysis methods for determining pressure drops and flow for transpiration heating for thermal anti-icing are defined. The control scheme used to observe and modulate suction distribution in flight is described. |   |  |  |  |
| 14. SUBJECT TERMS<br>Laminar Flow Control, Boundary Layer Suction, LFC, Flight Experiment  |   |  | 15. NUMBER OF PAGES<br>105   |  |
|  |   |  | 16. PRICE CODE<br>A06  |  |
| 17. SECURITY CLASSIFICATION<br>OF REPORT<br>Unclassified   | 18. SECURITY CLASSIFICATION<br>OF THIS PAGE<br>Unclassified | 19. SECURITY CLASSIFICATION<br>OF ABSTRACT<br>Unclassified | 20. LIMITATION<br>OF ABSTRACT<br>UL  |  |